Scuola Internazionale Superiore di Studi Avanzati

Trieste



Chemosensory Systems: Sympathetic Modulation of Vomeronasal Neurons and Electrophysiological Insights from the Human Olfactory Epithelium

Thesis submitted for the degree of “Doctor Philosophiae”

Academic Year 2023/2024

CANDIDATE

Cesar Adolfo Sanchez Trivino

SUPERVISORS

Prof. Anna Menini

CO-SUPERVISORS

Prof. Simone Pifferi

Table of contents

1. ABSTRACT 3

2. LIST OF ABBREVIATIONS 5

3. INTRODUCTION 7

3.1. Olfaction 7
3.2. Pheromones 8
3.3. Vomeronasal Organ (VNO) 9
3.4. Vomeronasal transduction cascade 11
3.4.1. Vomeronasal Receptors (VRs) 11
3.4.2. Phospholipase C (PLC) pathway 13
3.5. Action potential machinery 16
3.5.1. Passive electrical properties and firing of VSNs 17
3.5.2. Sodium channels 19
3.5.3. Calcium channels 21
3.5.4. Potassium channels 25
3.6. Main Olfactory Epithelium (MOE) 26
3.7. Olfactory sensory neurons and transduction cascade 27
3.7.1. Odorant receptors 27
3.7.2. Adenylyl cyclase pathway 29
3.7.3. Voltage-gated currents and action potentials in OSNs 31
3.8. Comparison of human and mouse olfactory epithelium 32
3.9. Autonomic nervous system 34
3.10. Adrenergic receptor types 36
3.11. Autonomic nervous system and regulation of sensory systems 39
3.12. Autonomic nervous system in the VNO and MOE. 40

4. AIMS 41

5. RESULTS 42

5.1. Noradrenaline modulates sensory information in mouse vomeronasal sensory neurons 42
5.2. Shedding light on human olfaction: Electrophysiological recordings from sensory neurons in acute slices of olfactory epithelium 66

6. DISCUSSION 67

6.1.1. NA increases the excitability of VSNs 67
6.1.2. Identity of the AR expressed in VSNs 68
6.1.3. Calcium increase by NA stimulation and possible cellular mechanism 68
6.1.4. Sympathetic nervous system and NA on VSNs 69
6.2.1. OSNs in human epithelium 70
6.2.2. SCs in human epithelium 70

7. REFERENCES 71

1. Abstract

Olfaction enables the discrimination of millions of molecules across varied concentrations, with species adapting their olfactory systems to suit their ecological needs. Despite this variability, many mammals share a common olfactory anatomy involving the main olfactory epithelium (MOE) for detecting odorants and the vomeronasal organ (VNO) for sensing semiochemicals and pheromones. These functions are critical for identifying food sources, finding mates, and avoiding environmental dangers.

In the first part of this thesis, we explored the VNO, an organ housing vomeronasal sensory neurons (VSNs) located in a secluded sensory epithelium, accessible solely through a duct in the nasal cavity. The entry of mucus laden with pheromones into this organ is facilitated by muscle contractions orchestrated by the sympathetic nervous system. This system governs fight-or-flight responses through the secretion of noradrenaline (NA) from sympathetic nerves or adrenaline from the adrenal gland, both capable of activating adrenergic receptors (AR).

Our investigation focused on understanding how VSNs are modulated under sympathetic influence. Specifically, we examined NA's impact on the spiking activity of VSNs, which are crucial for detecting pheromones and other semiochemicals. Employing several techniques including patch-clamp whole-cell recordings, transcriptomic analysis, calcium imaging, and pharmacology, we identified alpha 1-AR as pivotal in mediating NA-induced increases in VSN firing frequency. Immunohistochemistry further revealed catecholaminergic fibers in the vomeronasal sensory epithelium, indicating localized NA release. These findings underscore NA’s critical role in VSNs and shed light on the intricate interplay between the sympathetic nervous system and chemosensory processing.

In the second part of this thesis, we delve into the MOE, the tissue harboring olfactory sensory neurons (OSNs), responsible for the detection of odorant molecules. These bipolar neurons have dendrites ending with several cilia that contain the essential components for olfactory transduction. Studies on several vertebrates have shown that, upon binding of odorant molecules to specific odorant receptors (ORs), a transduction cascade is initiated, converting the chemical signal into an electrical one, which is then transmitted and processed by the central nervous system. This cascade involves the activation of adenylyl cyclase III (ACIII), which generates cAMP, subsequently activating cyclic nucleotide gated (CNG) channels. These channels permit the entry of both Na^+ and Ca^{2+} ions into the cilia. The rise in Ca^{2+} levels then triggers the opening of the Cl^- channel TMEM16B, amplifying the primary CNG current response.

However, in the human MOE, there is a lack of information at the cellular physiology level, highlighting the necessity of developing a novel model to study it. Given the heightened focus on the MOE during the COVID-19 pandemic, we examined the cellular physiology of the MOE in humans, in acute slices of the human MOE from nasal biopsies. By using whole-cell patch-clamp techniques, we recorded voltage-gated currents in human OSNs and supporting cells (SCs). In OSNs, we recorded action potentials in response to current injections. Additionally, we found functional indications of a transduction cascade involving cAMP as a second messenger. Indeed, phosphodiesterase inhibitors and odorant mixtures triggered the activation of inward currents and action potential firing. This marks the first electrophysiological characterization of human OSNs, providing a foundation for future investigations into human olfactory physiology.

Together, these results advance our comprehension of chemical sensory modulation in both the OSNs and VSNs, emphasizing NA's significant regulatory role in VSNs and expanding the knowledge of olfactory mechanisms in human OSNs.

2. List of abbreviations

AA	Arachidonic acid
AC	Adenylyl cyclase
ACh	Acetylcholine
AMP	Adenosine monophosphate
AOB	Accessory olfactory bulb
APs	Action potentials
AR	Adrenergic receptors
ATP	Adenosine triphosphate
BCs	Basal stem cells
BK	Voltage- and Ca^{2+}-activated K^+ channel
CaCCs	Voltage-dependent and Ca^{2+}-activated Cl^--channels
CaM	Calcium calmodulin
CaMKII	Calcium calmodulin kinase II
cAMP	Cyclic adenosine monophosphate
Ca_V	Voltage-gated calcium channels
cDNA	Complementary DNA
cGMP	Cyclic guanosine monophosphate
CNG	Cyclic nucleotide–gated ion channels
CNS	Central nervous system
DAG	Diacylglycerol
DIDS	4,4'-Diisothiocyano-2,2'-stilbenedisulfonic acid
ESP1	Exocrine gland-secreting peptide 1
FPRs	Formyl peptide receptors
GC-D	Guanylyl cyclase D
GDP	Guanosine triphosphate
GFP	Green fluorescence protein
GIRK1	G protein-gated inwardly rectifying potassium channel 1
GPCRs	G-protein-coupled receptors
GTP	Guanosin triphophate
HCN	Hyperpolarization-activated cyclic nucleotide–gated channel
I_K	Outward rectifier potassium currents
IP3	inositol 1,4,5-triphosphate
IP3R	Inositol 1,4,5-trisphosphate receptor
KcsA	Potassium channel of streptomyces A
K_v	Voltage-gated potassium channels
MHC	Major histocompatibility complex class I
MOB	Main olfactory bulb
MOE	Main olfactory epithelium
MUP	Major urinary proteins
NA	Noradrenaline
Na_V	Voltage-gated sodium channel
NFA	Niflumic acid
OB	Olfactory bulb
OR	Olfactory receptor
OSNs	Olfactory sensory neurons

PDE	Phosphodiesterase
PIP2	Phosphatidylinositol bisphosphate
PKA	Protein kinase A
PKC	Protein kinases C
PLC	Phospholipase C
RT-PCR	Reverse-transcription PCR
SCs	Sustentacular cells or supporting cells
SK3	small conductance Ca^{2+}-activated potassium channel 3
SNX-482	$Ca_V2.3$ channel blocker
T1R	Taste receptor, family 1
TAARs	Trace-amine-associated receptors
TEA	Tetraethylammonium
TMEM16A	Transmembrane member 16A or anoctamin-1
TMEM16B	Transmembrane member 16B or anoctamin-2
TRP	Transient Receptor Potential Cation Channel
TRPV1-4	Transient Receptor Potential, vanilloid-receptor 1-4
TTX	Tetrodotoxin
V1R	Vomeronasal receptor 1
V2R	Vomeronasal receptor 2
VNO	Vomeronasal
VR	Vomeronasal receptor
VSNs	Vomeronasal sensory neurons
WT	Wild-type

3. Introduction

3.1. Olfaction

Olfaction enables the discrimination of millions of chemical structures across a wide range of concentrations (Sharma et al., 2019) playing a crucial role in detecting food, and locating mates, and helping organisms avoid environmental threats (Hoover, 2010). The binding of odorants to cellular proteins to gather information about the environment has catalyzed significant phenotypic and genomic changes throughout evolution. This is evident in the transition of vertebrates from aquatic environments to terrestrial ones, challenging their physiology in many ways, including olfaction.

Fishes have been specialized in detecting water-soluble odorants in a medium where diffusion is approximately 10,000 times slower than in air, where the viscosity is higher and the detection of molecules strongly depends on their solubility (Freitag et al., 1998). Due to these environmental constraints, aquatic organisms evolved mechanisms to facilitate the water movement onto the olfactory surface such as nostril structures and active beating cilia (Reiten et al., 2017).

Amphibians, especially anurans, represent an intermediate step in this transition. During metamorphosis, adaptive changes occur in the olfactory system, which recapitulates the accommodation to terrestrial olfaction. Tadpoles are characterized by a water-type olfactory epithelium composed of ciliated, and microvillous receptors as well as two types of supporting cells. In contrast, adult frogs, adapted to air-type olfaction, have a ciliary epithelium enriched with Bowman's glands that increase mucus production (Weiss et al., 2021).

Two types of molecules challenge the olfactory system in a terrestrial environment: volatile odor molecules, which disperse easily in the air, and non-volatile or hydrophobic molecules, which cannot be freely distributed. These evolutionary pressures have led to the development of specialized structures, resulting in the specialization of the main olfactory epithelium (MOE), responsible for the detection of odorants, and the vomeronasal organ (VNO), which detects semiochemicals and pheromones, aiding in communication with other animals (Bigiani et al., 2005; Silva & Antunes, 2017).

3.2. Pheromones

The word pheromone was initially described in insects by Karlson and Lüscher in 1959 (Karlson & Luscher, 1959) to identify biologically active substances "*which are secreted to the outside by an individual and received by a second individual of the same species, in which they release a specific reaction, for example, a definite behavior or a developmental process*". The sources of pheromones are body fluids such as urine, vaginal secretions, or saliva (Tirindelli et al., 2009; Voznessenskaya et al., 2022). For example, mouse urine contains several pheromone types classified according to their chemical structures and physical properties, such as volatility.

High volatile pheromones (Figure 1.1A) are organic chemical compounds with low molecular weight, such as 2-heptanone, 2-*sec*-butyl dihydrothiazole, β-farnese and dehydro-exo-brevicomin (Novotny et al., 1999; Tirindelli et al., 2009). They are released in the male urine in a testosterone-dependent manner, working as a chemo-signal informing about the presence of reproductive and socially dominant males (Ihara et al., 2013).

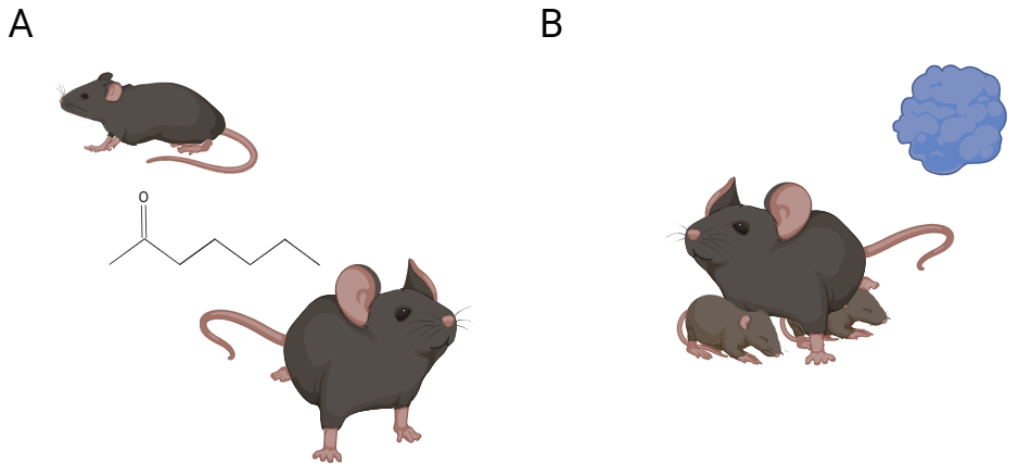


Figure 1.1: Volatility of pheromones plays different roles during recognition between individuals. **A.** Volatile molecules advertise the presence of other animals to save long distances. **B.** Non-volatile molecules are involved in close social interactions.

The signaling mediated by nonvolatile molecules (Figure 1.1B) requires physical contact between individuals, such as during the sniffing of genitalia or facial interactions. In mice, the peptides of the major histocompatibility complex class I (MHC) and major urinary proteins (MUP) are excreted in urine and are responsible for individual recognition and the avoidance of inbred progeny (Leinders-Zufall et al., 2004; Roberts et al., 2010; Sherborne et al., 2007).

Moreover, several peptides with higher molecular weight are secreted by the lacrimal gland into male tears and have been identified as pheromones, such as exocrine gland-secreting peptide 1 (ESP1) which induces receptive sexual behavior in females (Kimoto et al., 2005; Yoshinaga et al., 2013).

In mice, pheromones are primarily detected by VSNs in the VNO, where they bind to specific receptors, activating a sensory transduction cascade that generates action potentials reaching directly the accessory olfactory bulb (AOB) (Tirindelli, 2021). After processing in the AOB, this information is transmitted to several brain circuits to induce physiological and behavioral responses (Stowers & Kuo, 2015; Voznessenskaya et al., 2022).

3.3. Vomeronasal Organ (VNO)

Initial descriptions of the vomeronasal structure were obtained from anatomical investigation on domestic and model animals (Døving & Trotier, 1998; Jacobson et al., 1998), where Jacobson reported the presence of a tubular structure associated with the nasal septum, communicating through ducts to either the nasal or oral cavity (Figure 1.2A-B).

Early experiments on the VNO's function demonstrated its crucial role as a primary source of chemosensory inputs for conspecific communication through pheromones and for other semiochemical detection. For instance, behavioral experiments showed that male mice with VNO ablation significantly decreased their preference for estrous female urine compared to control mice (Pankevich et al., 2006).

The VNO consists of two main histological regions arranged around a lumen (Mechin et al., 2021). One is the vomeronasal sensory epithelium, located close to the medial line. The sensory epithelium is a pseudostratified epithelium composed of three cell types: VSNs, SCs, and basal stem cells (BSc) (Figure 1.2C). VSNs have a bipolar morphology, with an axon traveling to the AOB and a sensory dendrite reaching the lumen, ending with a knob with several microvilli (Liman & Corey, 1996). The microvilli create a large surface for the receptor proteins and ion channels involved in the transduction pathway. SCs are glial-like cells (Fieni et al., 2003; Ghiaroni et al., 2003) capable of sustaining significant fluxes of K^+, Na^+, and Cl^-, thereby controlling osmotic

and excitability processes through the redistribution of ion species often concentrated in some pheromone-delivering fluids such as urine (Figure 1.2C).

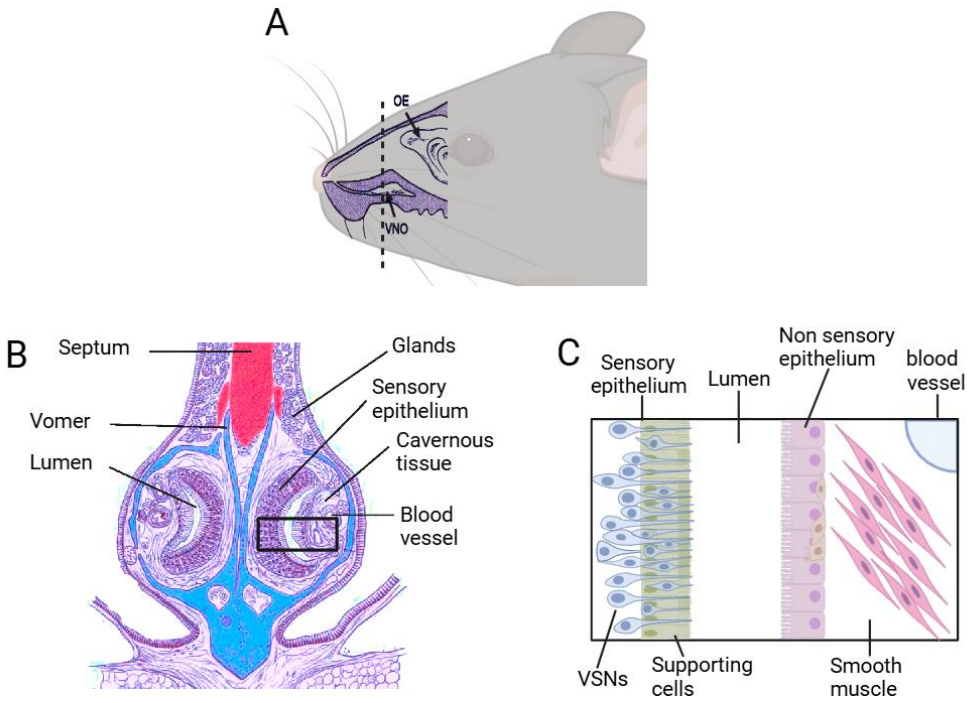


Figure 1.2: Structure of VNO in mouse. **A.** Localization of the VNO in the bottom part of the nasal cavity and in the palate roof. **B.** Coronal section at the dashed line level in A, showing the bilateral organization in the VNO. **C.** Histological regions in the VNO identifying its main cellular types (from inset in B). Adapted from (Doving & Trotier, 1998) and (Liman & Corey, 1996).

The second histological region facing the lumen is the non-sensory epithelium, consisting of ciliated and non-ciliated columnar cells accompanied by a continuous layer of BCs adjacent to the basement membrane (Elgayar et al., 2017). Adjacent to this epithelium, the lateral region of the VNO is mainly composed of smooth muscle innervated by autonomous nerves. These nerves regulate fluid entry into the VNO lumen by controlling blood flow through coordinated vasoconstriction in the cavernous tissue of the lateral VNO, similar to mechanisms observed in penile erectile tissue (Hamacher et al., 2024; Meredith et al., 1980; Meredith & O'Connell, 1979)

3.4. Vomeronasal transduction cascade

3.4.1. Vomeronasal Receptors (VRs)

In rodents, VSNs express three main types of G-protein-coupled receptors (GPCRs): vomeronasal receptors 1 and 2 (V1Rs and V2Rs), and formyl peptide-like receptors (FPRs), totaling around 300 protein receptors (Dulac & Axel, 1995; Herrada & Dulac, 1997; Ibarra-Soria et al., 2014; Liberles et al., 2009; Matsunami & Buck, 1997; Rivière et al., 2009; Ryba & Tirindelli, 1997).

V1Rs and V2Rs have seven transmembrane domains but differ in their extracellular domains and the number of exons in the encoding sequence. V1Rs have a short extracellular N-terminal encoded by genes with a single exon, while V2Rs have a long extracellular domain typically encoded by genes with six exons (Silva & Antunes, 2017). All VR genes are located on the long arm of chromosome 6 within restricted clusters (Figure 1.3A).

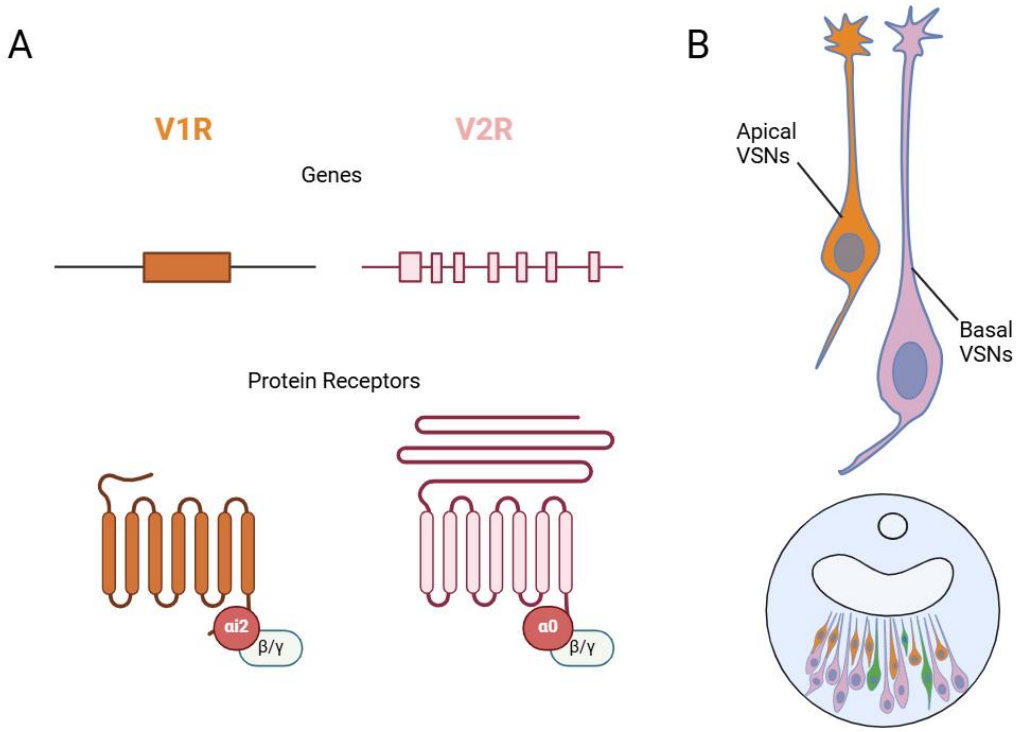


Figure 1.3: Apical and basal neurons express different VRs. **A.** Differences occur at the level of gene structure and translation of the protein receptors for V1R and V2R. Each receptor type is co-expressed with a different G-protein: V1Rs co-express with G-protein G alpha-i2 and V2Rs co-express with G-protein G alpha-o. **B.** Expression of V1Rs or V2Rs correlates respectively with apical or basal localization of VSNs within the sensory epithelium of the VNO. VSNs expressing FPRs are shown in green, V1R-positive neurons in orange, V2R-positive neurons in pink.

FPRs exhibit a broad expression pattern in various tissues and were initially identified in lymphocytes and macrophages where they regulate chemotactic responses (Migeotte et al., 2006). Their gene structure is highly heterogeneous, composed of several exons (Le et al., 2002). The main characteristic lies at the protein structure level, with a widely open extracellular region fostering a promiscuous binding capability compared to V1Rs and V2Rs (Zhuang et al., 2020). FPRs bind molecules with diverse physical properties, such as bacteria-derived formyl peptides (e.g., formyl-Met-Leu-Phe and formyl-MGIIAGIIKFIKGLIEKFTGK), eicosanoids (e.g., LipoxinA4), and other small molecules like Quinazolinones and Benzimidazoles (He & Ye, 2017). Phylogenetically, FPRs are divided into three clades, with one of them, termed FPRL1 in mice, representing an exclusive branch expressed in the VNO (Liberles et al., 2009).

The expression patterns of VRs and FPRs, along with their related transduction cascades, highlight segregated subpopulations of VSNs with distinct localizations (Dulac & Axel, 1995; Spehr, 2010). For instance, the apical layer of VSNs expresses the trimeric G-protein G alpha-i2 along with members of the V1R subtypes primarily involved in detecting volatile social molecules (Figure 1.3B). Experimental evidence supporting this notion includes studies on mice with a deletion of a 600-kilobase genomic region containing two of the twelve V1R families. These mice could not respond to 2-heptanone in field potential recordings (Del Punta et al., 2002; Ihara et al., 2013; Isogai et al., 2011; Novotny et al., 1999). Regarding the pattern of expression of V1R, in-situ hybridization experiments on mice genetically tagged for V1rb2 and other V1r-related genes demonstrated monogenic expression, where each apical VSN expresses only one V1R receptor type (Roppolo et al., 2007). These receptors in mice seem to derive from a few copies present in the ancestor of rodents, leading to the evolution of species-specific repertoires (Miller et al., 2020; Park et al., 2011; Rodriguez et al., 2002).

The VSNs of the basal region of VNO express V2Rs that are coupled with G alpha-o protein. V2Rs are involved in non-volatile molecule detection (Figure 1.3B). This association was initially inferred from an analysis of the extracellular large N-terminal domain of the V2R sequence, which exhibits striking similarities with other chemoreceptors, such as the sweet/umami-sensing T1R taste receptors and the glutamate metabotropic receptor (Mombaerts, 2004; Spehr, 2010). Experimental evidence supporting the detection of non-volatile

molecules by V2Rs includes the detection of MUP in calcium imaging experiments only in VSNs positive for G alpha-o expression (Chamero et al., 2007) or the stimulation with the lacrimal peptide ESP1(Cavaliere et al., 2014), which activates V2Rp5, eliciting a specific sexual behavior in females(Haga et al., 2010). Moreover, a member of the V2R family, V2r1b, is likely responsible for detecting MHC peptides (Kimoto et al., 2005; Yoshinaga et al., 2013).

V2R receptors are classified into five families from A to E, where family A includes 95% of the V2Rs present in mice, and exhibits orthology only among closely related species (Silva & Antunes, 2017). Unlike apical neurons, basal neurons demonstrate a partial rule of multigenic expression of V2R. Families A, B, and D exhibit mutually exclusive expression, with minimal co-expression (less than 2%) observed through in-situ hybridization assays (Silvotti et al., 2007). On the other hand, immunohistochemistry using an antibody to recognize family C, combined with in-situ hybridization for family A, revealed that over 90% of neurons positive for Vmn2r2 (a member of family C) co-express with members of family A (Ishii & Mombaerts, 2011; Silvotti et al., 2007). Similar approaches showed that basal neurons are divided into at least two subpopulations. One subpopulation expresses members of families A, B, D, and E with family C1, while a second cluster of neurons expresses subfamilies of A (A1-A6) with family C2 members.

Regarding the FPRs expression in VSNs, experiments using in-situ hybridization against Fpr-rs3, Fpr-rs4, Fpr-rs6, and Fpr-rs7, showed that they are localized in the apical G alpha-i2 expressing layer of the neuroepithelium. Moreover, specific probes for FPRs did not show co-hybridization, indicating monogenic transcription of these receptors similar to what was observed for V1R receptor genes (Rivière et al., 2009).

3.4.2. Phospholipase C (PLC) pathway

Transduction in the VSNs begins with the binding of pheromones to the vomeronasal receptor, inducing the activation of two heterotrimeric G-proteins (Figure 1.4)(Berghard & Buck, 1996; Menco et al., 2001). These G alpha subunits (G alpha-i2 and G alpha-o) interact distinctly with beta-gamma G-subunits (Clapham & Neer, 1997), all VSNs express the beta 2-subunit and two distinct gamma-subunits, gamma-2, and gamma-8, which have restricted apical and basal neurons expression, respectively (Figure 1.4). Antibodies

targeting these subunits decrease inositol 1,4,5-triphosphate (IP3) production upon urine stimulation, suggesting their involvement in the activation of PLC (Rünnenburger et al., 2002). Additional evidence supporting the activation of PLC during the VSNs transduction process comes from studies using multielectrode arrays that demonstrated the inhibition of spiking activity responses to urine by the specific inhibitor U73122 (Holy et al., 2000).

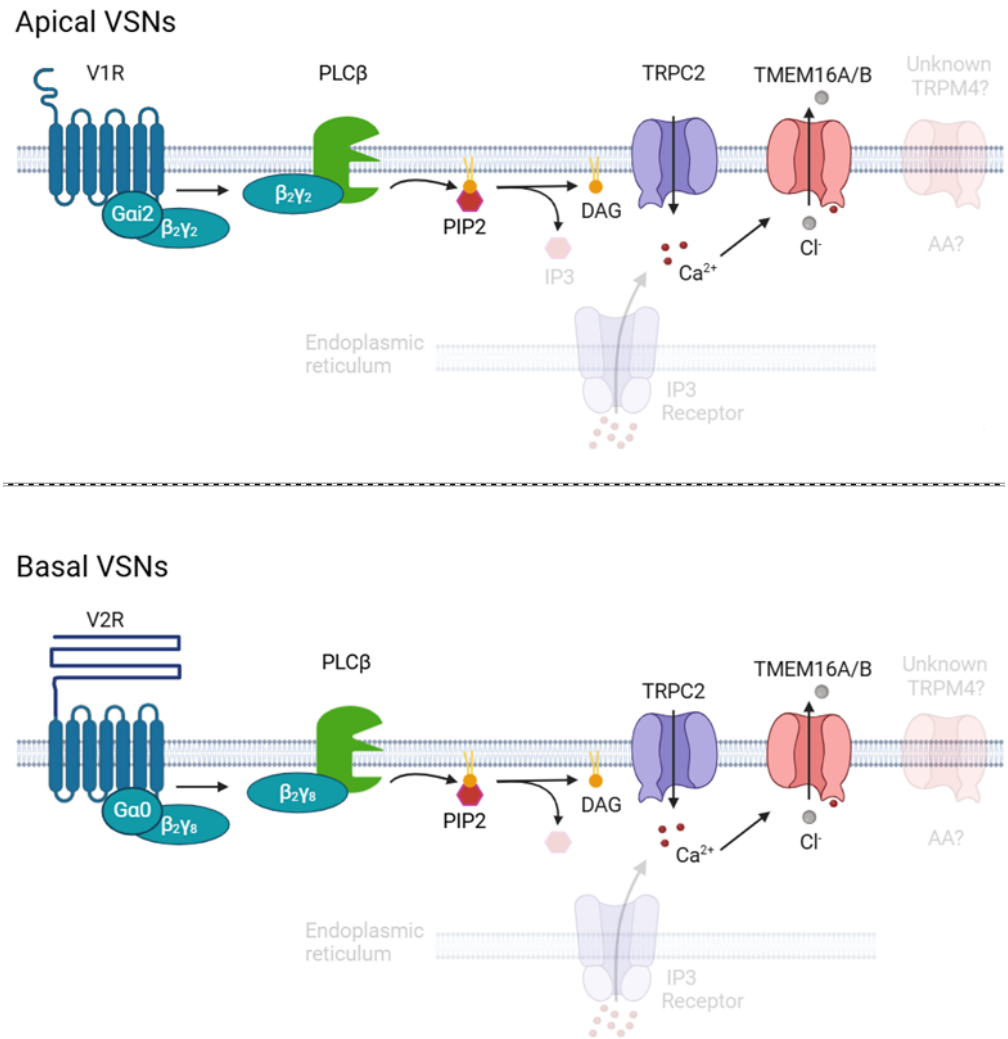


Figure 1.4: When pheromone molecules bind to VRs located in the microvilli, they trigger a signaling cascade. In the apical neurons, this involves the V1R receptor and the Gαi2β2γ2 protein complex, while in the basal neurons, it involves the V2R receptor and the Gαoβ2γ8 protein complex. The βγ subunits activate PLC, increasing the levels of IP3 and/or DAG. This process leads to the opening of the TRPC2 channel, allowing Na^+ and Ca^{2+} ions to enter the neuron, resulting in membrane depolarization. Additionally, anion-selective channels, TMEM16A and TMEM16B, activated by Ca^{2+}, amplify the depolarization process playing an important role in this signaling pathway. The TRPC2 channel is thought to be the main transduction channel in VSNs. Adapted from (Tirindelli et al., 2009).

Activation of the PLC induces the production of diacylglycerol (DAG) and IP3 from Phosphatidylinositol bisphosphate (PIP2), DAG's role in the transduction cascade is well-documented through the activation of a highly expressed channel (Figure 1.4) called Transient Receptor Potential Cation Channel, Subfamily C, Member 2 (TRPC2) (Liman et al., 1999; Lucas et al., 2003; Menco et al., 2001).

TRPC2 channel is present in the VSN microvilli as the Immunofluorescence experiments of Liman et al. 1999 demonstrated, as well that Knockout mice for TRPC2 showed a significant decrease in the number of developed VSNs and an inability to discriminate gender, phenocopying knockout mice for G alpha subunits (G alpha-i2 and G alpha-o) expressed in VSNs (Chamero et al., 2011; Norlin et al., 2003; Stowers et al., 2002). However, functional experiments on TRPC2 knockouts revealed a complex landscape in VSN physiology. At the level of electrical responses, experiments using microelectrode arrays reported a complete abolition of the responses to urine stimulation in VSNs of TRPC2 knockout mice (Stowers et al., 2002), whereas recordings of the VNO field potential described a reduction in the response to urine stimulation with a persistent component (Leypold et al., 2002). This last observation is consistent with the normal Bruce effect found in mice lacking TRPC2, which still respond to MHC class I peptides (Kelliher et al., 2006). Thus, an ion channel different from TRPC2 may be involved in the transduction of some stimuli.

In contrast, the effects of the IP3 messenger are controversials. Incubation of rat VSNs with thapsigargin and Xestospongin C during calcium imaging experiments indicated that IP3 might have a negligible contribution, as there was an increase in calcium under urine stimulation (Spehr, 2010), However, electrophysiological whole-cell experiments involving the dialysis of IP3 in mouse VSNs activated a conductance with several seconds of delay, suggesting the presence of another conductance regulated by this second messenger, the identity of which remains unknown (Lucas et al., 2003).

Additional reports suggest possible contributions from other molecules produced by the metabolism of DAG, such as arachidonic acid (AA). Electrophysiological experiments have proposed the opening of a separate Ca^{2+}-permeable channel dependent on AA (Yang & Delay, 2010).

Recently, an additional channel, TRPM4, has been identified as a sex-specific potential modulator of the primary transduction current. TRPM4 is expressed in VSNs of female mice and its expression is cyclically controlled by ovarian sex hormones. Although it is activated by calcium and has an ion permeability similar to that of TRPC2, TRPM4 is not expressed in microvilli of VSNs and therefore is not likely to contribute to the primary transduction current (Eckstein et al., 2020). Additional functional experiments are necessary to fully understand the role of TRPM4 in VSN transduction.

Some studies have highlighted the expression of Ca^{2+}-activated Cl− channels in VSNs. These channels may be activated by both Ca^{2+} influx through TRPC2 channels and/or Ca^{2+} release mediated by IP3 (Kim et al., 2011; Yang & Delay, 2010). RT-PCR experiments have identified members of the TMEM16/anoctamin family, particularly TMEM16A and TMEM16B, as being expressed in the VNO. These channels were shown to co-localize with TRPC2 at the apical surface of the vomeronasal epithelium (Dibattista et al., 2012). suggesting their involvement in vomeronasal transduction. At the resting potential of VSNs, these channels are expected to mediate chloride efflux, inducing depolarization due to the high internal concentration of chloride (Kim et al., 2015; Untiet et al., 2016). Later studies on knockout mice for TMEM16A and TMEM16B have confirmed that their activation is crucial for amplifying the cation current and setting the membrane potential, which controls neuronal activity (Amjad et al., 2015; Hernandez-Clavijo et al., 2021)

Additional ion channels have been identified in VSNs, potentially playing crucial roles in signal transduction or regulation of firing activity through mechanisms that are still not fully understood. These include the Ca^{2+}-activated potassium channel SK3, the G-protein activated inwardly rectifying potassium channel GIRK1 (Kim et al., 2012), the large-conductance Ca^{2+}-activated potassium channel (BK) (Zhang et al., 2008), and HCN channels, which are associated with the regulation of spiking activity in dependence on the urine pH (Cichy et al., 2015; Dibattista et al., 2008).

3.5. Action potential machinery

VSNs have evolved to ensure maximum sensitivity to stimuli present in very low concentrations (tens or hundreds of nanomolars). In this context, when barely detectable pheromones bind to VRs in the microvilli, the transduction

cascade should be capable of ultimately inducing changes in somatic membrane conductances, triggering the generation of action potentials (APs) that are sent to the AOB.

3.5.1. Passive electrical properties and firing of VSNs

VSNs have high input resistance as recordings from dissociated apical or basal VSNs reported an average input resistance of around 3 GΩ (Fieni et al., 2003; Liman & Corey, 1996). Similar values were obtained from recordings of acute slices (Shimazaki et al., 2006; Ukhanov et al., 2007). However, it is noteworthy that these values significantly underestimate the resistance of the membrane, as the seal resistance in whole-cell voltage clamp experiments typically falls within the previously reported range (1-10 GΩ).

The membrane capacitance in mice VSNs varies from 5 to 20 pF, as expected from their small size (Dibattista et al., 2008; Liman & Corey, 1996; Ukhanov et al., 2007).

The resting membrane potential measured in the VSNs is between -63 to -70 mV in slices(Dibattista et al., 2008; Ukhanov et al., 2007), however, this data is different from dissociated cells used in early reports where the value is between -58 to -63 mV (Fieni et al., 2003; Liman & Corey, 1996).

VSNs express a vast repertoire of ion conductances, generating a unique firing pattern. When stimulated with small current step amplitudes (Figure 1.5, less than 2 pA), most VSNs show tonic firing for several seconds without adaptation. Similar results were obtained under short stimulation with urine (2-3 seconds) (Dibattista et al., 2008; Lucas et al., 2003; Ukhanov et al., 2007). However, paired pulses of stimulation with concentrated urine (1:50) and injections between 3 to 5 pA induce adaptation in VSNs (Sarno et al., 2022; Spehr, 2010). This short-term spike frequency adaptation to repeated stimuli was shown to involve slow inactivation of sodium channels (Sarno et al., 2022).

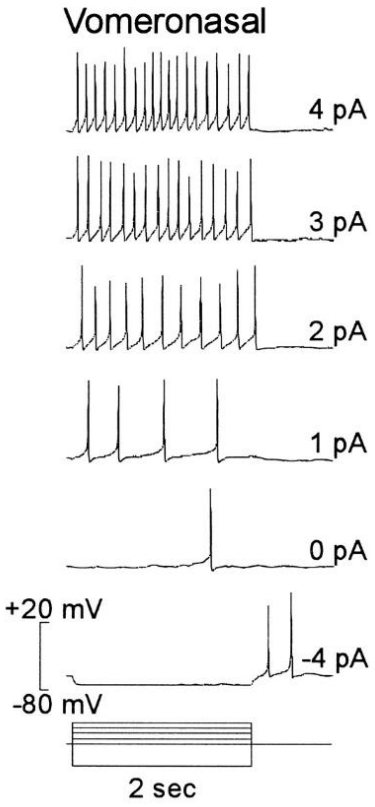


Figure 1.5: Firing properties of a mouse VSN in response to injection of current between -4 to 4 pA. Currents steps with an amplitude of 1 or 2 pA induce a tonic firing of VSNs. Adapted from (Liman & Corey, 1996).

The spiking frequency of VSNs exhibits an increase in response to small current injections reaching a maximal value varying between 8 to 20 Hz at about 10-20 pA (Liman & Corey, 1996; Shimazaki et al., 2006; Ukhanov et al., 2007). This wide range of saturation has been correlated with differences in the VSN subsets. Evidence for this comes from experiments performed using two lines of transgenic mice in which VSNs express GFP under the control of a specific V1R (V1rb2) or V2R (V2r1b) (DelPunta et al., 2002; Rodriguez et al., 1999). Apical VSNs expressing the V1rb2 receptor, showed frequency saturation at frequencies below 10 Hz, whereas basal VSNs expressing the V2r1b receptor, showed a higher frequency of saturation, around 20 Hz (Ukhanov et al., 2007).

The diverse firing patterns observed in VSNs underscore the intricate interplay of ion conductances expressed within the neuron subsets, indicating differences in the voltage-gated ion channels of apical and basal neurons (Fieni et al., 2003; Ukhanov et al., 2007).

3.5.2. Sodium channels

Voltage-gated sodium channels (Na_v) are transmembrane proteins composed of several subunits. The main alpha subunit alone is sufficient to form a functional channel, while the interaction with beta subunits modifies its biophysical properties (Figure 1.6). The alpha subunit contains four internal homologous domains (I-IV), each comprising six transmembrane segments. These domains fold to form a central pore, with the internal part of this structure being crucial for sodium selectivity (Marban et al., 1998). Advances in protein structure, along with physiological evidence from site-directed mutagenesis, demonstrate the importance of the S5-S6 linker segment (P segment) in determining permeability (Figure 1.6B) (Heinemann et al., 1992).

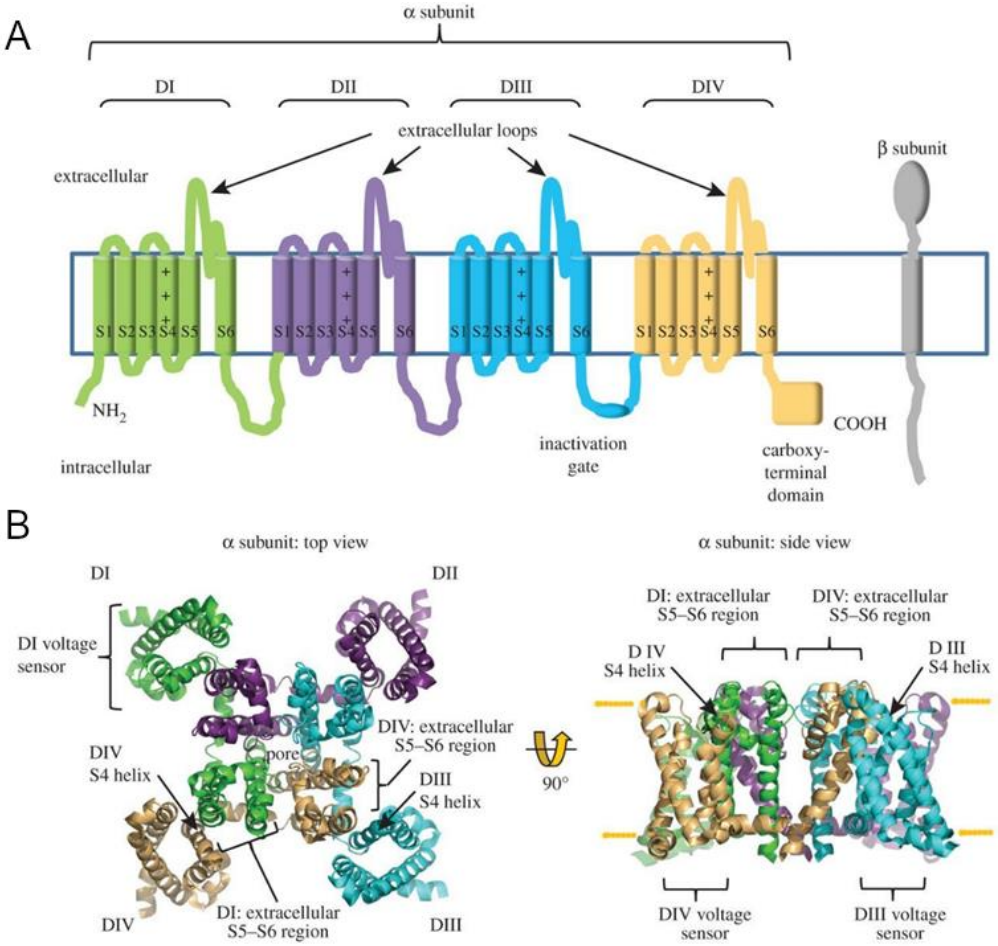
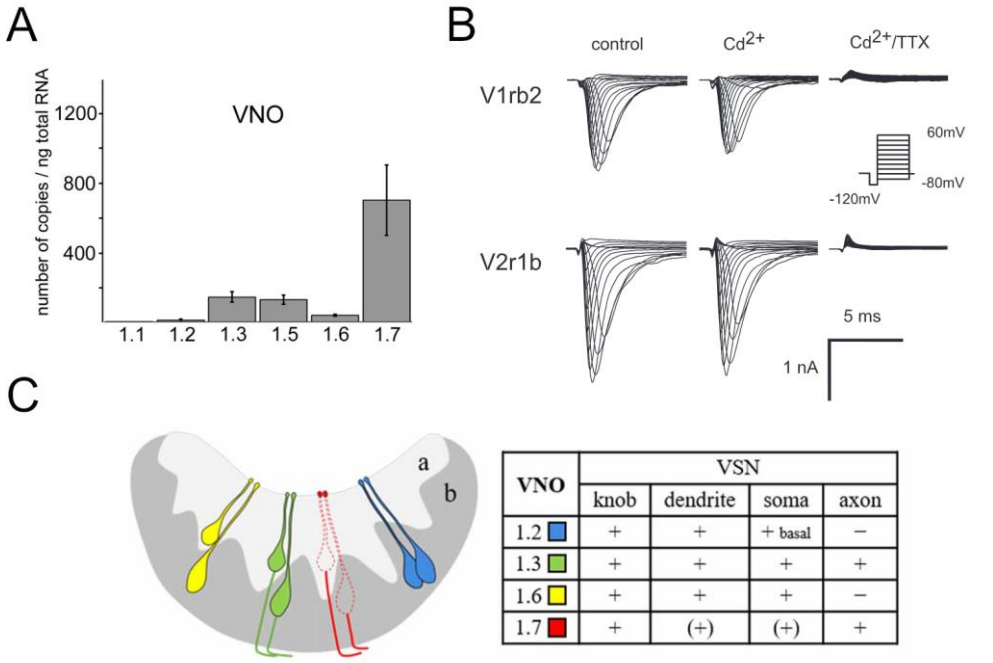


Figure 1.6: Structure of the voltage-gated Nav channel. **A.** Representation of the alpha and beta subunits. alpha subunit has four domains I–IV, where each domain contains the amphipathic helix S4 as a voltage sensor, the extracellular region between helices S5 and S6, the fast inactivation gate, and the carboxy-terminus. **B.** Top view from the extracellular face and side view of the Nav channel from the bacterium Arcobacter butzeri (PDB ID code 3RVY). color-coded match with figure 1.6A. (Namadurai et al., 2015).

In mice, nine genes coding for the voltage-gated sodium channel alpha subunit share more than 50% similarity in their transmembrane and extracellular domains (Yu & Catterall, 2003). These genes cluster into four groups, each mapping to specific chromosome segments. The sodium channels $Na_v1.1$, $Na_v1.2$, $Na_v1.3$, and $Na_v1.7$ are located on chromosome 2 in humans and mice, exhibiting similar characteristics such as sequence, biophysics, and sensitivity to the neurotoxin tetrodotoxin (TTX). Another cluster on human chromosome 3, housing $Na_v1.5$, $Na_v1.8$, and $Na_v1.9$, shares 75% sequence identity with the first group but shows variations that confer varying degrees of TTX resistance. Phylogenetic analysis suggests a more distant evolutionary relationship for $Na_v1.4$ and $Na_v1.6$, located on different chromosomes from the first group. $Na_v1.4$ is expressed in skeletal muscle, while $Na_v1.6$ is abundant in the central nervous system (Goldin et al., 2000; Yu & Catterall, 2003).



VNO	VSN			
	knob	dendrite	soma	axon
1.2	+	+	+ basal	–
1.3	+	+	+	+
1.6	+	+	+	–
1.7	+	(+)	(+)	+

Figure 1.7: Voltage-gated sodium channels expressed in VSNs and sensitivity to TTX. **A.** Sodium channel transcripts levels analyzed through RT-PCR analysis in the whole VNO. **B.** Voltage-gated sodium currents isolated from apical (top) and basal VSNs (bottom). **C.** Proposed localized expression of different sodium channel subtypes. Adapted from (Ukhanov et al., 2007) and (Bolz et al., 2017)

The alpha subunits of sodium channels expressed in the VNO have been characterized using molecular and electrophysiological approaches. Transcriptomic data and RT-PCR assays (Figure 1.7) indicate a high expression of $Na_v1.7$, followed by an intermediate expression of $Na_v1.5$, $Na_v1.3$, $Na_v1.6$,

and $Na_V1.2$ (Bolz et al., 2017; Ibarra-Soria et al., 2014). However, as these data were obtained from the whole organ, some analyzed transcripts may come from different cell types, including SCs (Ghiaroni et al., 2003). A study using immunofluorescence assays with antibodies against several sub-types of Na_V showed that $Na_V1.2$ and $Na_V1.6$ are localized in the soma of VSNs, while $Na_V1.7$ is highly expressed in the axon bundles (Bolz et al., 2017).

Voltage-gated sodium currents recorded from dissociated VSNs or VSNs in acute slices exhibit similar characteristics. The current amplitude when the holding of the neurons is at -70 mV, is around 1 nA. Upon depolarization to -20 mV, approximately 80-95% of the inward current is sensitive to TTX, with the non-TTX-sensitive component completely abolished by adding blockers of voltage-gated calcium currents (Liman & Corey, 1996; Shimazaki et al., 2006).

Later experiments were conducted on dissociated VSNs to distinguish apical and basal neurons in the base of length of the dendrite obtaining significant differences in the sodium current density where the apical ones have a lower value than the basal ones (Fieni et al., 2003). These findings were later confirmed by in-depth studies isolating sodium currents from a subpopulation of neurons in transgenic mice (Ukhanov et al., 2007). These mice expressed GFP protein under the control of a specific vomeronasal receptor V1rb2 to label apical VSNs and V2r1b to identify basal VSNs, They established some common characteristics in the biophysical parameters of the sodium currents, such as the Vhalf for the activation curve (approximately -45 mV) (Figure 1.7B). Despite this, their comparison of the maximal sodium currents showed that apical neurons had lower amplitudes than basal ones as well as a more negative Vhalf for the inactivation curve (Ukhanov et al., 2007).

3.5.3. Calcium channels

Voltage-gated calcium channels (Ca_V) are large heteromeric proteins composed of several subunits. The initial identification of this complex took place in the T-tubules of skeletal muscle, where researchers identified five components, called alpha-1, alpha-2, beta, gamma, and delta subunits (Figura 1.8) (Dolphin, 2018; Neely & Hidalgo, 2014). Like Na_V channels, Ca_V alpha-1 subunits consist of four homologous domains, each comprising six transmembrane segments. These subunits can assemble into channels mediating the current flow.

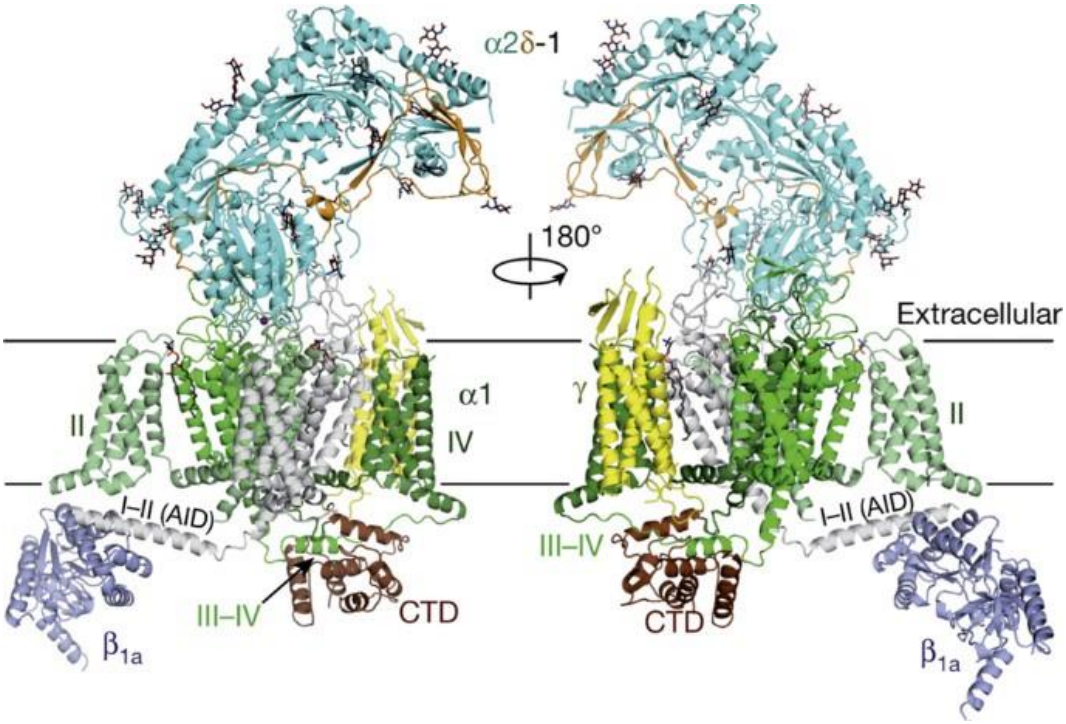


Figure 1.8: Subunit structure of $Ca_V1.1$ channel with 3.6 Å of resolution. The subunit composition and structure of calcium channels follow a color code where the alpha subunit is colored dark green, alpha-2 in pale blue, Beta in dark blue, Gamma in yellow, and delta in brown. The structure shows the interaction between the III-IV linker, S6 segment, and helices in the carboxy-terminal domain (CTD). Taken From (Wu et al., 2016).

Based on pharmacological, molecular, and biophysical properties, alpha-1 subunits are classified into three families: Ca_V1, Ca_V2, and Ca_V3. Family Ca_V1 and Ca_V3 consist of four and three members, respectively, and exhibit high sensitivity to dihydropyridine blockers. The main differences lie in their biophysical properties. Ca_V1, also known as L-Type channels because of large and long-lasting Ca^{2+} fluxes, are characterized by large single-channel conductance and very slow inactivation kinetics, as well as activation at high voltages. On the other hand, family Ca_V3, or T-Type channels (transient), are low-voltage activated with a very small single conductance and faster kinetics compared to other families (Catterall et al., 2005).

The Ca_V2 family comprises three members that are not sensitive to dihydropyridines. This family displays significant heterogeneity, with each channel isolated in different models exhibiting slight variations in biophysics and sensitivity to different blockers. $Ca_V2.1$, or P/Q-Type channel, called like this because of the initial discovery in Purkinje neurons, is sensitive to ω-

agatoxin IVA, this channel is found in many neurons involved in neurotransmitter release. $Ca_V2.2$, or N-Type channel (N because is involved in neurotransmitter release), is inhibited by ω-conotoxin, while $Ca_V2.3$, or R-Type channel characterized because is particular resistance to different general calcium channel blockers, this is blocked by a tarantula toxin called SNX-482 (Neely & Hidalgo, 2014; Newcomb et al., 1998).

In VSNs, isolation of voltage-dependent calcium currents using Ba^{2+} as a carrier ion to increase the amplitude of the current, showed that depolarized steps activate inward currents almost completely inhibited by 100 μM cadmium (Fieni et al., 2003; Liman & Corey, 1996; Ukhanov et al., 2007). Depolarization steps reveal that calcium currents comprise two components: a transient and a sustained component (Figure1.9 A-B). Depolarization between -60 mV to -20 mV activates an inward current with fast inactivation and only when the depolarization reaches -10 mV does a sustained current develop reaching a peak at +20 mV. Kinetics and pharmacology of the two components indicate the presence of L-Type and T-Type currents in VSNs (Fieni et al., 2003; Liman & Corey, 1996; Sarno et al., 2022).

These currents are only slightly different between basal and apical neurons (Fieni et al., 2003; Ukhanov et al., 2007). Specific inhibitors showed an important role of the L-type current in the maintenance of tonic firing during depolarized current injection and the interplay function with BK channels. Furthermore, basal and apical VSNs produce TTX-insensitive action potentials indicating the involvement of Ca_v channels in the spiking activity (Figure1.9 C) (Ukhanov et al., 2007).

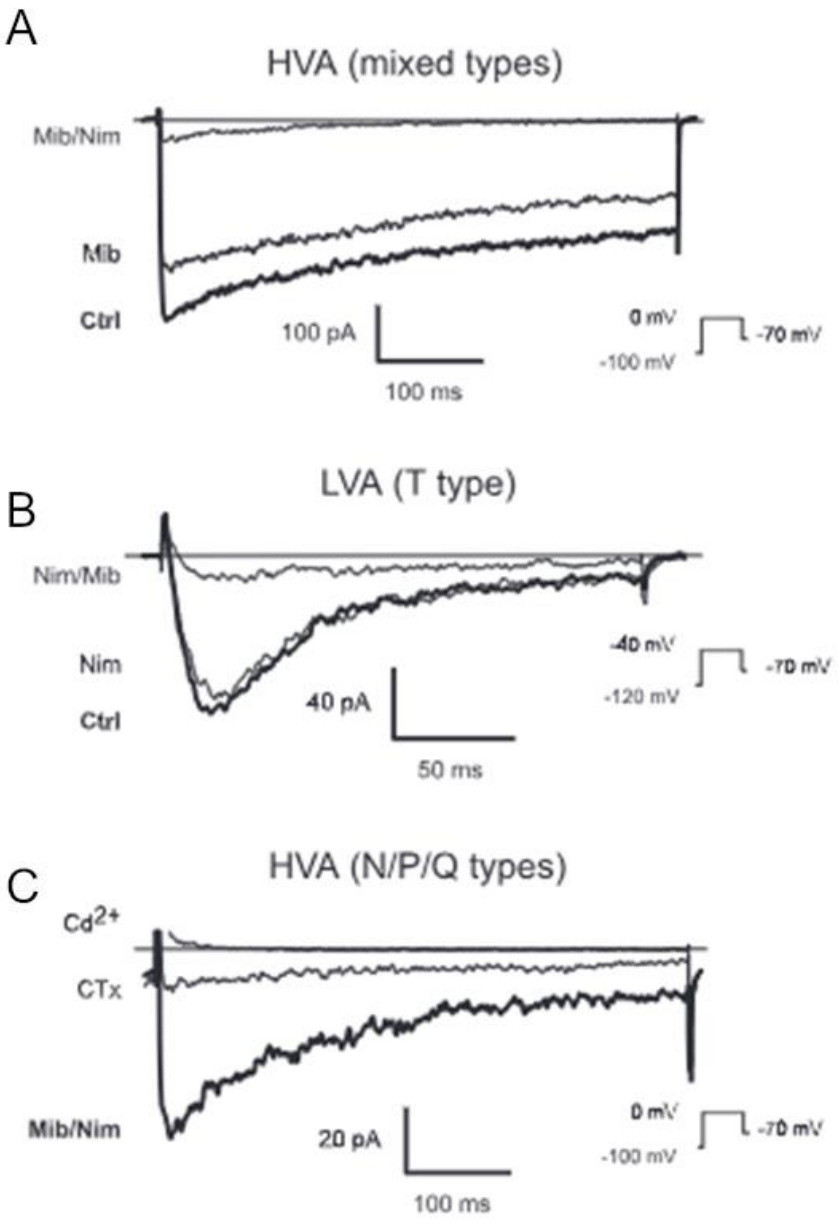


Figure 1.9: Calcium currents isolated on VSNs. **A.** voltage step from -100 mV to 0 mV for 500 ms shows the activation of a slowly inactivating inward current (Ctrl, thick and bottom trace); 10 µM mibefradil (Mib) induce a partial inhibition, treatment with nimodipine (5 µM, Mib/Nim) block the current leaving a small amount. **B.** A voltage from -120 mV to -40 mV activated a low-voltage-activated (LVA) T-type Ca_v current, where the addition of mibefradil significantly produces the inhibition of this current. **C.** The resistance current to the previous treatments (Mib/Nim, thick line) was blocked by ω-conotoxin MVIIC (1 µM, CTx). The different Ca_V conductance was completely suppressed by treatment with Cd^{2+}. From (Ukhanov et al., 2007)

3.5.4. Potassium channels

Voltage-gated potassium channels (K_v) are homotetramers of alpha subunits, each composed of six transmembrane segments. The four identical alpha subunits are arranged around a central axis that forms a pore (Ranjan et al., 2019). K^+ ions are stabilized within the pore of the K^+ channel by specific binding sites, composed of oxygen dipoles forming a "bracelet." This region is a cylindrical pore with an inner diameter of 3–3.4 Å(Bezanilla & Armstrong, 1972). Identification of a signature amino acid sequence, highly conserved among K^+-selective channels, led to the hypothesis for the identity of the K^+ channel selectivity filter. Functional studies confirmed that mutation of this signature sequence disrupts K^+ selectivity (Heginbotham et al., 1992). The crystal structure of the KcsA potassium channel (bacterial channel) validated these predictions, revealing a narrow pore with dimensions of ∼3 Å, where specific potassium binding sites are formed of carbonyl oxygen atoms from residues in the signature sequence TVGYG (Kim, & Nimigean, 2016).

K_v channels are classified into 12 subfamilies. Transcriptomic analysis of the entire VNO reveals the expression of seven of these subfamilies (Ibarra-Soria et al., 2014). However, these findings encompass diverse cell types in the VNO, including smooth muscle and SCs, which have been shown to express K_v channels (Amberg et al., 2003; Ghiaroni et al., 2003). Further molecular and immunohistochemical investigations are necessary to pinpoint the specific K_v subtypes present in VSNs.

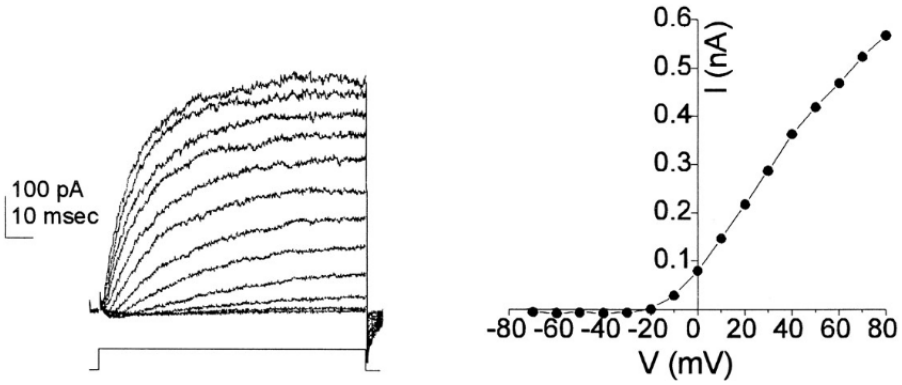


Figure 1.10: K^+ currents in mouse VSN. Family (left) and current-voltage curve (right) of K^+ currents in response to step depolarizations between −30 and +80 mV from a prepulse potential of −120 mV. K^+ currents were isolated by addition of 10 µM TTX and 100 µM $CdCl_2$. From (Liman & Corey., 1996)

Functional analysis via electrophysiology reveals that the predominant potassium conductance observed in VSNs is a slowly inactivating delayed-rectifying current (Figure1.10). Tetraethylammonium (TEA) at 10 mM blocks 85% of this current while an internal solution based on cesium completely abolishes it. Prolonged depolarization (10-50 seconds) results in inactivation with two exponential time constants of 2.4 and 49 seconds (Fieni et al., 2003; Liman & Corey, 1996). This slow-inactivated current becomes active around -40 mV, with a half-activation voltage of -10 mV and a slope of 16 mV, indicating high channel availability within the range where sodium channels are active. This characteristic enables VSNs to sustain repetitive firing without adaptation (Ukhanov et al., 2007).

3.6. Main Olfactory Epithelium (MOE)

The primary olfactory system comprises the MOE in the nasal cavity and the main olfactory bulb (MOB), from which the lateral olfactory tract projects to the olfactory cortex, the olfactory tubercle, the piriform and entorhinal cortex, as well as several structures in the limbic system, involved in the emotional aspects of the odorant detection (Haberly, 2001). The MOE is a pseudostratified epithelium located in the back-upper part of the nasal cavity, containing olfactory OSNs, SCc, BCs, and various glands (Figure 1.11). OSNs are specialized bipolar neurons with a sensory dendrite ending in a tuft of cilia in direct contact with the nasal cavity. These neurons detect odorants using specific receptors, the odorant receptors (ORs), on their ciliary membrane (Menini et al., 2004; Purves et al., 2001). The OSNs then send signals through their axons to the MOB, where OSNs expressing the same odorant receptor type project into specific and independent spherical structures called glomeruli (Maresh et al., 2008). The glomeruli are the functional unit of the olfactory bulb. There, OSNs connect with mitral and tufted cells that send signals to higher brain areas. This precise connection between ORs and glomeruli forms a map in the MOB, allowing the brain to accurately recognize different odorants (Zhou et al., 2019).

SCs have a columnar-cylindrical morphology and are characterized by their apical microvilli. These cells produce mucus through granules located in the cytoplasm near the microvilli, a crucial process for maintaining a hydrated mucus layer on the surface of the epithelium (Okano & Takagi, 1974). In addition, SCs are involved in the phagocytosis of the dead OSNs (Suzuki et al.,

1996), the metabolism of toxic chemicals (Hegg et al., 2009), and the regulation of extracellular ionic gradients necessary to maintain the activity of ionic conductances mediating sensory transduction (Vogalis et al., 2005a). Interestingly, SCs express various ion channel types, such as voltage-gated sodium and potassium channels (Henriques et al., 2019; Vogalis et al., 2005b). Moreover, purinergic stimulation with ATP induces an intracellular calcium increase, which then activates TMEM16A and BK channels (Czesnik et al., 2006; Henriques et al., 2019).

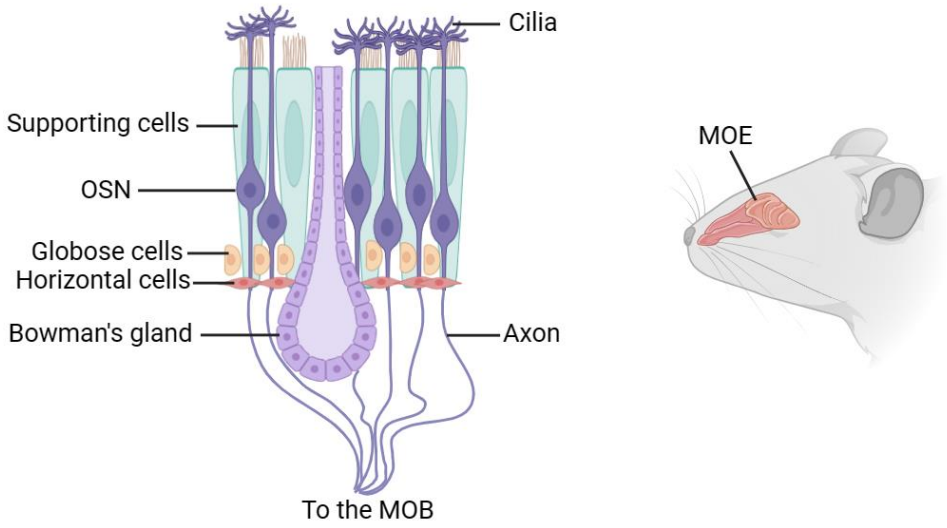


Figure 1.11: Location and histological composition of the MOE in mice. OSNs in blue

BCs are necessary for replacing OSNs and SCs. Indeed, these stem cells ensure the regeneration of OSNs and SCs during normal turnover and when the MOE is exposed to environmental and mechanical stress. BCs comprise two subpopulations: globose and horizontal BCs, both of which contribute olfactory cells' regeneration (Carter et al., 2004; Hassenklöver et al., 2009).

3.7. Olfactory sensory neurons and transduction cascade

3.7.1. Odorant receptors

An important milestone in understanding how OSNs code odorants was reached by Lynda Buck and Richard Axel in 1991, when they revealed a multigene family that encode ORs. This significant finding aligns with the

sensory needs of the MOE, which must detect a wide range of chemical structures, requiring a diverse repertoire of ORs (Lewcock & Reed, 2004).

In mice, there are 1296 OR genes (including about 20% pseudogenes), grouped into 228 families and distributed throughout the genome except for the 12 and Y chromosomes (Zhang & Firestein, 2002). These genes encode GPCRs categorized into two subtypes: class I receptors, known as 'fish-like', mainly expressed in the dorsal region of the MOE, and class II receptors, located in the dorsal and ventral parts of the epithelium. This distinct spatial organization is also reflected in the axon projections within the MOB. However, it is not clear whether there are functional differences between these OR classes (Spehr & Munger, 2009).

Analysis of receptor variability showed that transmembrane domains 4 and 5 exhibit the highest variability, with the extracellular regions being the primary loci of this variability. This is expected as odorants are detected extracellularly through hydrophobic and van der Waals interactions with amino acid residues of the OR (Katada et al., 2005).

In addition to classical ORs, non-classical odorant receptors such as trace-amine-associated receptors (TAARs) and receptor guanylyl cyclase D (GC-D) have been identified in the mouse MOE. TAARs, belonging to family A GPCRs, are phylogenetically linked to serotonin and dopamine receptors. There are 15 different TAAR genes, 14 of which are expressed in the MOE (Liberles & Buck, 2006). TAARs specifically respond to volatile amines, including odorants that serve as social cues and predator-derived signals. For example, compounds like 2-phenylethylamine, found in carnivore urine, may act as warning signals for mice (Liberles, 2015). Removal of even a single olfactory TAAR gene may have an important impact in the response to aversive odorants (Dewan et al., 2013).

GC-D receptors have a variable extracellular segment for binding molecules, a single transmembrane domain, unlike classical GPCR receptors, and a distinctive intracellular C-terminal with GMP-cyclase catalytic activity. Further evidence supporting the role of these receptors as chemosensors include the expression of other key components of the transduction cascade, such as the cGMP-gated channel subunit 3 (CNGA3) and phosphodiesterase 2 (PDE2),

which are localized within the cilia (Duda et al., 2004; Leinders-Zufall et al., 2007).

3.7.2. Adenylyl cyclase pathway

The transduction process converts chemical energy from odorant binding to ORs into electrical signals (Katada et al., 2005). Each OR can recognize multiple odorants, while a single odorant can be recognized by several receptors(Araneda et al., 2000; Firestein, 2001). Upon odorant binding to an OR, conformational changes activate a G-protein (Figure1.12). Initial biochemical assays identified this specific G-protein and its role in cAMP synthesis in the cilia, revealing the restricted expression of a tissue-specific trimeric G-protein called Golf (Jones & Reed, 1989). Activated Golf dissociates into an active G alpha-olf subunit and a G beta-gamma complex. The G alpha-olf subunit then stimulates ACIII to convert ATP to cAMP (Jones & Reed, 1989; Takeuchi & Kurahashi, 2003; Wong et al., 2000).

Increased cAMP activates CNG channels (Kurahashi & Yau, 1993; Liman & Buck, 1994). Each CNG channel is composed of four subunits: two CNGA2, one CNGA4, and one CNGBlb subunit. Each subunit has six transmembrane domains, with the pore located between the S5 and S6 domains, and a cyclic nucleotide-binding site near the C-terminal (Dhallan et al., 1990; Li et al., 2017). There are four binding sites for cAMP, which exhibit an allosteric effect and display cooperativity. The channels are permeable to monovalent ions such as Na+ and K+, as well as Ca^{2+}, with Ca^{2+} influx playing a significant role in olfactory transduction and adaptation (Pifferi et al., 2010).

The unitary conductance of a single CNG channel is approximately 30 pS in the absence of divalent cations. However, this conductance decreases in the presence of Ca^{2+} or Mg^{2+} ions due to open channel block. This blockage reduces the current carried by all cations, leading to a small single-channel conductance of about 1.5 pS (Matthews & Reisert, 2003).

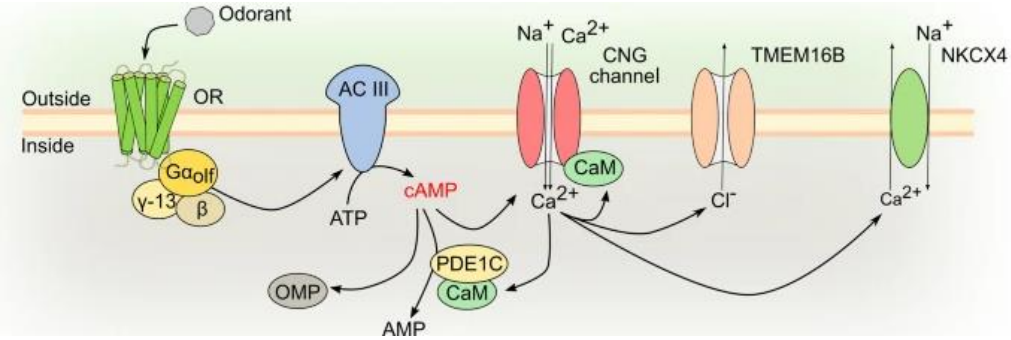


Figure 1.12: The molecular mechanism of olfactory transduction. When an odorant binds to an OR, it activates a trimeric G-protein, which then stimulates ACIII to produce cAMP. This cAMP opens CNG channels, allowing Na^+ and Ca^{2+} to enter. The influx of Ca^{2+} activates the Cl^- channel TMEM16B. Ca^{2+} also binds to CaM, which reduces the sensitivity of the CNG channel to cAMP and activates the phosphodiesterase PDE1C. Finally, Ca^{2+} is expelled by the NKCX4 exchanger (Boccaccio et al., 2021).

The calcium entry through CNG channels plays several roles in the transduction process, inducing the activation of a Ca^{2+}-dependent chloride channel, known as TMEM16B. This channel plays an important role in the physiology of OSNs, contributing to the amplification of the odorant response through Cl- efflux (Figure1.12). This cascade results in a depolarizing receptor potential, initiating olfactory perception (Kleene, 2008; Pifferi et al., 2010).

Initial evidence about the identity of the chloride channel came from immunochemistry assays showing the co-expression of TMEM16B with ciliary markers and proteins involved in the transduction cascade (Rasche et al., 2010). Functional confirmation of the role of Ca^{2+}-activated chloride channels was provided by electrophysiological experiments, showing that chloride ions carry up to 90% of the inward current in mice. This current can be blocked by chloride channel inhibitors such as NFA and DIDS (Boccaccio & Menini, 2007; Dibattista & Menini, 2009; Pifferi et al., 2009, 2012) Experiments on TMEM16B knockout mice confirmed that the chloride component of the transduction current is absent (Boccaccio & Menini, 2007; Dibattista et al., 2024; Pifferi et al., 2006). Surprisingly, OSNs in TMEM16B knockout mice showed reduced transduction currents but a higher frequency of action potentials compared to WT mice (Pietra et al., 2016). Additionally, the action potential train was significantly prolonged in these knockout mice. These observations suggest that the depolarizing Ca^{2+}-activated Cl^- current normally acts as a "clamp", shortening the firing duration by adjusting it according to the strength of the odorant stimulus. This modulation changes the response time course, causing

rapid inactivation of voltage-dependent Na^+ channels (Dibattista et al., 2024; Li et al., 2018).

Inhibitory action is crucial for the adaptation and recovery process, involving the Ca^{2+}-dependent activation of the Ca^{2+}-calmodulin complex (Ca^{2+}-CaM). This complex regulates the activity of the CNG channel, ACIII, and PDE (Boccaccio et al., 2021; Kaupp, 2010). Specifically, Ca^{2+}-CaM increases the activity of PDE, which hydrolyzes cAMP, thereby decreasing its concentration in the knob and reducing the open probability of the CNG channel(Kurahashi & Menini, 1997; Molday, 1996; Yan et al., 1995). Another important mechanism is the Na^+-dependent Ca^{2+} extrusion through the Na^+-Ca^{2+} exchanger, which helps expel calcium and aids in the recovery of the response(Reisert & Matthews, 1998).

3.7.3. Voltage-gated currents and action potentials in OSNs

OSNs in mice have a membrane resistance of about 2 GΩ and membrane capacitance of about 4.5 pF (Boccaccio, 2018; Vogalis et al., 2005b). Due to the high membrane resistance, injection of a few pA induces large changes in the voltage membrane and triggers the action potential activation. The pattern of OSN spiking under current injections of 2-6 pA and 1-5 seconds duration, is characterized by a strong silencing (Kawai, 2024; Kawai et al., 1999; Liman & Corey, 1996): initially, OSNs show a fast train of action potentials with subsequent spikes decreasing in amplitude until reaching a voltage plateau.

OSNs have voltage-gated currents for Na^+, Ca^{2+}, and K^+ in their somatic membrane. The main Na^+ channel is $Na_v1.7$, as experiments of RT-PCR and immunohistochemistry recently reported (Bolz et al., 2017). The activation voltage of the Na^+ current in mice is from -50 to -40 mV and the maximum current is reached at -10 mV to 0 mV (Kawai, 2024). About 80% of the current is blocked by 1 µM TTX (Boccaccio, 2018; Ma et al., 1999; Vogalis et al., 2005b). Voltage-dependent calcium currents in mouse OSNs were studied on cell-attached experiments from patches of the soma and dendritic knob, (Maue & Dionne, 1987) showed that depolarized steps induce the activation of an inward current that increases with elevated concentration of barium with a single channel conductance of 16 pS, suggesting the presence of L-type currents (Kawai, 2024; Maue & Dionne, 1987).

Voltage-dependent potassium currents in mouse OSNs have two components: a transient I_A and a delayed rectifier I_K (Boccaccio, 2018; Lagostena & Menini, 2003; Maue & Dionne, 1987). The I_A current is characterized by rapid activation and inactivation and the repolarization to potentials negative to −50 mV is typically required for restoration of channel availability. I_A is inhibited by 4-aminopyridine (4-AP). The delayed rectifier current has very slow inactivation in the order of seconds and is sensitive to TEA (Hodgkin & Huxley, 1952). In OSNs, the activation of I_A current occurs at -30 mV, and its exponential time constant of inactivation is hundreds of milliseconds. Both components (I_A and I_K) of the outward current have a high sensitivity to TEA, which blocks the outward current with a concentration of 20 mM (Ma et al., 1999; Maue & Dionne, 1987).

3.8. Comparison of human and mouse olfactory epithelium

The morphology and cellular physiology of the MOE in rodents and amphibians have been studied extensively (Genovese et al., 2021; Kaupp, 2010; Weiss et al., 2021). However, research on the human MOE remains limited, primarily focused on its anatomical and histological characteristics, with little information on cellular physiology.

In mice, the MOE is situated on the roof of several turbinates within the nasal cavity, covering about 45% of the surface area, with a distinct transition zone between sensory and non-sensory epithelium (Hong et al., 2023). In humans, the MOE is located in the upper and posterior regions of the nasal cavity, constituting approximately 5 to 10% of the surface area (Figure 1.13), and is distributed in patchy regions within the respiratory epithelium (Hernandez-Clavijo et al., 2022; Holbrook et al., 2011; Morrison & Costanzo, 1990).

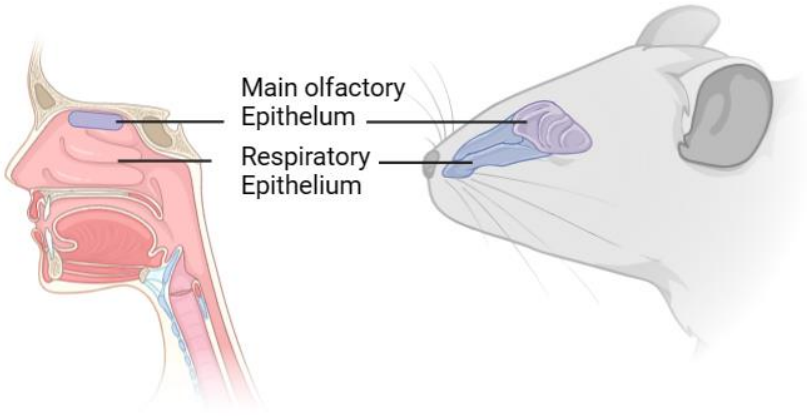


Figure 1.13: Location of the MOE and RE in humans and mice. The surface covered by the olfactory epithelium in the upper is purple, and the respiratory epithelium is pink in humans and blue in mice, note the different areas covered in each of them.

Several similarities exist in the histological composition of the MOE in mice and humans, in both cases mainly composed of OSNs, SCs, and BCs. In humans, OSNs have a single dendrite process with a diameter of 1-2 µm, from which a slightly larger, spherical knob protrudes to the epithelial surface, containing a variable number of cilia (between 10 to 25) measuring 50 µm in length (Morrison & Costanzo, 1990). These numbers are similar to those measured for OSNs in mice (Menco & Morrison, 2003).

The biophysical properties of the voltage-gated currents in human OSNs were characterized using dissociated cells from nasal biopsies. Compared to OSNs in mice, human OSNs were shown to have a delayed outward current sensitive to TEA but surprisingly lack inward currents (Tamari et al., 2019). However, the dissociation process may have compromised the integrity of these neurons hiding the presence of the inward currents.

Regarding the ORs, the human genome contains about 350 sequences with an intact open reading frame, encoding genes for ORs, accounting for 2.4% of the entire genome and constituting the largest gene family (Mombaerts, 2004). In comparison, an olfactory-dependent animal such as the mouse, has three times as many OR genes in its genome. Despite this difference, it has been reported that humans can discriminate 1 trillion olfactory stimuli (Bushdid et al., 2014).

In mice, OSN expresses one of 1,100 possible ORs. The axons from OSNs with the same OR converge into about 1,800 glomeruli in the olfactory bulb (OB)(Potter et al., 2001), resulting in a convergence ratio of 2:1. Humans, with only 350 intact ORs, have over 5,500 glomeruli in the OB, resulting in a convergence ratio of about 16:1. This suggests that odor processing in humans is more complex than in mice, with more glomeruli involved per OR, potentially leading to a more detailed representation of odors (Maresh et al., 2008).

Several homologous proteins involved in the transduction process in the olfactory cilia of mice have also been found in humans, such as G protein alpha and gamma subunits, ACIII, CNGA2, and the Ca^{2+}-activated chloride channel TMEM16B (Durante et al. 2020). However, functional evidence about the transduction cascade in human OSNs is limited to experiments on dissociated neurons obtained from biopsies of human epithelium. Calcium imaging assays performed in these neurons reported paradoxical changes in calcium concentration under odor stimulation (Restrepo et al., 1993), An additional study on the physiological mechanisms behind the transduction process in humans reported that protein kinase A and C inhibitors affected the responses to different sets of odorants, indicating differences in the transduction process compared to what was known in mice (Gomez et al., 2000).

3.9. Autonomic nervous system

The autonomic nervous system is a fundamental regulator of homeostasis in the body, controlling involuntary functions such as heart rate, blood flow, breathing, and digestion. These functions are regulated by two traditionally antagonistic branches: the sympathetic and parasympathetic systems. The sympathetic system governs the fight-or-flight response, while the parasympathetic system controls the rest-and-digest response. Both systems share an efferent organization based on two synapses. The first synapse occurs at the level of the autonomic ganglia outside of the central nervous system, where acetylcholine (ACh) serves as the neurotransmitter in both systems (McCorry, 2007; Wehrwein et al., 2016).

The main difference between these branches lies in the localization of the autonomic ganglia. In the sympathetic branch, these ganglia form a bilateral chain close to the spinal cord at the cervical and thoracic levels, distant from

their target organs. In contrast, the parasympathetic branch has ganglia near its targets, located at various levels in the body (O'Donnell et al., 2012).

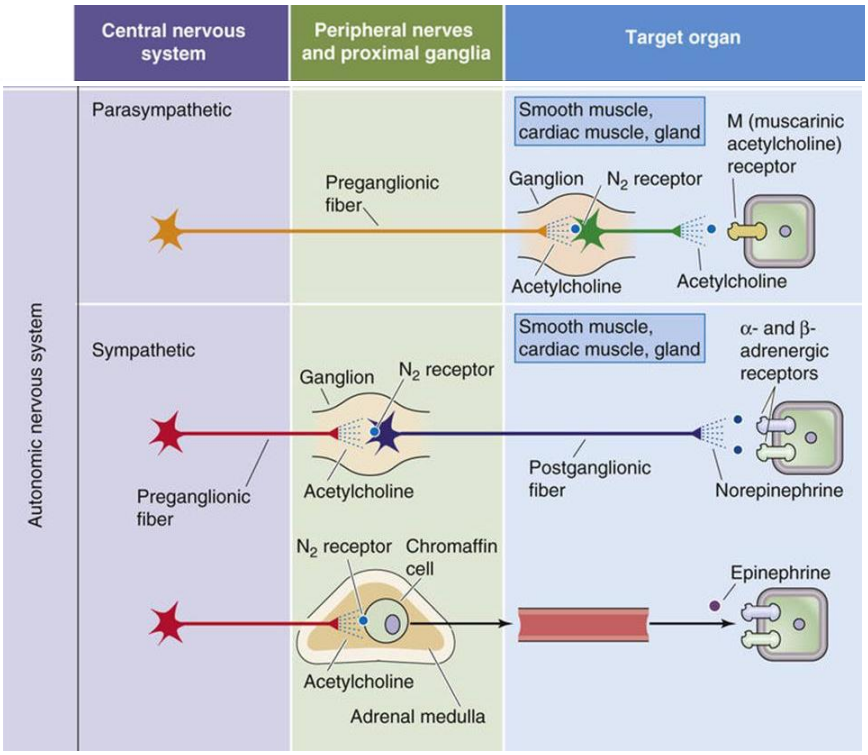


Figure 1.14: Differences between the Sympathetic and Parasympathetic branches of the autonomous nervous system (Waxenbaum et al., 2024).

Another difference is the effector neurotransmitter released (Figure 1.14). In the sympathetic system, noradrenaline (NA, also known as norepinephrine), a crucial neurotransmitter belonging to the catecholamines group, induces the activation of Adrenergic Receptors (ARs). These receptors can be also activated by another internal catecholamine called adrenaline, primarily produced in the adrenal glands. Adrenaline acts as a hormone, playing a fundamental role in the body's stress response system. Regarding the parasympathetic system, the neurotransmitter released by the postganglionic fiber is ACh, which activates muscarinic receptors, inducing antagonist responses to the ARs (Drouin et al., 2017).

In the following sections, I will provide some more details on the sympathetic system because this information will be useful in understanding my work on the VNO.

3.10. Adrenergic receptor types

ARs constitute a class of GPCRs widely distributed throughout the body, where they play critical roles in regulating various physiological processes, including heart rate, blood pressure, smooth muscle contraction, metabolism, and neurotransmitter release (Graham, 1990).
Structurally, ARs consist of a single polypeptide chain sharing several features: seven transmembrane domains, an extracellular region with two glycosylated amino-acid residues of asparagine, and an intracellular carboxyl-terminal containing phosphorylated sites (Insel, 1989). Traditionally classified based on pharmacological effects, ARs are categorized into two types: Alpha-adrenergic receptors (Alpha-AR) and beta-adrenergic receptors (Beta-AR). Alpha ARs primarily mediate vasoconstriction and smooth muscle contraction upon activation by adrenaline or NA, while beta-AR typically mediate vasodilation, bronchodilation, and increased cardiac contractility.

There are three main types of AR: Alpha 1, Alpha 2, and beta. These receptors are classified based on molecular characterization, pharmacology, and the signaling pathways they activate (Michelotti et al., 2000).

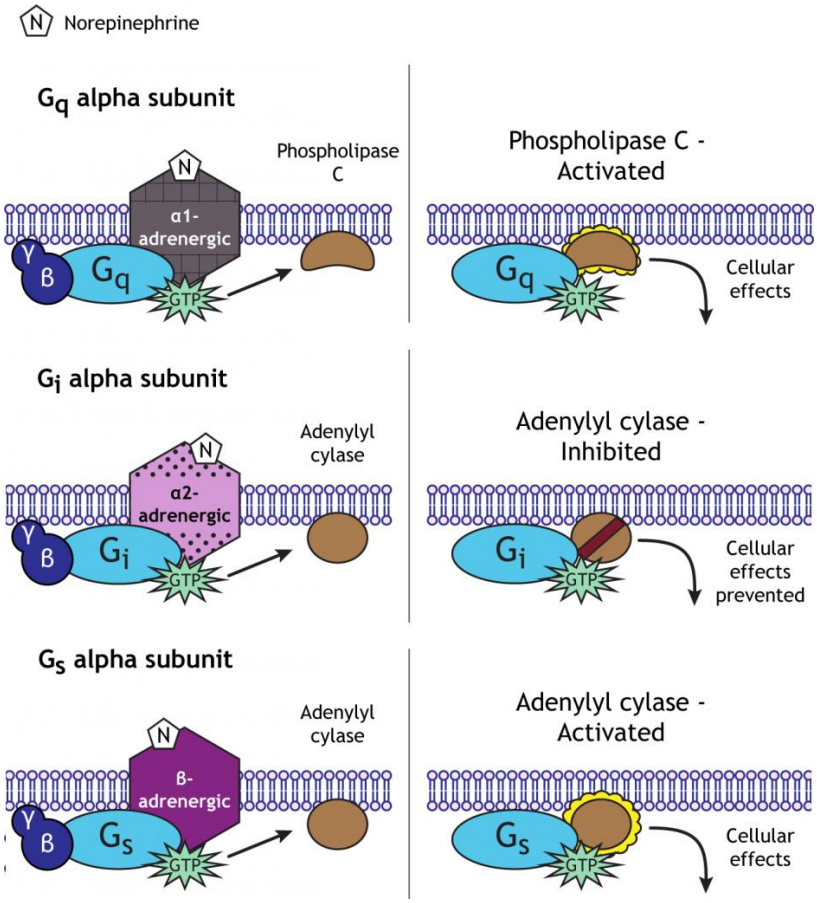


Figure 1.15: Effector enzyme and G-protein associated with each Adrenergic receptor subtype (Taken from the library weber State University. chemistry (weber.edu))

There are three members of the Alpha 1-ARs type: Alpha 1a, Alpha 1b, and Alpha 1d. All of them activate the Gq/11 trimeric G-protein, which stimulates PLC and leads to the subsequent release of calcium ions from intracellular stores (Figure 1.15). In smooth muscle, the activation of this receptor leads to the contraction and vasoconstriction of blood vessels. Another intracellular signal, DAG, activates protein kinase C (PKC), which mediates further downstream signaling events, including the activation of transcription factors or phosphorylation of calcium channels helping in the contraction process (Webb, 2003). In hepatocytes, the activation of Alpha 1 receptors induces the activation of glycogen phosphorylase (Tsujimoto et al., 1989). In the central nervous system, Alpha-1-ARs are expressed in many regions, including the tegmental area, where their activation enhances glutamate release (Velásquez-Martinez et al., 2012).

For alpha 2-ARs, three distinct subtypes have been identified from multiple species: Alpha 2a, Alpha 2b, and Alpha 2c. These receptors activate Gi/o protein, which inhibits adenylate cyclase, leading to decreased levels of cAMP and subsequent inhibition of PKA (Figure 1.15)(Philipp et al., 2002). In the sympathetic nervous system, the expression of Alpha 2a, and Alpha 2b mediates a negative loop to decrease the release of NA (Rump et al., 1995). In the control of blood pressure, Alpha 2 receptors induce a biphasic effect. The hypotension effect, well-known for decades, occurs when stimulation of Alpha 2a receptors in the brainstem induces a decrease in blood pressure. Conversely, the application of Alpha 2 analogs in a bolus inside the carotid and femoral artery results in smooth muscle contraction and increased blood pressure, demonstrating the expression of Alpha 2 receptors in blood vessels which induce contraction similarly to Alpha 1 receptors (Gavras & Gavras, 2001).

Lastly, the beta-AR type consists of three members: beta 1, beta 2, and beta 3. Upon activation by NA, beta-AR couples to Gs proteins, activating AC and increasing cAMP levels (Figure 1.15). However, in certain tissues, beta-AR may also couple to Gi proteins, leading to inhibition of AC and subsequent reduction in cAMP levels, resulting in opposing effects (De Blasi, 1990).

beta-ARs are the most studied receptors due to their implication in heart physiology, where beta-1 stimulation induces an increase in heart rate, contractility, and conduction velocity. These receptors are widely distributed in many tissues of the heart, including the sinoatrial node, atria, His-Purkinje system, and ventricles (Hoffman & Lefkowitz, 1982). In other tissues, such as the smooth muscle of the trachea and bronchi, the stimulation of beta 2 receptors induces relaxation, increasing the expansion of the airways (Strosberg, 1995).

Furthermore, extensive understanding of ARs structure, signaling pathways, and pharmacology has facilitated the development of pharmacological agents targeting these receptors, providing valuable therapeutic options for clinical use.

3.11. Autonomic nervous system and regulation of sensory systems

ARs play crucial roles in sensory systems, contributing to the modulation of sensory perception and the transmission of sensory information. ARs are expressed in sensory organs of the olfactory, visual, auditory, taste and nociceptive systems (Firestein & Menini, 1999; Hoffman & Lefkowitz, 1982; Philipp et al., 2002).

In the visual system, sympathetic innervation triggers pupil dilation releasing NA from the postganglionic fibers of the superior cervical ganglia. This release activates Alpha 2 receptors, promoting relaxation and enlarging the pupil through the contraction of the dilator muscle, which pulls the iris radially during low-light or night vision (Ostrin & Glasser, 2010). On the other hand, the parasympathetic system works in opposition, contracting the radial sphincter muscle to decrease the aperture of the pupil. This interaction between the sympathetic and parasympathetic systems constantly adjusts the pupillary aperture, controlling the amount of light entering the eye to stimulate the retina (McDougal & Gamlin, 2015).

In the auditory system, a recent study has shown the expression of Alpha 2a receptor on outer hair cells, correlating its activation with a protective effect against oxidative damage induced by noise-induced hearing loss (Tian et al., 2024).

Concerning the perception of pain, nociceptors and interneurons in the dorsal horns of the spinal cord in mice express Alpha ARs, and studies using conditional knockout mice for Alpha 2 receptors demonstrated the role of these receptors in inducing analgesia (Philipp et al., 2002).

Regarding the taste receptors, some reports show the expression of several adrenergic receptors in the posterior taste buds as well as positive signals for markers involved in the synthesis of NA (Zhang et al., 2010), functional studies inducing sympathetic stimulation produced the inhibition of potassium outward current in taste receptors deviling a role of NA in the perception of flavors (Herness et al., 2002).

3.12. Autonomic nervous system in the VNO and MOE.

ARs are expressed in both VNO and MOE and central associated structures, such as the AOB and MOB. In the AOB, ARs serve a crucial function in mate recognition memory (Bruce effect) by modulating the firing patterns of granular and mitral cells through synaptic plasticity modifications (Huang et al., 2018; Zimnik et al., 2013). In the MOE, functional experiments have shown that adrenaline enhances odorant contrast by regulating the sensitivity of OSNs through the activation of beta-ARs and the following synthesis of cAMP, activation of PKA, and modulation of voltage-gated sodium channels (Firestein & Menini, 1999; Hall, 2011; Kawai, 1999).

The regulation of VSNs by adrenaline or NA remains elusive. Nevertheless, a transcriptomic study indicated the presence of ARs in the VNO (Ibarra-Soria et al., 2014) and other studies showed the presence of a complex vasculature with dense innervation originating from adrenergic and cholinergic nerves (Hamacher et al., 2024; Iwanaga & Nio-Kobayashi, 2020). These findings indicate a potential physiological role for ARs in VSNs.

4. Aims

This work is focused on the investigation of molecular mechanisms involved in the modulation of VSNs and of the basic physiological properties of human OSNs.

The specific aims of this work were:

- To investigate the potential neuromodulator role of Noradrenaline in Vomeronasal Sensory Neurons activity.
- To identify functionally expressed adrenergic receptors in Vomeronasal Sensory Neurons.
- To verify possible sources of autonomic innervation of the Vomeronasal Epithelium.
- To perform the first electrophysiological characterization of human Olfactory Sensory Neurons and Supporting cells in slices of Main Olfactory Epithelium obtained from nasal biopsies.

5. Results

5.1. Noradrenaline modulates sensory information in mouse vomeronasal sensory neurons

Cesar Adolfo Sánchez Triviño[#], Andres Hernandez- Clavijo, Kevin Y. Gonzalez-Velandia, Simone Pifferi and Anna Menini

[#] conceptualized the project and performed experiments of electrophysiology and calcium imaging.

Manuscript under revision

Noradrenaline modulates sensory information in mouse vomeronasal sensory neurons

Cesar Adolfo Sánchez Triviño[1,#], Andres Hernandez- Clavijo[1,2#], Kevin Y. Gonzalez-Velandia[1§], Simone Pifferi[3*] and Anna Menini[1*]

[1] Neurobiology Group, SISSA, Scuola Internazionale Superiore di Studi Avanzati, 34136 Trieste, Italy.

[2]Department of Chemosensation, Institute for Biology II, RWTH Aachen University, 52074 Aachen, Germany

[3] Department of Experimental and Clinical Medicine, Università Politecnica delle Marche, 60126 Ancona, Italy.

[§] Current address: Department of Neuroscience, University of Rochester School of Medicine and Dentistry, 14642, Rochester, USA.

[#]These authors contributed equally

*Corresponding authors

Simone Pifferi P017884@staff.univpm.it

and

Anna Menini menini@sissa.it

Short title: NA modulates firing in VSNs

Keywords: VNO, adrenergic receptor, sympathetic system

Summary

During the induction of the body's alert state, the sympathetic system modulates sensory modalities and fine-tunes peripheral organs for improved stimulus detection. We explored noradrenaline (NA)'s role in modulating signaling in vomeronasal sensory neurons (VSNs), responsible for detecting pheromones and other semiochemicals. In current-clamp recordings, NA increased the firing frequency in response to natural stimuli of responsive VSNs and induced spiking activity in previously unresponsive neurons. Current injections showed an increase in firing frequency during NA application. Combining transcriptomic analysis, electrophysiology, Ca^{2+} imaging and a pharmacological approach, we identified alpha 1 adrenergic receptors as crucial for NA-induced firing frequency increases in VSNs. Immunohistochemistry revealed catecholaminergic fibers in the vomeronasal sensory epithelium, suggesting localized NA release near VSNs. This study unveils NA as a key regulator of VSN signaling, shedding light on the intricate interplay between the sympathetic nervous system and chemosensory processing, advancing our understanding of sensory modulation.

Introduction

The autonomic nervous system is one of the most relevant regulatory systems in the body, managing the internal environment and engaging the organism in either a "flight-or-fight" response or in "rest-and-digest" state, depending on which division of the autonomic system is more active. The sympathetic system is mainly responsible for inducing an alert state of the body through the release of the neurotransmitter noradrenaline (NA) and the hormone adrenaline, both activating adrenergic receptors (McCorry 2007; Graham 1990). During the induction of the body's alert state, the sympathetic system also influences several sensory modalities and fine-tunes peripheral organs for improved stimulus reception. For example, in the visual system, NA triggers pupil dilation, controlling the amount of light entering the eye to stimulate the retina (Ostrin and Glasser 2010). In the peripheral olfactory system, adrenaline enhances odorant contrast by regulating the sensitivity of olfactory sensory neurons (OSNs) (Firestein and Menini 1999; Kawai, Kurahashi, and Kaneko 1999; Hall 2011). However, little is known about the potential regulation of the peripheral vomeronasal system, primarily responsible for detecting pheromones and other semiochemicals, by the sympathetic system. Some studies showed that the vomeronasal organ (VNO) is functionally innervated by the sympathetic system (Ben-Shaul et al. 2010; Meredith 1994; Hamacher et al. 2024).

The VNO is one of the chemosensory organs used by many mammals to detect chemical stimuli in the environment, a crucial ability that plays a significant role in survival, communication, and interaction with the external world (Døving and Trotier 1998). The VNO is composed of two main regions: a non-sensory region containing non-sensory epithelium and blood vessels, and a sensory region, the vomeronasal sensory epithelium. These structures run parallel along the antero-posterior axes, with the lumen space between them filled with mucus and in direct contact with the nasal cavity (Salazar et al. 2008; Adams 1992; Døving and Trotier 1998).

The VNO non-sensory region is largely composed of venous blood vessels and smooth muscle fibers (Tirindelli 2021; Hamacher et al. 2024). Its principal function is to provide the mechanical force necessary for the chemicals dissolved in the mucus to enter into the VNO lumen, a process known as VNO pumping. Recent evidence has enhanced our understanding of the pumping mechanism in the VNO, demonstrating the crucial involvement of the sympathetic system (Hamacher et al. 2024). This system innervates the intricate smooth muscle fibers and vasculature, inducing repetitive contractions that drive the pumping action, introducing chemicals into the VNO (Iwanaga and Nio-Kobayashi 2020; Hamacher et al. 2024). The pumping mechanism involves the alternating activation of NA-sensitive muscle fibers and acetylcholine-activated muscle fibers, which, due to their different orientations within the organ, generate opposing effects on the volume of the lumen (Hamacher et al. 2024).

In the sensory epithelium, vomeronasal sensory neurons (VSNs) detect chemicals that enter the VNO lumen and bind to specific vomeronasal receptor proteins at the apical microvili of the VSNs. Each VSNs express only one or few members of three families of G protein coupled vomeronasal receptors: V1Rs, V2Rs or formylated peptide receptors (FPRs) and each receptor binds different ligands. The binding activates a phospholipase C (PLC)-based signaling cascade, leading to membrane depolarization and subsequent firing of action potentials. This firing activity is sent to the accessory olfactory bulb (AOB) in the brain for further processing, modulating the physiological and behavioral responses of the animal (Tirindelli et al. 2009; Tirindelli 2021; Mohrhardt et al. 2018; Zufall 2005; Stowers et al. 2002; Hernandez-Clavijo et al. 2021; Dibattista et al. 2012; Francia et al. 2014).

Here, to investigate the potential role of NA in modulating signaling in VSNs, we recorded the firing activity of VSNs in acute slices of the mouse VNO. Surprisingly, we found that not only NA causes an increase in firing frequency in VSNs responsive to a natural stimulus composed of diluted mouse urine, but also elicits a response in VSNs that did not initially respond to urine, indicating a modulatory effect of NA on VSNs responsiveness. Moreover, we found that, independently of the transduction mechanism, NA affects the generation of action potential in VSNs, as current injection experiments showed an increase in firing frequency during NA application, in the absence of urine stimuli. Through transcriptomic analysis of previously published data from the whole VNO single cell RNA-seq data (Katreddi et al., 2022), we identified the expression in VSNs of Adra1a, encoding the alpha 1a adrenergic receptor. We obtained a functional validation of the involvement of alpha 1 adrenergic receptors in the modulatory effect of NA through electrophysiological and calcium imaging experiments, combined with a pharmacological approach. Our experimental findings establish 1, likely alpha 1a, as the primary adrenergic receptor type activated by NA in VSNs. Futhermore, by immunohistochemistry we provide evidence that the sensory epithelium of the VNO is innervated by catecholaminergic fibers indicating that NA could be released in close proximity of VSNs.

Results

NA increases firing frequency of responses to natural stimuli in VSNs

To evaluate the NA's potential impact on VSNs during their response to natural stimuli, we performed current-clamp whole-cell recordings from VSNs in acute murine VNO slices, using diluted mouse urine (1:50) as a natural stimulus. Indeed, urine is often used as a stimulus for VSNs because it is a rich source of pheromones and ligands that interact with vomeronasal receptors and activate the transduction cascade leading to action potential generation (Tirindelli et al. 2009; Moss et al. 1997; Wong et al. 2018; Sarno et al. 2022; Doyle et al. 2016; Hernandez-Clavijo et al. 2021). We measured spiking activity induced by diluted urine application in 42% of the viable VSNs (10 out of 24). Subsequently, we applied 50 µM NA and, after 3 min, challenged the same recorded VSNs, whether initially responsive or not, with a second diluted urine application identical to the first one. We measured that 70% (7 out of 10) of the initially responsive VSNs exhibited an increased mean spiking frequency when stimulated a second time in the presence of NA. The average spiking frequency in response to urine rose from 1.37 ± 0.83 Hz under control conditions to 2.48 ± 1.30 Hz during NA application (n = 7), returning to 1.31 ± 0.78 Hz after washout (n = 7; Fig. 1 *A*, *B*). Surprisingly, 36% (5 out of 14) initially unresponsive VSNs showed a clear spiking activity in response to urine when NA was present (Fig. 1 *C*, *D*). Importantly, the effect of NA on spiking activity following urine stimulation was entirely reversible upon washout (Fig. 1*A-D*). These results clearly show that NA can increase VSNs' responsiveness to their natural ligands.

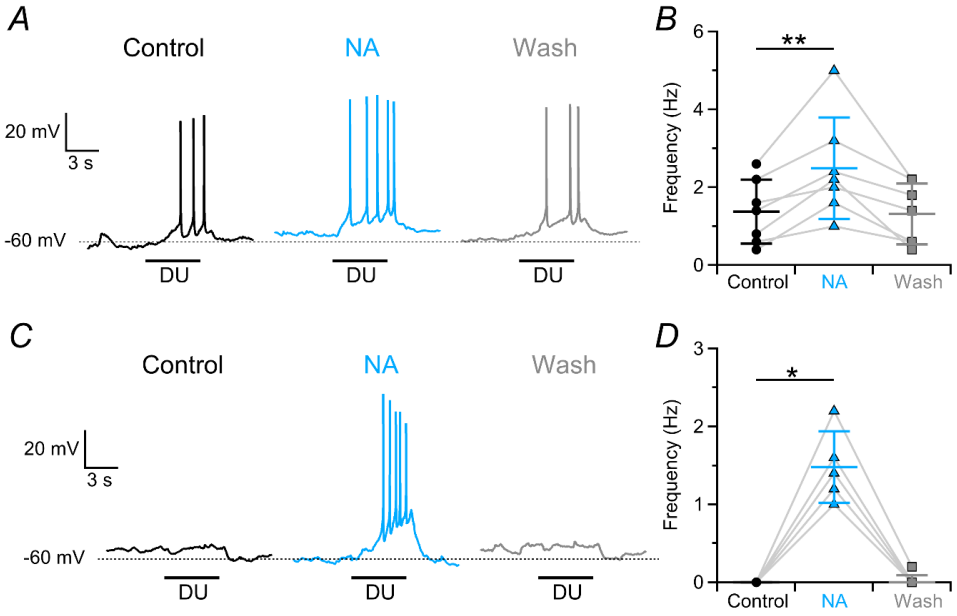


Fig. 1 Noradrenaline increases urine-induced action potential firing in VSNs.
A, C, representative whole-cell current-clamp recordings from VSNs stimulated for 5 s with diluted urine (DU, 1:50) in control condition, during application of 50 µM NA and after washout. Recordings with NA started 3 min after application of NA and washout was measured 5 min after removal of NA. Neuron in *C* responded to urine only during application of NA. Bars at the bottom

indicate the time of urine application. *B, D,* scatter plots with averages ± SD of the firing frequencies. *B,* n=7; P=0.00917 (Control-NA) P=1 (control-wash) t-test with Bonferroni's correction after ANOVA for repeated measurements P=0.0007. ***D*****,** n=5; P=0.026 (Control-NA) P=1 (control-wash) Demsar test after Friedman test P=0.0087.

NA increases firing frequency by activating alpha 1 adrenergic receptors

Changes in firing activity driven by NA during responses to natural stimuli in VSNs could arise from two mechanisms: i) modulation of elements within the complex and heterogeneous signal transduction cascade, and/or ii) modulation of the action potential machinery. To assess if NA's effect on VSNs could be observed independently of signal transduction activation, we bypassed the transduction cascade by using direct current injections to activate the action potential machinery in VSNs.

In a first set of experiments, we applied repetitive 3 pA current steps lasting 3 s, at 1 min intervals (to prevent adaptation, as previously described by Sarno et al. (2022), under three conditions: control, NA application, and subsequent washout (Fig. 2). Remarkably, NA application led to a progressive increase in action potential frequency, which subsequently decreased during washout (Fig. 2*A*). In a second set of experiments, we expanded the range of current stimulation step amplitudes from 0 to 6 pA (Fig. 2*B,C*), increasing by 1 pA increments. NA significantly increased the frequency of action potentials elicited by current injections ranging from 2 to 6 pA (Fig. 2*C*). Specifically, using 3 pA current steps, the average firing frequency increased from 2.0 ± 1.1 Hz in the control state to 2.8 ± 1.4 Hz in the presence of NA (n = 10), subsequently returning to 1.8 ± 1.0 Hz after washout (n = 10; Fig. 2*C*). NA had no significant impact on the resting membrane potential measured at zero-current injection, indicating that NA does not modulate the resting ionic conductances (-72 ± 4 mV in control, -69 ± 5 mV in the presence of NA, -69 ± 5 mV after washout (n=10; Fig. 2*D*). Overall, 67% of VSNs (18 out of 27) tested with 3 pA current injection displayed reversible increases in firing frequency during NA application.

These results collectively demonstrate that NA exerts a direct effect on action potential generation in VSNs, producing a firing frequency increase.

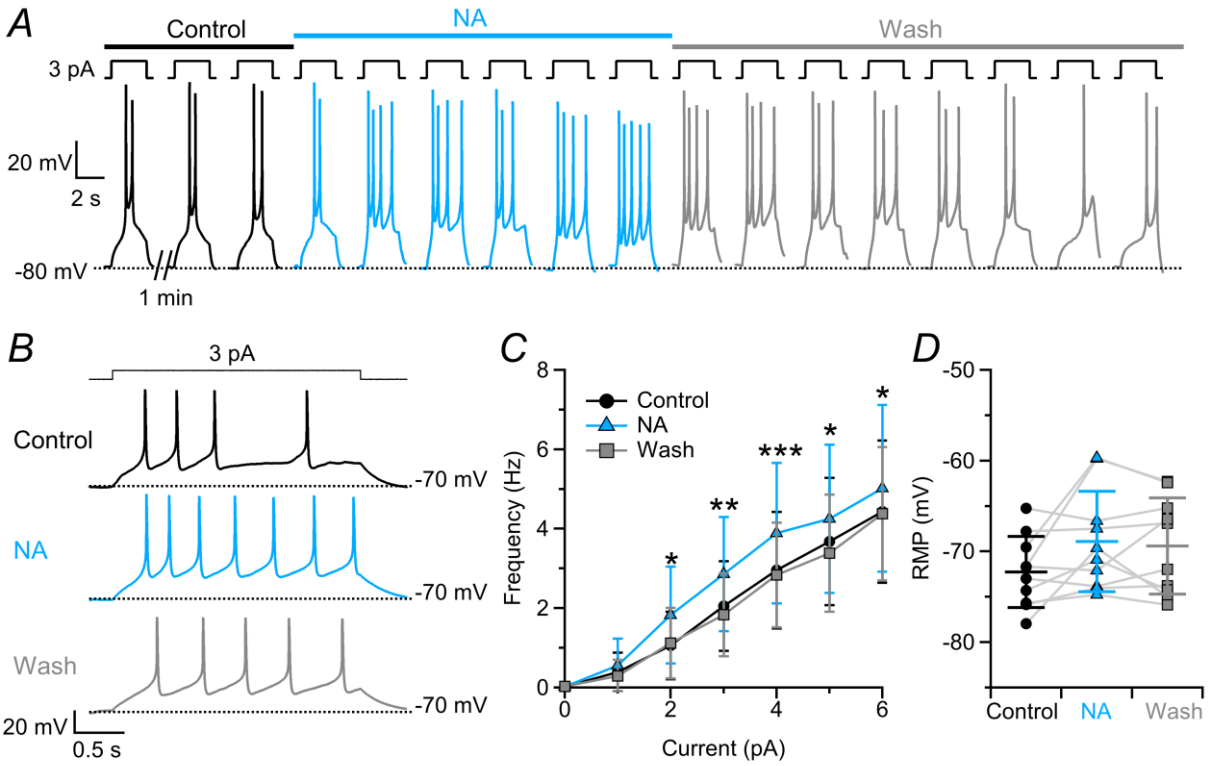


Fig. 2 Noradrenaline increases spike frequency in response to current injections in VSNs.

A, representative whole-cell current-clamp recordings from a VSN repetitively stimulated with 3 pA current steps for 3 s at 1 min intervals in control, during application of 50 µM NA and during washout. Steps at the top indicate the time of current injections. *B*, representative current-clamp recordings from VSNs stimulated with 3 pA current steps for 3 s in control, during application of 50 µM NA and after washout. Recordings with NA started 3 min after application of NA and washout was measured 5 min after removal of NA. *C*, averages ± SD of firing frequencies as a function of current injection amplitude in the indicated conditions (n=10; for 1 pA, P=0.426 (C-NA), P=1 (C-wash); for 2 pA, P=0.082 (C-NA), P=1 (C-wash); for 3 pA, P=0.004 (C-NA), P=0.51 (C-wash); for 4 pA, P<0.001 (C-NA), P=1 (C-wash); for 5 pA, P=0.012 (C-NA), P=0.127 (C-wash); for 6 pA, P=0.032 (C-NA), P=1 (C-wash), paired t test with Bonferroni correction after mixed model two way ANOVA P<0.001). *D*, scatter plot with the averages ± SD of the resting membrane potentials (RMP) in the indicated conditions (n=10, P=0.06 Friedman test).

To assess which adrenergic receptors mediate the effect of NA, we examined the transcriptional profile of adrenergic receptors in mature VSNs (Fig. 3A and B) analyzing previously published scRNA-seq data from the VNO (Katreddi et al. 2022). We found that *Adra1a*, the transcript for alpha 1a adrenergic receptors, was the most abundant among adrenergic receptor transcripts in mature VSNs (Fig. 3B), indicating that alpha 1a is likely to be the main receptor type activated by NA.

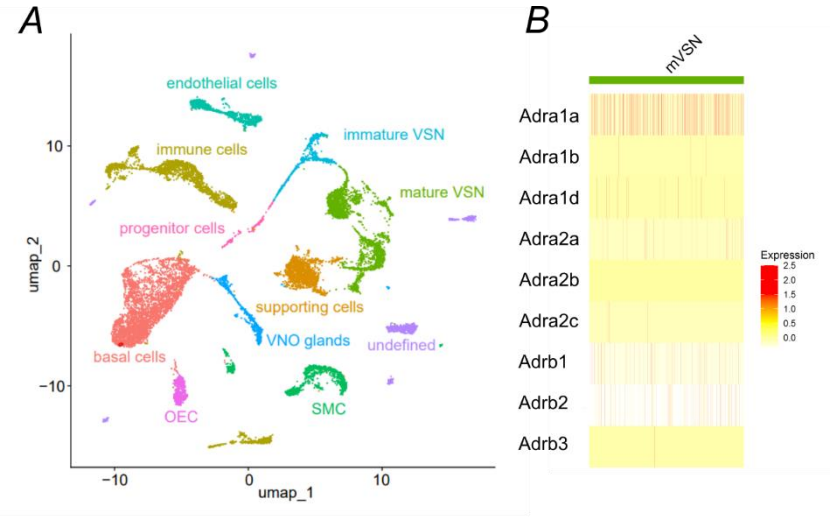


Fig. 3 Expression of adrenergic receptors in VSNs.
A, visualization of the clustering results from the whole VNO scRNA-seq data produced in Katreddi et al. (2022) on a Uniform Manifold Approximation and Projection (UMAP) plot. The cell type annotation of each cluster is noted on the color key legend and labels. *B*, heatmap showing expression levels of the transcripts of adrenergic receptors in mature VSNs.

To investigate the involvement of alpha 1 receptors in the response to NA, we measured the effects of selective alpha 1 receptor agonists and antagonists on VSNs excitability (Fig. 4). Methoxamine (50 µM), a selective agonist of alpha 1 receptors (Langer, Cavero, and Massingham 1980; Tsujimoto et al. 1989; Velásquez-Martinez, Vázquez-Torres, and Jiménez-Rivera 2012), increased the firing frequency, indicating that the activation of alpha 1 receptors produces an enhancement of VSNs excitability (Fig. 4*A* and *B*), without modifying the resting membrane potential (Fig. 4*C*). By using prazosin (2.5 µM), a selective antagonist of alpha 1 receptors (Graham, 1990; Zhong and Minneman 1999; Michelotti et al., 2000), application of 50 µM NA failed to increase firing frequency elicited by current injections and did not affect the resting membrane potential (n=5-6; Fig. 4 *D-F*).

In summary, these findings show that NA modulates VSNs firing frequency by acting on alpha 1 adrenergic receptors.

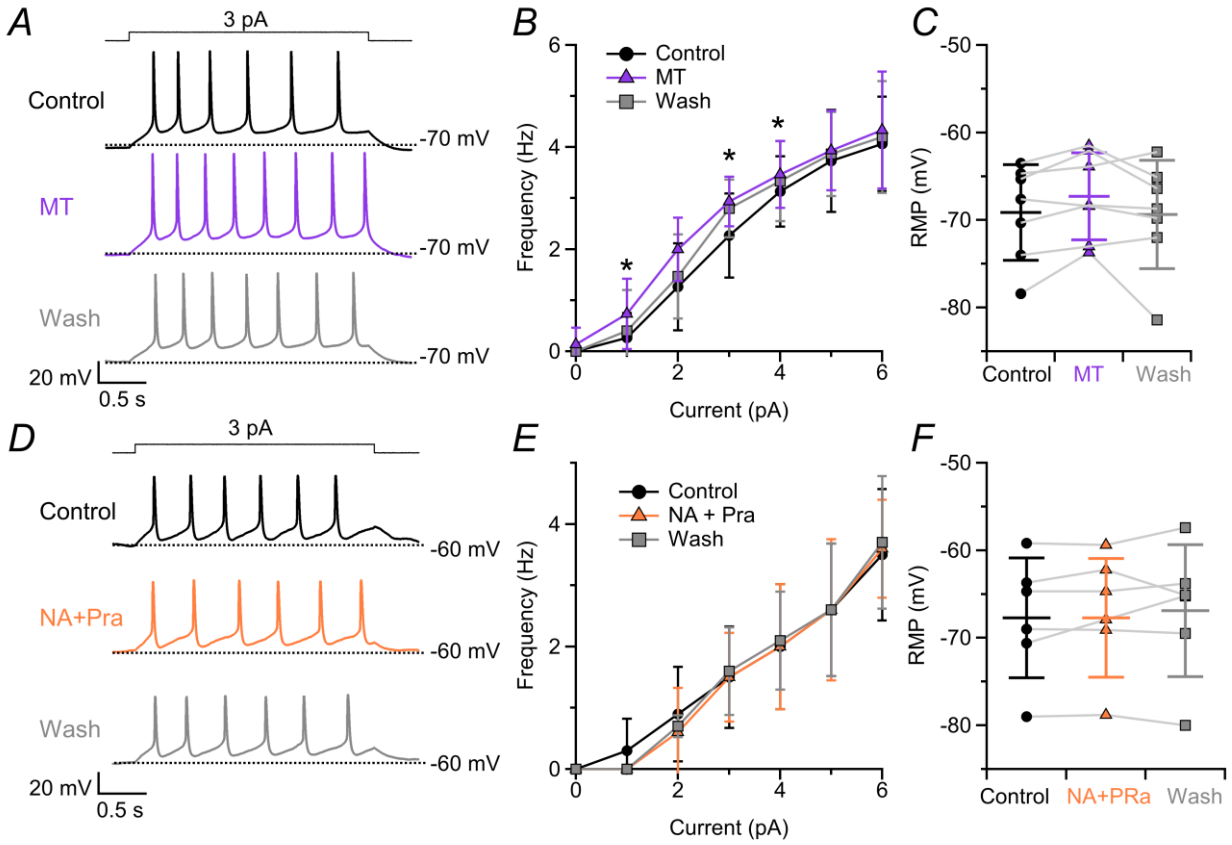


Fig. 4 Noradrenaline increases spike frequency of VSNs through alpha 1 adrenergic receptors.

A, representative current-clamp recordings from a VSN stimulated with 3 pA current steps for 3 s in control, during application of 50 µM methoxamine (MT) and after washout. Recordings with methoxamine started 3 min after its application and washout was measured 5 min after removal. *B*, average ± SD of firing frequency as a function of current injection in the indicated conditions (n = 7; for 1 pA, P=0.038 (C-NA), P=1 (C-wash); for 2 pA, P=0.059 (C-NA), P=0.887 (C-wash); for 3 pA, P=0.032 (C-NA), P=0.247 (C-wash); for 4 pA, P=0.012 (C-NA), P=0.227 (C-wash); for 5 pA, P=0.609 (C-NA), P=0.1 (C-wash); for 6 pA, P=0.306 (C-NA), P=1 (C-wash), paired t test with Bonferroni correction after mixed model two way ANOVA P=0.002). *C*, scatter plot with the average ± SD of the resting membrane potential (RMP) in the indicated conditions (n = 7; P=0.094 ANOVA for repeated measurements). *D*, representative current-clamp recordings from a VSN stimulated with 3 pA current steps for 3 s in control, after application of 50 µM NA and 2.5 µM prazosin (Pra) and after washout. NA and prazosin were applied for 3 min and washout was measured 5 min after removal. *E*, scatter plot with the average ± SD of the resting membrane potentials (RMP) in the indicated conditions (n = 6; P=0.56 ANOVA for repeated measurements). *F,* average ± SD of firing frequency as a function of current injection in the indicated conditions (n = 5; P=0.4 mixed model two way ANOVA).

NA induces intracellular Ca^{2+} increase

As it is well established that alpha 1 receptors activation leads to an increase in cytosolic Ca^{2+} (Graham 1990;Michelotti et al., 2000; Insel 1989), we investigated whether the stimulation of VSNs with NA produces a rise in intracellular Ca^{2+}, which could potentially contribute to the molecular mechanisms that produce a higher firing frequency. Thus, we conducted Ca^{2+} imaging experiments on dissociated mouse VSNs loaded with the Ca^{2+} indicator Fluo4-AM.

To distinguish viable VSNs from other cells and exclude non-viable neurons, we used a depolarizing high K^+ solution and selectively analyzed only VSNs responding to high K^+ with a Ca^{2+} increase. Following 100 µM NA stimulation for 20 s, a notable increase in fluorescence was observed in several viable dissociated VSNs. This rise in fluorescence persisted across three consecutive NA stimulations at an interstimulus interval of 3 min (n=18; Fig. 5*A* and *B*). Overall, 52% of VSNs (48 out of 93) exhibited an increase in intracellular Ca^{2+} concentration in response to NA stimulation. To evaluate if the rise in fluorescence was mediated by alpha 1 receptors, we applied the antagonist prazosin (2.5 µM), which effectively blocked the Ca^{2+} increase induced by NA in dissociated VSNs (Fig. 5*C* and *D*). Furthermore, we explored whether the alpha 1 agonist methoxamine (50 µM) could induce intracellular Ca^{2+} increases in dissociated VSNs similar to NA. Our findings revealed that dissociated VSNs responded to methoxamine with an elevation in intracellular Ca^{2+} concentration (Fig. 5*E* and *F*).

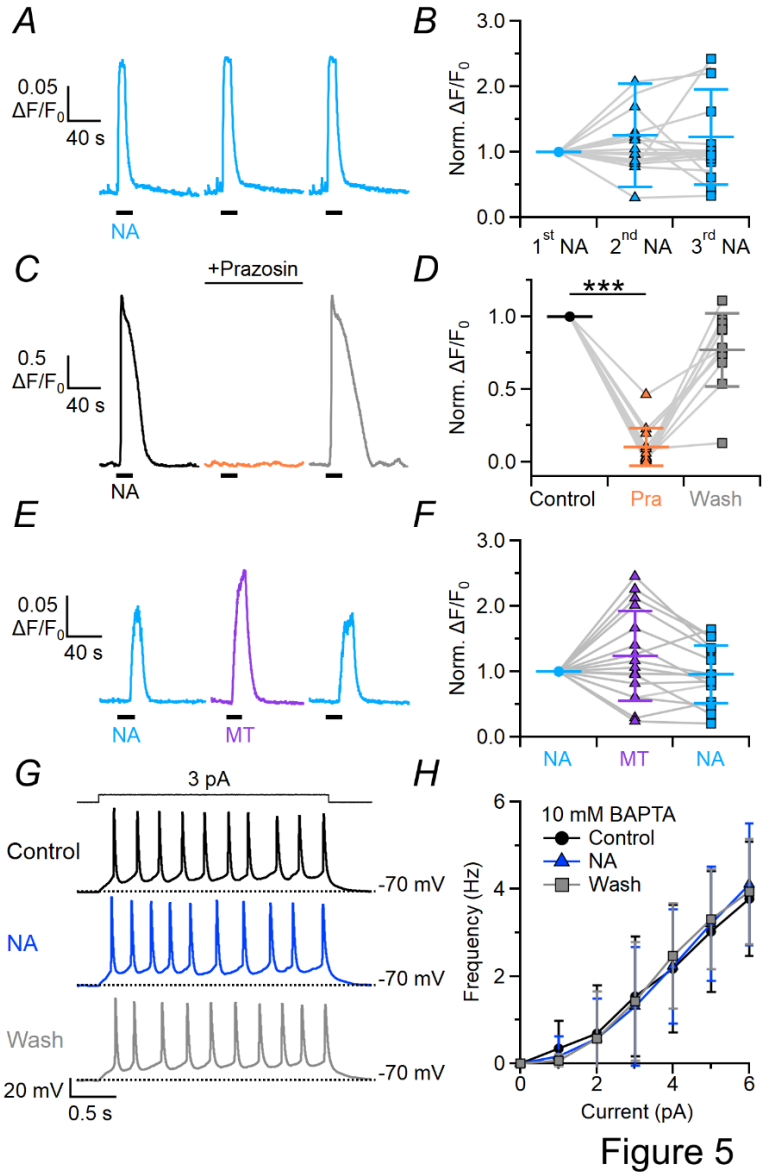


Figure 5

Fig. 5 Alpha 1 adrenergic receptor activation increases intracellular calcium in VSNs. *A, C, E,* representative recordings of cytosolic Ca^{2+} signals from VSNs in response to: *A*, three repetitive stimulations with 100 µM NA (20 s); *C*, stimulations with 100 µM NA (20 s) in control, during the application of 2.5 µM prazosin and after its washout; *E*, stimulations with 100 µM NA (20 s) or 50 µM methoxamine (MT, 20 s). The interval between stimulations was 3 min. *B, D, F,* scatter plot with average ± SD of normalized changes in fluorescence intensity following stimulations as indicated in *A, C, E* respectively. All data were normalized to the peak value obtained from the first stimulation. *B,* n=19; P=0.805 Friedman test. *D,* n=12; P=5.3*10^{-6} (Con-Pra), P=0.082 (Con-wash) Demsar test after Friedman test P=1.5*10^{-5}. *F,* n=16; P=0.144 Friedman test. *G*, representative whole-cell current-clamp recordings from a VSN in a VNO coronal slice repetitively stimulated with 3 pA current steps for 3 s at 1 min intervals in control, during application of 50 µM NA and after washout. The intracellular solution contained the rapid Ca^{2+} chelator BAPTA (10 mM). Recordings with NA started 3 min after its application and washout was measured 5 min after

removal. *H,* average ± SD of firing frequencies as a function of current injection in the indicated conditions (n = 7; P=0.994 mixed model two way ANOVA).

These results collectively demonstrate that NA induces Ca^{2+} increases in VSNs through the activation of alpha 1 receptors.

We reasoned that, if the increase in firing frequency induced by NA in current-clamp whole-cell recordings is indeed caused by an intracellular Ca^{2+} increase, then reducing the Ca^{2+} increase by dialyzing the cytosol of VSNs with an intracellular solution containing the rapid Ca^{2+} chelator BAPTA, should decrease, or abolish, the effect of NA on VSNs. Thus, we recorded from VSNs in VNO acute slices and measured the effect of NA on firing frequencies induced by current steps by using BAPTA instead of EGTA as Ca^{2+} chelator inside the patch pipette. We found that, when the rapid Ca^{2+} chelator BAPTA was used in the patch pipette, NA failed to significantly increase the firing frequency elicited by current injections (Fig. 5*G* and *H*).

Taken together, these results provide compelling evidence that a Ca^{2+} increase induced after the activation of alpha 1 receptors by NA is involved in the increase of firing frequency in VSNs.

Sympathetic nerve fibers in the vomeronasal sensory epithelium

To investigate if NA could be released in the direct proximity of VSNs, we investigated if the sensory epithelium in the VNO is innervated by catecholaminergic fibers. Indeed, previous studies showed a functional innervation of the VNO by the sympathetic system in mice and hamsters (Ben-Shaul et al. 2010; Meredith 1994) and a recent work found that the release of NA by sympathetic fibers controls the contraction of smooth muscles in the non-sensory epithelium responsible for VNO pumping playing a pivotal role in the stimulus intake (Hamacher et al. 2024).

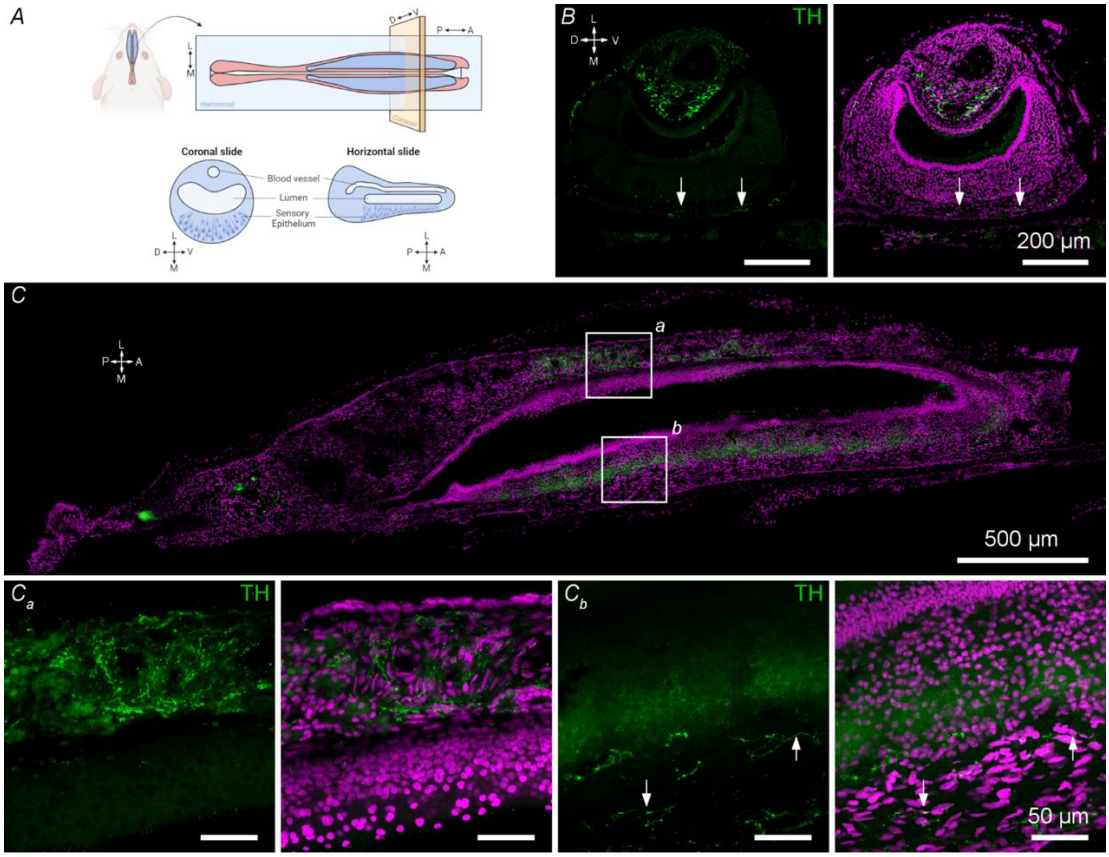


Fig. 6 Catecholaminergic fibers innervate the VNO sensory epithelium.
A, schematic representation of the VNO and the tissue distribution after coronal or horizontal sectioning. *B-C*, Immunostaining against tyrosine hydroxylase (TH) enzyme (green) on coronal (*B*) and horizontal (*C*) sections of the VNO. White squares in *C* denote the zoomed in areas for the non-sensory epithelium (C_a) and sensory epithelium (C_b). White arrows indicate the presence of TH-positive fibers in the basal zone of the sensory epithelium. Note the high innervation by TH-positive fibers on the non-sensory epithelium. Nuclei were stained with DAPI (magenta).

We labeled coronal and horizontal cryosections of adult VNOs with antibodies targeting tyrosine hydroxylase (TH). In both sectioning planes, coronal or horizontal, a comprehensive morphology of the VNO can be observed, including: the non-sensory epithelium characterized by a large blood vessel; the sensory epithelium, and the lumen, a mucus-filled cavity separating the two epithelia (Fig. 6). Consistent with the findings of Hamacher et al. (2024), a dense network of TH positive nerve fibers was observed in the non-sensory epithelium of the VNO (Fig.6*B*, C and C_a). Importantly, we identified TH positive nerve fibers also innervating the basal region of the vomeronasal sensory epithelium (Fig. 6*B, C* and C_b; arrows). The presence of catecholaminergic innervation within the sensory epithelium implies a potential for a localized and precise release of NA in close proximity to VSNs.

These results show that catecholaminergic fibers of the sympathetic system innervate both the sensory and non-sensory epithelia of the mouse VNO.

Discussion

In this study, we demonstrate that NA increases VSNs action potential firing through activation of alpha 1 adrenergic receptors, leading to an increase in intracellular Ca^{2+} concentration. Furthermore, through the analysis of available single-cell transcriptomic data, we show that mature VSSs predominantly express alpha 1a adrenergic receptors. In addition, we show that catecholaminergic fibers innervate the sensory epithelium, indicating that NA could be released near VSNs.

In current-clamp whole-cell recordings, we measured spiking activity in response to natural stimuli in mouse diluted urine, which contains a rich blend of pheromones, in 42% of the viable VSNs. As individual VSNs are known to express different vomeronasal receptors belonging to the V1R, V2R or FPR receptor families and each receptor binds different ligands (Tirindelli, 2021), is not surprising that not all VSNs respond to a given stimulus. This could be because unresponsive neurons may express receptors that do not bind to any of the stimulus components, or the stimulus concentration was too low to elicit action potentials. Furthermore, we cannot exclude the possibility that some VSNs were not viable.

NA caused an increase of the firing frequency in all neurons responding to urine and the frequency returned to the initial value after washout of NA, showing that the increase was reversible. Surprisingly, also 36% of the initially unresponsive neurons fired action potentials in response to urine when NA was present and returned to be unresponsive after NA washout, providing an additional clear demonstration that NA modulates responses to natural stimuli by increasing the responsiveness of VSNs.

As the binding of ligands to vomeronasal receptors first activate transduction cascades that may lead to action potential firing, NA modulation of the responses may occur at various stages during the transduction cascade and/or on ion channels producing action potentials. To bypass the transduction cascade and therefore the activation of specific vomeronasal receptors, we performed current-clamp experiments by using current steps. In these experimental conditions, NA caused a reversible increase in firing frequency in 67% of neurons (tested with 3 pA current steps). Although we cannot exclude the possibility that NA produces effects on components of the transduction cascade, these results demonstrate that NA affects the generation of action potentials causing an increase in firing frequency.

We investigated the expression of adrenergic receptors in VSNs with several approaches: by analyzing publicly available VNO single cell RNA-seq data (Katreddi et al. 2022) and by performing electrophysiological and Ca^{2+}-imaging experiments combined with pharmacological compounds. Single-cell transcriptomic data revealed that mature VSNs predominantly express Adra1a, encoding the alpha 1a adrenergic receptor. From a functional point of view, although we could not validate the involvement of alpha 1a, because selective agonists or antagonists are unknown, we used selective compounds for alpha 1 receptors: the agonist methoxamine and the antagonist prazosin (Zhong and Minneman 1999). Methoxamine mimicked the increase in firing frequency in current-clamp experiments measured with NA stimulation and prazosin blocked such increase, confirming the activation by NA of alpha 1 receptors in VSNs. Since it is well known that alpha 1 receptors activation leads to an increase in cytosolic Ca^{2+} (Graham 1990; Michelotti

et al., 2000; Insel 1989), we provided a further demonstration of the activation of alpha 1 receptors in VSNs by NA by performing Ca^{2+} imaging experiments on dissociated cells from the VNO. Indeed, stimulation with NA caused a clear increase in intracellular Ca^{2+} concentration in 52% of the tested VSNs that was mimicked by the selective alpha 1 agonist methoxamine and blocked by the selective antagonist prazosin.

Is the NA-induced increase in intracellular Ca^{2+} involved in the higher VSNs excitability? In current-clamp experiments, when we reduced the increase in intracellular Ca^{2+} using the fast Ca^{2+} chelator BAPTA in the intracellular solution, we did not measure any increase in firing frequency induced by NA, indicating that a Ca^{2+} increase is involved in the higher VSN excitability.

It is of interest to note that in the peripheral olfactory system, adrenaline plays a role in enhancing odorant contrast by regulating the sensitivity of OSNs. Indeed, Kawai et al. (1999) demonstrated that adrenaline modulates action potential firing and induces a negative shift in the activation curve of voltage-gated Na^{+} channels in sensory neurons of the main olfactory epithelium. Their study showed the involvement of beta adrenergic receptors in the soma of OSNs. Upon binding to their agonists, these receptors trigger the synthesis of cAMP, leading to the subsequent activation of protein kinase A, which in turn could modulate voltage-gated Na^{+} channels in OSNs. Interestingly, cathecolamines enhance stimulus responses in both OSNs and VSNs by using distinct pathways: beta-adrenergic receptors in OSNs and alpha1 adrenergic receptors in VSNs.

Where is NA released within the vomeronasal sensory epithelium? While it is conceivable that there may be a systemic release of NA during states of arousal in the animal, there is also evidence indicating that the sympathetic system innervate the mouse and hamster VNOs (Ben-Shaul et al. 2010; Meredith 1994; Hamacher et al. 2024). A recent study by Hamacher et al. (2024) reported the abundant presence of catecholaminergic fibers in the non-sensory epithelium of the mouse VNO and demonstrated that adrenergic stimulation controls the pumping activity of the VNO, contributing to the regulation of pheromone concentration reaching the organ.

Here, we showed that catecholaminergic fibers not only innervate the non-sensory epithelium, but also the basal region of the sensory epithelium of the VNO. This sympathetic innervation within the sensory epithelium suggests the possibility of a localized release of NA in close proximity to VSNs. Moreover, the shared innervation of both sensory and non-sensory epithelia, suggests the potential for synchronized release of NA within the VNO, thereby coordinating the uptake of stimuli with higher excitability of VSNs thus improving the detection of pheromones or other semiochemicals.

The overall action of NA in the control of vomeronasal signaling also depends on its modulation of the AOB, where signals from VSNs undergo further processing, and higher brain centers (Tirindelli et al. 2009). NA is released within the AOB from fibers originating in the locus coeruleus (McLean et al. 1989) and several studies have demonstrated that NA induces changes between excitation and inhibition of mitral and granule cells, ultimately resulting in a decrease of mitral cells activity (Brennan et al. 1995; Brennan 2004; Araneda and Firestein 2006; Smith et al. 2009; Doyle and Meeks 2017; Lorenzon et al. 2023). Furthermore, Doyle and Meeks (2017) revealed that this inhibition

of mitral cell activity is not uniform but is selective for the stimuli present during NA release, suggesting that different mitral cells respond distinctively to NA stimulation.

In summary, our data provide evidence that NA can be released near VSNs and increase the spiking frequency of VSNs through the activation of alpha 1a adrenergic receptors, leading to a cytosolic increase in Ca^{2+} levels. This study shows that NA is a crucial regulator of VSN signaling and provides a foundation for future work investigating molecular aspects underlying NA modulation and interactions between the sympathetic nervous system and chemosensory processing.

Limitations of the study

In our study, several questions remain unanswered. Determining whether NA selectively influences specific subsets of VSNs (e.g., V1R, V2R or FPR-expressing VSNs), and/or the detection of particular classes of signal molecules (e.g., high or low molecular weight molecules) would yield valuable insights, also related to heterogenous responses in AOB mitral cells (Doyle and Meeks 2017). Furthermore, confirming whether the same nerve fibers innervate both sensory and non-sensory epithelia would support the hypothesis of coordinated stimulus uptake and VSN sensitivity regulation driven by NA. Investigating the precise temporal and spatial dynamics of NA on VSNs, would require the use of genetic tools for stimulating neurotransmitter release in the intact tissue, thus avoiding artifacts associated with an external perfusion system stimulation.

Methods

Animals and ethical approval

Mice were handled according to the guidelines of the Italian Animal Welfare Act (Decreto legislativo 26/2014) and European Union guidelines on animal research (2010/63) under a protocol approved by SISSA's Animal Care Committee and the Italian Ministry of Health. Mice had free access to water and food. Every effort was made to reduce the number of animals used. C57BL/6 mice of both sexes (age range, 2–3 months) were anesthetized with CO_2 and decapitated before removal of the VNO.

Electrophysiological recordings from VSNs in acute VNO slices

Acute slices of mouse VNO were prepared as previously described (Dibattista et al. 2012; Hernandez-Clavijo et al. 2021; Shimazaki et al. 2006; Wong et al. 2018; Sarno et al. 2022). The VNO was removed and transferred to ice-cold artificial cerebrospinal fluid (ACSF). The capsule and all cartilaginous tissues were removed using fine forceps obtaining the two clean halves of the VNO. Each half was embedded in 3% agarose (A7002, Sigma-Aldrich) prepared in ACSF, once the agar had cooled to 37 °C. Upon solidification, the agarose block was fixed in a glass Petri dish filled by ice-cold oxygenated ACSF solution and sliced with a vibratome (Vibratome 1000 Plus Sectioning System, Vibratome Company) at 200 µm. Slices were then left to recover for over 30 min before electrophysiological experiments were initiated.

Slices were viewed with an upright microscope (Olympus BX51WI) using infrared differential contrast optics with water immersion 20X or 60X objectives. The slice was attached to the base of the recording chamber using a home-made U-shaped silver wire and VSNs could be distinguished based on their morphology. Patch pipettes, pulled from borosilicate capillaries (WPI) with a PC-10 puller (Narishige), had a resistance ranging from 3 to 6 MΩ. Electrophysiological recordings were made using a Multiclamp 700B amplifier controlled by Clampex 10 via a Digidata 1440 (Molecular Devices). Data were low-pass filtered at 2 kHz and sampled at 10 kHz. Experiments were performed at room temperature (20–25°C). The recording chamber was continuously perfused by gravity flow with oxygenated (95% O2 and 5% CO2) ACSF.

For current-clamp recordings, the intracellular solution filling the patch pipette contained the following (in mM): 80 K-gluconate, 60 KCl, 2 Mg-ATP, 10 HEPES, and 1 EGTA, adjusted to pH 7.2 with KOH. For some experiments, 1 mM EGTA was replaced with 10 mM BAPTA. An extracellular high K^+ solution, prepared from ACSF by replacing 25 mM NaCl with KCl, was used to test the viability of neurons. Urine was collected from both sexes of C57BL-BALB/c mice, filtered with a 0.2 µm filter, and frozen at −80°C for no more than 2 months to maintain the integrity of pheromones. Before use, male and female urine samples were mixed in a 1:1 ratio, and the mixture was diluted to 1:50 in ACSF, pH 7.4.

Stimuli were delivered through an 8-into-1 multibarrel perfusion pencil connected to a ValveLink8.2 pinch valve perfusion system (AutoMate Scientific). Adrenergic agonists or antagonists were applied for 3 min before starting recordings and washout was measured 5 min after removal of compounds with perfusion with ACSF, unless otherwise indicated.

Igor Pro 6.7/8 software (WaveMetrics, Lake Oswego, OR, USA) was used for data analysis.

Calcium imaging from dissociated VSNs

VSNs were dissociated using enzymatic and mechanical treatments as previously described (Dibattista et al. 2008; 2012; Amjad et al. 2015). The whole VNOs were carefully dissected and cut into 5 coronal sections under a stereoscopic microscope (Olympus SZ60) in artificial cerebrospinal fluid (ACSF) solution containing (in mM): 120 NaCl, 20 $NaHCO_3$, 5 KCl, 2 $CaCl_2$, 1 $MgSO_4$, 10 HEPES, and 10 glucose, pH 7.4. VNO sections were incubated with collagenase II (1 mg/ml in PBS) for 25 minutes at 37°C, then transferred to a stop solution containing ACSF with 5% FBS. Subsequently, mechanical dissociation was performed using fire-polished glass pipettes in ACSF solution containing the Ca^{2+} indicator Fluo-4 AM (5 μM; Thermo Fisher Scientific), 0.001% pluronic F-127 (20% solution in DMSO; Thermo Fisher Scientific), and 5% FBS. Dissociated cells were plated for 1-4 hours at 4 °C in dishes (FluoroDishTM; World Precision Instruments) coated with concanavalin-A (5 mg/ml) and then washed with ACSF.

Ca^{2+}-imaging experiments were performed using an epifluorescence inverted microscope with a mercury fluorescence lamp U-RF-T (IX70; Olympus). A dish containing dissociated cells was placed on the stage of the microscope and continuously perfused by gravity flow with oxygenated (95% O_2 and 5% CO_2) ACSF. The microscope was equipped with a Filter Block U-MWIB2 (Excitation filter EX 460-90, Dichromatic mirror DM 505, Emission filter EM 510IF) and a 40X (0.75 NA) objective (UPlanFL; Olympus). An ORCA-Flash4.0 V3 Digital CMOS camera (C13440-22CU, Hamamatsu) was used with the sotware HCImage Live (Hamamatsu). Data were acquired at 5 Hz with 512 × 512 pixel resolution. Changes in fluorescence signals were measured from specific regions of interest (ROIs) delineated around single neurons using ImageJ 1.51 s (National Institute of Health). Data were normalized and plotted as fluorescence changes: $\Delta F/F_0 = (F(t) - F_0)/F_0$, where F_0 is the average fluorescence intensity before the initial stimulus application and F(t) is the fluorescence amplitude at time t. Subsequent analysis and generation of figures were conducted employing IgorPro 6.3.7.2 (Wavemetrics). A neuron was considered responsive if it statisfied the following criteria: (a) high K^+ stimulation (25 mM) induced a Ca^{2+} transient, and (b) after the stimulus, $\Delta F/F_0$ was higher than the mean intensity measured during the prestimulus (15 s), plus three standard deviations for at least 5 s. In some experiments, the reduction of fluorescence signal due to photobleaching was mathematically corrected using the exponential decay observed in non-responding cells

Stimuli were delivered through an 8-into-1 multibarrel perfusion pencil connected to a ValveLink8.2 pinch valve perfusion system (AutoMate Scientific). Adrenergic agonists were applied for 20 s followed by 3 min washout with ACSF. Prazosin was applied for 5 min followed by 3-5 min washout with ACSF.

Single-cell RNA sequencing data analysis

Single-cell RNA sequencing (scRNA-seq) dataset was downloaded from NCBI GEO: GSE190330 and was related to the study by Katreddi et al. (2022). Data consist of single cell 3' RNAseq of dissociated VNO cells from 5 male C57BL/6J mice at postnatal

day 60. 10X Genomics Chromium platform and Illumina Novaseq 6000 technology was used for sequencing. The data was analysed in R version 4.1.2 using the Seurat R package version 4.1.0, a widely used toolkit for quality control, analysis and exploration of single cell RNA sequencing data. The procedures described in Katreddi et al. (2022), with minimal modifications were used for analysing this dataset. Cells that expressed >7000 genes, <700 genes, or >10% mitochondrial genes were not included in analysis. After filtering, data from 14,851 cells were included for clustering and analysis. We used NormalizeData() function with LogNormalize as normalization method. With FindVariableFeatures() function we selected the top 2,000 highly variable genes across the population to perform principal component analysis using RunPCA(), FindNeighbors(), FindClusters() and RunUMAP() Seurat functions. The first 30 principal components were used for cell clustering, which was visualized using UMAP. We identified cell types based on known gene expression as previously shown (Katreddi et al. 2022).

Immunohistochemistry

VNO tissue was dissected and immediately fixed in Glyoxal 9% + acetic acid 8% solution in PBS overnight at 4 C (Konno et al. 2023). For cryoprotection tissue was equilibrated overnight in 30% (w/v) sucrose in PBS at 4 °C. Then, the tissue was embedded in Tissue Freezing Medium (Leica Biosystems) and immediately frozen at -80 °C. 20 µm coronal sections and 50 µm horizontal sections were cut on a Leica CM3050 cryostat (Leica Biosystems), mounted on Superfrost Plus slides (Menzel, Braunschweig, Germany), and stored at -20°C. To remove the cryostat embedding medium from tissue, the slices were incubated for 15 min with PBS, then incubated in blocking solution (5% normal donkey serum, 0.2% Triton X-100 in PBS) for 90 min and finally overnight at 4 °C in primary antibody anti-Tyrosine Hydroxylase Vio® R667-conjugated 1:500 (Miltenyi Biotec, cat # 130-131-157). After removal of the excess of primary antibody with PBS washes, sections were incubated with DAPI (5 µg/ml) for 30 min at RT for nuclear staining. Excess of DAPI was washed and the sections were mounted in Fluoromount-G Mounting Medium (ThermoFisher, cat # 00-4958-02) Immunofluorescence was visualized with a confocal laser scanning microscope (Leica Microsystems, TCS SP5 DM6000 CFS). Images were acquired using LAS-X acquisition software (Leica Microsystems) at 1024 × 1024 pixels resolution and analyzed with ImageJ software (National Institute of Health, USA). The maximum projections of 5 µm optical slices were displayed. Control experiments, excluding primary antibodies, were performed for each immunolocalization.

Chemicals

All chemicals were obtained from Sigma-Aldrich unless otherwise specified. NA and methoxamine were prepared as 100 mM stock solutions, while prazosin was prepared as 1 mM stock solution and diluted to the final concentrations in ACSF.

Data and statistical analysis

Igor Pro 6.7/8 software (WaveMetrics, Lake Oswego, OR, USA) was used for data analysis and figure preparation. Averaged data from individual experiments in different VSNs are presented as mean ± standard deviation (SD) along with the number of cells (n).

Statistical significance was determined through the following tests. The Shapiro–Wilk test was employed to verify data normality (performed by R). For normally distributed data, repeated measures ANOVA followed by a paired t-test with Bonferroni correction (performed by Igor Pro) or mixed model two way ANOVA followed by paired t test with Bonferroni correction (performed by GraphPad). In the case of not normally distributed data, statistical significance was assessed using Friedman's test followed by Demsar's test. The P values associated to Desmar test were calculated using the algorithm in R developed by Eisinga et al. (2017).

Data availability

All relevant data are available from the corresponding authors.

Competing interests

The authors declare no competing interests.

Author contributions

C.A.S.T., A.H.C., S.P. and A.M. conceptualized the project and designed experiments. C.A.S.T., A.H.C. and K.Y.G.V. performed experiments and data analysis. C.A.S.T. , S.P. and A.M. wrote the manuscript with comments from all the other authors.

References

Adams, D. R. 1992. "Fine Structure of the Vomeronasal and Septal Olfactory Epithelia and of Glandular Structures." *Microscopy Research and Technique* 23 (1): 86–97. https://doi.org/10.1002/jemt.1070230108.

Amjad, Asma, Andres Hernandez-Clavijo, Simone Pifferi, Devendra Kumar Maurya, Anna Boccaccio, Jessica Franzot, Jason Rock, and Anna Menini. 2015. "Conditional Knockout of TMEM16A/Anoctamin1 Abolishes the Calcium-Activated Chloride Current in Mouse Vomeronasal Sensory Neurons." *The Journal of General Physiology* 145 (4): 285–301. https://doi.org/10.1085/jgp.201411348.

Araneda, Ricardo C., and Stuart Firestein. 2006. "Adrenergic Enhancement of Inhibitory Transmission in the Accessory Olfactory Bulb." *The Journal of Neuroscience: The Official Journal of the Society for Neuroscience* 26 (12): 3292–98. https://doi.org/10.1523/JNEUROSCI.4768-05.2006.

Ben-Shaul, Y., L. C. Katz, R. Mooney, and C. Dulac. 2010. "In Vivo Vomeronasal Stimulation Reveals Sensory Encoding of Conspecific and Allospecific Cues by the Mouse Accessory Olfactory Bulb." *Proceedings of the National Academy of Sciences of the United States of America* 107 (11): 5172–77. https://doi.org/10.1073/pnas.0915147107.

Brennan, P. A., K. M. Kendrick, and E. B. Keverne. 1995. "Neurotransmitter Release in the Accessory Olfactory Bulb during and after the Formation of an Olfactory Memory

in Mice." *Neuroscience* 69 (4): 1075–86. https://doi.org/10.1016/0306-4522(95)00309-7.
Brennan, P. A. 2004. "The Nose Knows Who's Who: Chemosensory Individuality and Mate Recognition in Mice." *Hormones and Behavior* 46 (3): 231–40. https://doi.org/10.1016/j.yhbeh.2004.01.010.
Dibattista, Michele, Asma Amjad, Devendra Kumar Maurya, Claudia Sagheddu, Giorgia Montani, Roberto Tirindelli, and Anna Menini. 2012. "Calcium-Activated Chloride Channels in the Apical Region of Mouse Vomeronasal Sensory Neurons." *The Journal of General Physiology* 140 (1): 3–15. https://doi.org/10.1085/jgp.201210780.
Dibattista, Michele, Andrea Mazzatenta, Francesca Grassi, Roberto Tirindelli, and Anna Menini. 2008. "Hyperpolarization-Activated Cyclic Nucleotide-Gated Channels in Mouse Vomeronasal Sensory Neurons." *Journal of Neurophysiology* 100 (2): 576–86. https://doi.org/10.1152/jn.90263.2008.
Døving, K. B., and D. Trotier. 1998. "Structure and Function of the Vomeronasal Organ." *The Journal of Experimental Biology* 201 (Pt 21): 2913–25.
Doyle, Wayne I., Jordan A. Dinser, Hillary L. Cansler, Xingjian Zhang, Daniel D. Dinh, Natasha S. Browder, Ian M. Riddington, and Julian P. Meeks. 2016. "Faecal Bile Acids Are Natural Ligands of the Mouse Accessory Olfactory System." *Nature Communications* 7 (June): 11936. https://doi.org/10.1038/ncomms11936.
Doyle, Wayne I., and Julian P. Meeks. 2017. "Heterogeneous Effects of Norepinephrine on Spontaneous and Stimulus-Driven Activity in the Male Accessory Olfactory Bulb." *Journal of Neurophysiology* 117 (3): 1342–51. https://doi.org/10.1152/jn.00871.2016.
Eisinga, Rob, Tom Heskes, Ben Pelzer, and Manfred Te Grotenhuis. 2017. "Exact P-Values for Pairwise Comparison of Friedman Rank Sums, with Application to Comparing Classifiers." *BMC Bioinformatics* 18 (1): 68. https://doi.org/10.1186/s12859-017-1486-2.
Firestein, S., and A. Menini. 1999. "The Smell of Adrenaline." *Nature Neuroscience* 2 (2): 106–8. https://doi.org/10.1038/5661.
Francia, Simona, Simone Pifferi, Anna Menini, and Roberto Tirindelli. 2014. "Vomeronasal Receptors and Signal Transduction in the Vomeronasal Organ of Mammals." In *Neurobiology of Chemical Communication*, edited by Carla Mucignat-Caretta. Frontiers in Neuroscience. Boca Raton (FL): CRC Press/Taylor & Francis. http://www.ncbi.nlm.nih.gov/books/NBK200993/.
Graham, R. M. 1990. "Adrenergic Receptors: Structure and Function." *Cleveland Clinic Journal of Medicine* 57 (5): 481–91. https://doi.org/10.3949/ccjm.57.5.481.
Hall, Randy A. 2011. "Autonomic Modulation of Olfactory Signaling." *Science Signaling* 4 (155): pe1. https://doi.org/10.1126/scisignal.2001672.
Hamacher, Christoph, Rudolf Degen, Melissa Franke, Victoria K. Switacz, David Fleck, Raghu Ram Katreddi, Andres Hernandez-Clavijo, et al. 2024. "A Revised Conceptual Framework for Mouse Vomeronasal Pumping and Stimulus Sampling." *Current Biology: CB*, January, S0960-9822(24)00034-4. https://doi.org/10.1016/j.cub.2024.01.036.
Hernandez-Clavijo, Andres, Nicole Sarno, Kevin Y. Gonzalez-Velandia, Rudolf Degen, David Fleck, Jason R. Rock, Marc Spehr, Anna Menini, and Simone Pifferi. 2021. "TMEM16A and TMEM16B Modulate Pheromone-Evoked Action Potential Firing in Mouse Vomeronasal Sensory Neurons." *eNeuro* 8 (5): ENEURO.0179-21.2021. https://doi.org/10.1523/ENEURO.0179-21.2021.

Insel, P. A. 1989. “Structure and Function of Alpha-Adrenergic Receptors.” *The American Journal of Medicine* 87 (2A): 12S-18S. https://doi.org/10.1016/0002-9343(89)90108-3.

Iwanaga, Toshihiko, and Junko Nio-Kobayashi. 2020. “Unique Blood Vasculature and Innervation in the Cavernous Tissue of Murine Vomeronasal Organs.” *Biomedical Research (Tokyo, Japan)* 41 (5): 243–51. https://doi.org/10.2220/biomedres.41.243.

Katreddi, Raghu Ram, Ed Zandro M. Taroc, Sawyer M. Hicks, Jennifer M. Lin, Shuting Liu, Mengqing Xiang, and Paolo E. Forni. 2022. “Notch Signaling Determines Cell-Fate Specification of the Two Main Types of Vomeronasal Neurons of Rodents.” *Development (Cambridge, England)* 149 (13): dev200448. https://doi.org/10.1242/dev.200448.

Kawai, F., T. Kurahashi, and A. Kaneko. 1999. “Adrenaline Enhances Odorant Contrast by Modulating Signal Encoding in Olfactory Receptor Cells.” *Nature Neuroscience* 2 (2): 133–38. https://doi.org/10.1038/5686.

Konno, Kohtarou, Miwako Yamasaki, Taisuke Miyazaki, and Masahiko Watanabe. 2023. “Glyoxal Fixation: An Approach to Solve Immunohistochemical Problem in Neuroscience Research.” *Science Advances* 9 (28): eadf7084. https://doi.org/10.1126/sciadv.adf7084.

Langer, S. Z., I. Cavero, and R. Massingham. 1980. “Recent Developments in Noradrenergic Neurotransmission and Its Relevance to the Mechanism of Action of Certain Antihypertensive Agents.” *Hypertension (Dallas, Tex.: 1979)* 2 (4): 372–82. https://doi.org/10.1161/01.hyp.2.4.372.

Lorenzon, Paolo, Kamil Antos, Anushree Tripathi, Viktoria Vedin, Anna Berghard, and Paolo Medini. 2023. “In Vivo Spontaneous Activity and Coital-Evoked Inhibition of Mouse Accessory Olfactory Bulb Output Neurons.” *iScience* 26 (9): 107545. https://doi.org/10.1016/j.isci.2023.107545.

McCorry, Laurie Kelly. 2007. “Physiology of the Autonomic Nervous System.” *American Journal of Pharmaceutical Education* 71 (4): 78. https://doi.org/10.5688/aj710478.

McLean, J. H., M. T. Shipley, W. T. Nickell, G. Aston-Jones, and C. K. Reyher. 1989. “Chemoanatomical Organization of the Noradrenergic Input from Locus Coeruleus to the Olfactory Bulb of the Adult Rat.” *The Journal of Comparative Neurology* 285 (3): 339–49. https://doi.org/10.1002/cne.902850305.

Meredith, M. 1994. “Chronic Recording of Vomeronasal Pump Activation in Awake Behaving Hamsters.” *Physiology & Behavior* 56 (2): 345–54. https://doi.org/10.1016/0031-9384(94)90205-4.

Michelotti, G. A., D. T. Price, and D. A. Schwinn. 2000. “Alpha 1-Adrenergic Receptor Regulation: Basic Science and Clinical Implications.” *Pharmacology & Therapeutics* 88 (3): 281–309. https://doi.org/10.1016/s0163-7258(00)00092-9.

Mohrhardt, Julia, Maximilian Nagel, David Fleck, Yoram Ben-Shaul, and Marc Spehr. 2018. “Signal Detection and Coding in the Accessory Olfactory System.” *Chemical Senses* 43 (9): 667–95. https://doi.org/10.1093/chemse/bjy061.

Moss, R. L., R. E. Flynn, X. M. Shen, C. Dudley, J. Shi, and M. Novotny. 1997. “Urine-Derived Compound Evokes Membrane Responses in Mouse Vomeronasal Receptor Neurons.” *Journal of Neurophysiology* 77 (5): 2856–62. https://doi.org/10.1152/jn.1997.77.5.2856.

Ostrin, Lisa A., and Adrian Glasser. 2010. “Autonomic Drugs and the Accommodative System in Rhesus Monkeys.” *Experimental Eye Research* 90 (1): 104–12. https://doi.org/10.1016/j.exer.2009.09.015.

Salazar, Ignacio, Pablo Sánchez-Quinteiro, Nuria Alemañ, and Dolores Prieto. 2008. "Anatomical, Immnunohistochemical and Physiological Characteristics of the Vomeronasal Vessels in Cows and Their Possible Role in Vomeronasal Reception." *Journal of Anatomy* 212 (5): 686–96. https://doi.org/10.1111/j.1469-7580.2008.00889.x.

Sarno, Nicole, Andres Hernandez-Clavijo, Anna Boccaccio, Anna Menini, and Simone Pifferi. 2022. "Slow Inactivation of Sodium Channels Contributes to Short-Term Adaptation in Vomeronasal Sensory Neurons." *eNeuro* 9 (3): ENEURO.0471-21.2022. https://doi.org/10.1523/ENEURO.0471-21.2022.

Shimazaki, Ranken, Anna Boccaccio, Andrea Mazzatenta, Giulietta Pinato, Michele Migliore, and Anna Menini. 2006. "Electrophysiological Properties and Modeling of Murine Vomeronasal Sensory Neurons in Acute Slice Preparations." *Chemical Senses* 31 (5): 425–35. https://doi.org/10.1093/chemse/bjj047.

Smith, Richard S., Christopher J. Weitz, and Ricardo C. Araneda. 2009. "Excitatory Actions of Noradrenaline and Metabotropic Glutamate Receptor Activation in Granule Cells of the Accessory Olfactory Bulb." *Journal of Neurophysiology* 102 (2): 1103–14. https://doi.org/10.1152/jn.91093.2008.

Stowers, Lisa, Timothy E. Holy, Markus Meister, Catherine Dulac, and Georgy Koentges. 2002. "Loss of Sex Discrimination and Male-Male Aggression in Mice Deficient for TRP2." *Science (New York, N.Y.)* 295 (5559): 1493–1500. https://doi.org/10.1126/science.1069259.

Tirindelli, Roberto. 2021. "Coding of Pheromones by Vomeronasal Receptors." *Cell and Tissue Research* 383 (1): 367–86. https://doi.org/10.1007/s00441-020-03376-6.

Tirindelli, Roberto, Michele Dibattista, Simone Pifferi, and Anna Menini. 2009. "From Pheromones to Behavior." *Physiological Reviews* 89 (3): 921–56. https://doi.org/10.1152/physrev.00037.2008.

Tsujimoto, G., A. Tsujimoto, E. Suzuki, and K. Hashimoto. 1989. "Glycogen Phosphorylase Activation by Two Different Alpha 1-Adrenergic Receptor Subtypes: Methoxamine Selectively Stimulates a Putative Alpha 1-Adrenergic Receptor Subtype (Alpha 1a) That Couples with Ca2+ Influx." *Molecular Pharmacology* 36 (1): 166–76.

Velásquez-Martinez, M. C., R. Vázquez-Torres, and C. A. Jiménez-Rivera. 2012. "Activation of Alpha1-Adrenoceptors Enhances Glutamate Release onto Ventral Tegmental Area Dopamine Cells." *Neuroscience* 216 (August): 18–30. https://doi.org/10.1016/j.neuroscience.2012.03.056.

Wong, Wen Mai, Maximilian Nagel, Andres Hernandez-Clavijo, Simone Pifferi, Anna Menini, Marc Spehr, and Julian P. Meeks. 2018. "Sensory Adaptation to Chemical Cues by Vomeronasal Sensory Neurons." *eNeuro* 5 (4). https://doi.org/10.1523/ENEURO.0223-18.2018.

Zhong, H., and K. P. Minneman. 1999. "Alpha1-Adrenoceptor Subtypes." *European Journal of Pharmacology* 375 (1–3): 261–76. https://doi.org/10.1016/s0014-2999(99)00222-8.

Zufall, F. 2005. "The TRPC2 Ion Channel and Pheromone Sensing in the Accessory Olfactory System." *Naunyn-Schmiedeberg's Archives of Pharmacology* 371 (4): 245–50. https://doi.org/10.1007/s00210-005-1028-

5.2. Shedding light on human olfaction: Electrophysiological recordings from sensory neurons in acute slices of olfactory epithelium

Andres Hernandez-Clavijo*, **Cesar Adolfo Sánchez Triviño**#, Giorgia Guarneri*, Chiara Ricci, Fabian A. Mantilla-Esparza, Kevin Y. Gonzalez-Velandia, Paolo Boscolo-Rizzo, Margherita Tofanelli, Pierluigi Bonini, Michele Dibattista, Giancarlo Tirelli, and Anna Menini.

Analyzed data and performed electrophysiological recordings.

iScience

Published: June 20, 2023

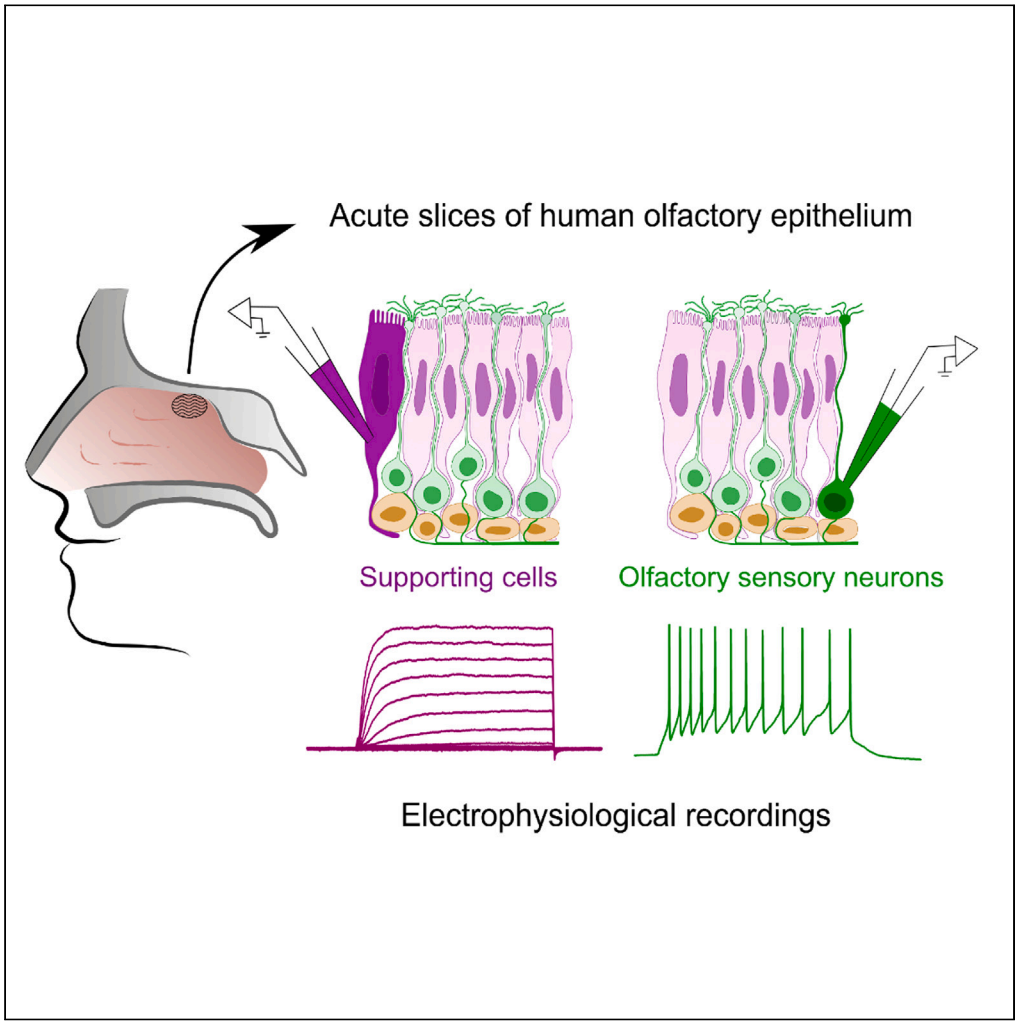
DOI: https://doi.org/10.1016/j.isci.2023.107186

iScience

CellPress
OPEN ACCESS

Article

Shedding light on human olfaction: Electrophysiological recordings from sensory neurons in acute slices of olfactory epithelium



Andres Hernandez-Clavijo, Cesar Adolfo Sánchez Triviño, Giorgia Guarneri, ..., Michele Dibattista, Giancarlo Tirelli, Anna Menini

michele.dibattista@uniba.it (M.D.)
anna.menini@sissa.it (A.M.)

Highlights

Acute slices of human olfactory epithelium are viable for patch-clamp recordings

Supporting cells (non-neuronal) exhibit outward voltage-gated currents

Olfactory sensory neurons display diverse patterns of action potentials

Olfactory sensory neurons respond to odorants and other stimuli

Hernandez-Clavijo et al., iScience *26*, 107186
July 21, 2023 © 2023 The Author(s).
https://doi.org/10.1016/j.isci.2023.107186

iScience

CellPress
OPEN ACCESS

Article

Shedding light on human olfaction: Electrophysiological recordings from sensory neurons in acute slices of olfactory epithelium

Andres Hernandez-Clavijo,[1,4,6] Cesar Adolfo Sánchez Triviño,[1,4] Giorgia Guarneri,[1,4] Chiara Ricci,[1] Fabian A. Mantilla-Esparza,[1] Kevin Y. Gonzalez-Velandia,[1] Paolo Boscolo-Rizzo,[2] Margherita Tofanelli,[2] Pierluigi Bonini,[2] Michele Dibattista,[3,*] Giancarlo Tirelli,[2] and Anna Menini[1,5,*]

SUMMARY

The COVID-19 pandemic brought attention to our limited understanding of human olfactory physiology. While the cellular composition of the human olfactory epithelium is similar to that of other vertebrates, its functional properties are largely unknown. We prepared acute slices of human olfactory epithelium from nasal biopsies and used the whole-cell patch-clamp technique to record electrical properties of cells. We measured voltage-gated currents in human olfactory sensory neurons and supporting cells, and action potentials in neurons. Additionally, neuronal inward current and action potentials responses to a phosphodiesterase inhibitor suggested a transduction cascade involving cAMP as a second messenger. Furthermore, responses to odorant mixtures demonstrated that the transduction cascade was intact in this preparation. This study provides the first electrophysiological characterization of olfactory sensory neurons in acute slices of the human olfactory epithelium, paving the way for future research to expand our knowledge of human olfactory physiology.

INTRODUCTION

Human olfaction has long been considered a neglected sense and the recent COVID-19 pandemic has highlighted the scarce knowledge we have of human olfactory physiology. The sudden and widespread olfactory loss experienced during the pandemic caught us unprepared, with many individuals struggling to recover their sense of smell.[1–7] Indeed, although the morphology of the human olfactory epithelium was well known, there was limited knowledge about the molecular and functional landscape of different cell types within the human olfactory epithelium. Molecular data became soon available in the early phase of the pandemic[8–11] but the functional properties of the cells are still largely unknown.

The human olfactory epithelium is located in the upper posterior part of the nasal cavity, and it is found in patchy regions that alternate with non-sensory epithelium. Its cellular composition and organization are similar to that of most other vertebrates.[12–15] The epithelium consists of three main cell types: olfactory sensory neurons, supporting (or sustentacular) cells, and basal cells. Olfactory sensory neurons are bipolar neurons that have one dendrite ending with a knob from which several cilia originate at the surface of the epithelium, a soma, and a single axon reaching the olfactory bulb. Supporting cells, the "unsung heroes"[10] of the olfactory epithelium, are columnar in shape, extending from the basal to the apical portion of the epithelium. They provide structural support to olfactory sensory neurons, and bear microvilli on their apical side.[16] Basal cells are located at the basal part of the epithelium and have the ability to regenerate various cell types within the olfactory epithelium.[11,16,17]

Recent research during the COVID-19 pandemic has identified supporting cells as the primary target of SARS-CoV-2 in the olfactory epithelium.[8–10] Furthermore, the compromised functionality of supporting cells, along with inflammatory processes, can exacerbate olfactory loss.[18,19]

Olfactory transduction in rodents and amphibians has been extensively studied and it is well established that it occurs in the cilia of olfactory sensory neurons.[20–24] This process begins with the binding of odorant

[1]Neuroscience Area, SISSA, Scuola Internazionale Superiore di Studi Avanzati, 34136 Trieste, Italy

[2]Department of Medical, Surgical and Health Sciences, Section of Otolaryngology, University of Trieste, 34149 Trieste, Italy

[3]Department of Translational Biomedicine and Neuroscience, University of Bari A. Moro, 70121 Bari, Italy

[4]These authors contributed equally

[5]Lead contact

[6]Present address: Department of Chemosensation, Institute for Biology II, RWTH Aachen University, Aachen, Germany

*Correspondence: michele.dibattista@uniba.it (M.D.), anna.menini@sissa.it (A.M.)

https://doi.org/10.1016/j.isci.2023.107186

This is an open access article under the CC BY-NC-ND license (http://creativecommons.org/licenses/by-nc-nd/4.0/).

molecules to specific G protein-coupled odorant receptors, which activate a biochemical cascade that increases cAMP concentration within the cilia. As a result, the open probability of cyclic nucleotide-gated (CNG) channels increases, allowing the entry of Na^+ and Ca^{2+} and inducing neuron depolarization.[25–28] The increase in Ca^{2+} concentration within the cilia then activates the Ca^{2+}-activated Cl^- channel TMEM16B (also named ANO2) that contributes to regulate neuron depolarization.[29–35] When the depolarization reaches the threshold, action potentials are generated and transmitted to the olfactory bulb.[36–38] In combination with calmodulin, Ca^{2+} also contributes to response termination by enhancing the activity of the phosphodiesterase PDE1C2, which hydrolyzes cAMP, reducing the open probability of CNG channels.[39,40] The use of the PDE inhibitor 3-isobutyl-1-methylxanthine (IBMX) has unveiled the presence of a basal cAMP concentration, as upon IBMX application, inward currents were measured in the whole-cell voltage-clamp configuration in olfactory sensory neurons in amphibians and rodents.[41–43] Basal cAMP fluctuations (hence the IBMX response) are caused by the constitutive activity of odorant receptors that activate the transduction cascade, producing a depolarization followed by action potential generation. Different odorant receptors show different levels of constitutive activity.[44–46]

The mature olfactory sensory neurons, which express the olfactory marker protein (OMP)[47,48] and only one odorant receptor type among about 400–1000,[10,49] are the main functional units in the olfactory epithelium in most vertebrates, including humans. In human mature olfactory sensory neurons, some genes coding for proteins known to be involved in odorant signal transduction in rodents are expressed, such as several odorant receptor genes, G protein alpha and gamma subunits, adenylyl cyclase type 3, cyclic nucleotide-gated channel alpha2, and the calcium-activated chloride channel (*TMEM16B*/ANO2).[8–11,50] However, while immunohistochemistry data have confirmed expression of the G protein alpha and gamma subunits in human olfactory sensory neurons,[11,13] no data have been published for the other proteins potentially involved in the human olfactory transduction cascade.

From a functional point of view, a pioneering study by Restrepo et al.[51] reported that viable human olfactory sensory neurons could be dissociated from olfactory tissue biopsies, and showed, by using Ca^{2+} imaging, that some neurons responded to odorants with an increase in intracellular Ca^{2+} concentration. Further studies by the same laboratory[52,53] showed that some human olfactory neurons also responded to odorants with a decrease in intracellular Ca^{2+} concentration, a response never observed in neurons from other vertebrates,[51,54–56] suggesting that human olfactory neurons have unique properties compared to other vertebrates. Moreover, Gomez et al.[57] found that protein kinases A and C modulate odorant responses in different ways in human and rat olfactory neurons, indicating additional differences between the two species. Overall, these studies provided insight into the odorant-induced Ca^{2+} changes in human olfactory neurons revealing differences from other vertebrates.

In rodents and amphibians, electrophysiological techniques have been extensively used to study the functional properties of olfactory sensory neurons while only a few studies have been reported in humans.[51,58,59] One of these studies used the inside-out patch-clamp technique from the dendritic knob of dissociated human olfactory neurons to characterize activation of CNG channels by cAMP, providing evidence that these channels may be involved in olfactory transduction in humans.[58] Two other reports investigated the electrical properties of isolated human olfactory neurons with the whole-cell patch-clamp technique.[51,59] Both studies consistently measured outward voltage-gated currents in response to depolarizing voltage steps, while transient inward currents were rarely observed in human olfactory neurons. The absence of transient inward currents in most human olfactory neurons is surprising, as they are found in other vertebrates,[60] and this may be due either to a unique aspect of human olfactory transduction[59] or to neuron damage during the dissociation procedure.[51]

Knowledge of the initial electrical events in human olfactory neurons is crucial for understanding the signals transmitted from the periphery to the brain. To achieve this, it is essential to use a preparation that closely mimics the physiological environment of human olfactory sensory neurons. In our study, we developed a technique to obtain acute slices from biopsies of the human olfactory epithelium, which provides a more physiological setting for olfactory neurons than dissociated cells. Using this preparation, we employed the whole-cell patch-clamp technique to measure the basic biophysical properties and voltage-gated currents of olfactory sensory neurons and supporting cells, and recorded action potential generation in olfactory neurons. Moreover, we were able to record IBMX and odorant-induced

transduction currents, providing the first functional characterization of olfactory sensory neurons from acute slices of the human olfactory epithelium.

RESULTS

Immunohistochemistry of the human olfactory epithelium

We performed an immunohistochemical analysis of biopsies of human nasal tissues using specific markers to identify the presence of olfactory sensory neurons and supporting cells.

We used β-tubulin III (TUJ1) a known marker for neurons and the OMP to stain mature olfactory sensory neurons and clearly identified the typical bipolar morphology of olfactory sensory neurons (Figure 1A) with cell bodies within the epithelium and a dendrite extending until the apical side. Axon bundles were also distinguishable under the basal lamina. To identify supporting cells, we used ERMN as their marker[13,15] and observed a staining of the apical part of the epithelium, mutually exclusive with TUJ1 staining (Figure 1D).

Although it is well known that in rodents, several proteins of the transduction cascade are expressed in the apical dendritic knob and ciliary regions of olfactory sensory neurons, in humans, the expression and cellular localization of most of these proteins have not been investigated yet. Immunostaining with antibodies against adenylyl cyclase type 3 (AC3) and the Ca^{2+}-activated Cl^{-} channel TMEM16B revealed the expression of both proteins in the apical knob and ciliary region of the TUJ1-positive neurons (Figures 1B and 1C).

These results extend previous immunohistochemistry data showing that AC3 and TMEM16B are localized in the dendritic knob and cilia of human olfactory sensory neurons, where olfactory transduction takes place.

Voltage-gated currents in human olfactory sensory neurons and supporting cells

Since a very limited number of studies have attempted to measure the electrophysiological properties of human olfactory sensory neurons and these studies have been performed only on isolated neurons, we asked whether it is possible to record the electrical activity from cells in acute slices of the human olfactory epithelium. Slices may provide a more physiological environment to the olfactory neurons and better cell viability, important for obtaining long lasting and stable recordings.

We first established the viability of obtaining electrophysiological recordings by measuring basic electrical properties and voltage-gated currents in the whole-cell voltage-clamp configuration. To visually identify cells, we dissolved Alexa Fluor 594 in the intracellular solution filling the patch pipette and took fluorescence images after obtaining the whole-cell configuration and the diffusion of the fluorophore inside the cell (Figures 2A and 2D). A human olfactory sensory neuron, with its typical morphology comprising a cell body toward the basal part and a dendrite extending to the apical part of the epithelium, is shown in Figure 2A, demonstrating that it is possible to reach a whole-cell configuration and to visually identify neurons in acute slices of the human olfactory epithelium. We then evaluated the resting membrane potential in current clamp at I = 0 in neurons and calculated an average value of -52 ± 5 mV (range -76 to -24 mV, n = 13). The membrane input resistance, estimated in voltage clamp, had an average value of 4.2 ± 1.2 GΩ (range 1.0–9.7 GΩ, n = 12).

Next, we measured voltage-gated currents in human olfactory sensory neurons. Transient inward currents followed by outward currents were activated upon depolarization from a holding potential of -80 mV (Figure 2B). Current-voltage relations were measured at the peak of the inward currents or at the end of the sustained outward currents, averaged from several neurons and plotted in Figure 2C. The average current-voltage relations show that the transient inward current activated between -60 and -50 mV and reached a peak at -30 mV, with an average value of -0.7 ± 0.1 nA (n = 10) and then decreased toward 0 between 50 and 60 mV. Outward currents activated at about -30 mV and increased their amplitude with the depolarizing step potential reaching an average value of 1.1 ± 0.1 nA (n = 10) at +50 mV (Figure 2C).

We also recorded from supporting cells in the whole-cell voltage-clamp configuration. Fluorescence images of supporting cells showed their typical columnar shape with fine processes extending toward the

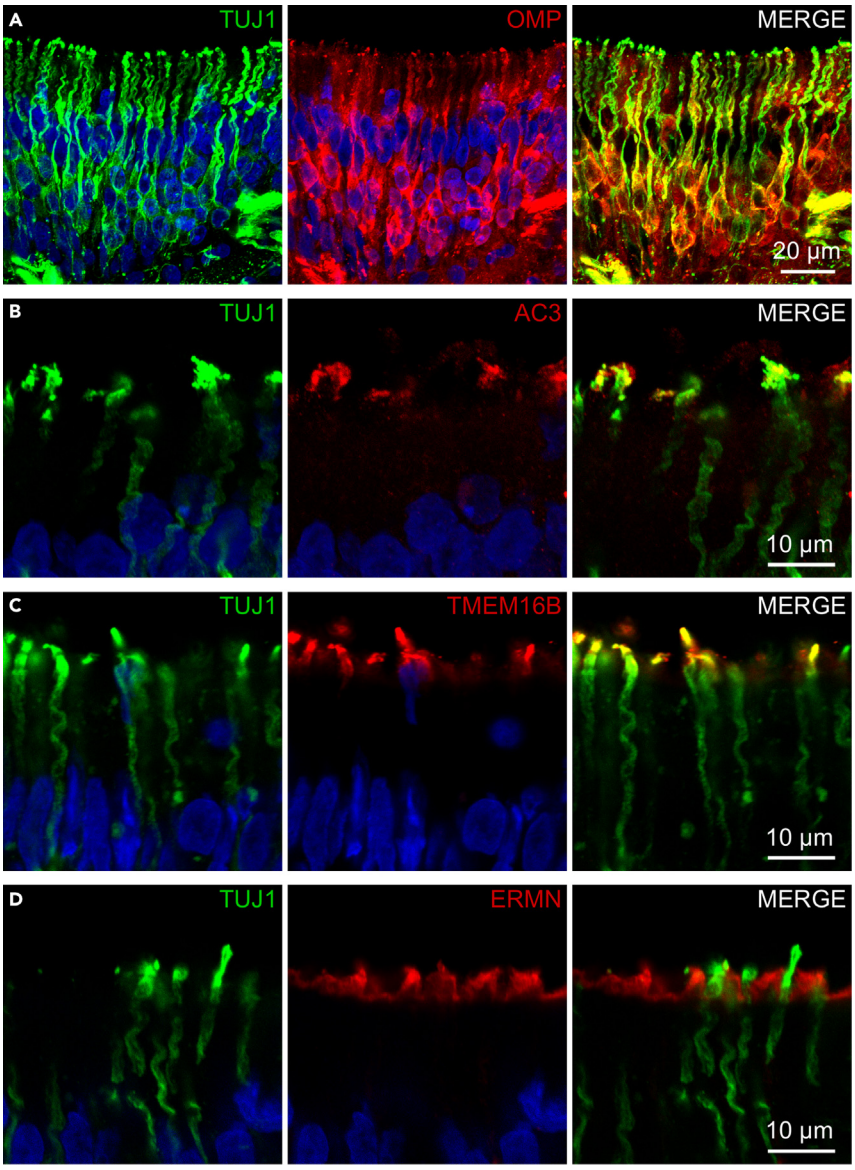


Figure 1. Olfactory sensory neurons from human olfactory epithelium express signal transduction proteins at the apical part

(A) Olfactory sensory neurons stained with the neuronal marker TUJ1 (green) and OMP (red).

(B) Co-expression of TUJ1 (green) and AC3 (red) at the apical part of olfactory sensory neurons.

(C) Co-expression of TUJ1 (green) and TMEM16B (red) at the apical part of olfactory sensory neurons. Note that AC3 and TMEM16B staining are present only in the dendritic knob and ciliary region of the neuron.

(D) Non-overlapping staining for the neuronal marker TUJ1 (green) and ERMN (red), a marker for the apical region of supporting cells. Cell nuclei were stained with DAPI (blue).

basal part of the epithelium (Figure 2D). The average membrane input resistance was 2.2 $\pm$ 0.6 GΩ (range 0.5–7.1 GΩ, n = 12). In a first set of experiments, we elicited voltage-gated currents with the same step protocol used for neurons from a holding potential of −80 mV and measured sustained outward currents (data not shown). As we and others have previously shown that supporting cells in mice also have voltage-activated transient inward currents,[61,62] in a second set of experiments, we lowered the holding potential to −120 mV before applying a depolarizing step protocol, also in this condition no transient inward currents were measured (Figure 2E). Outward currents activated at about −10 mV and increased with the depolarizing step potential (Figure 2F) reaching an average value of 0.7 $\pm$ 0.1 nA (n = 12) at +40 mV.

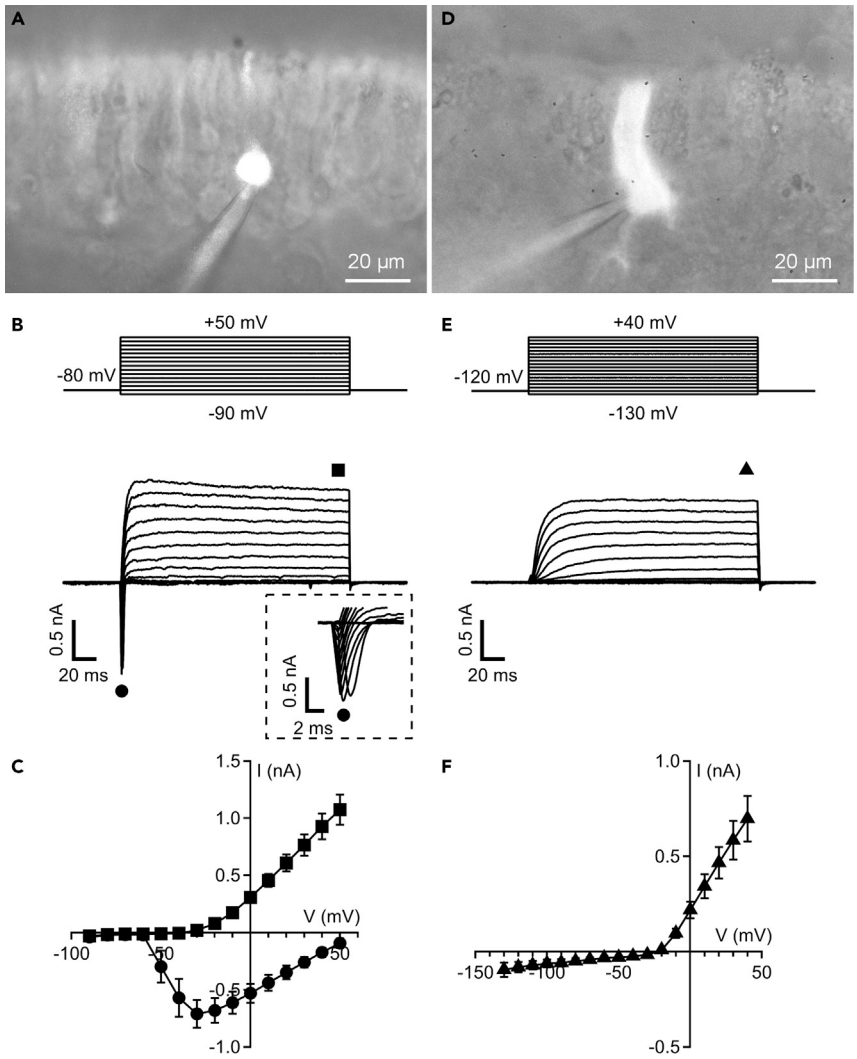


Figure 2. Voltage-gated currents in olfactory sensory neurons and supporting cells from acute slices of the human olfactory epithelium

(A and D) Fluorescence micrographs of an olfactory sensory neuron (A) and a supporting cell (D) filled with Alexa Fluor 594 through the patch pipette.

(B and E) Representative whole-cell currents recorded using the voltage protocols indicated at the top of the panels. The holding potential was −80 mV for olfactory sensory neurons (B) and −120 mV for supporting cells (E). Voltage steps in 10 mV increments were applied. The inset in (B) shows details of the inward currents on an expanded timescale.

(C and F) Plot of average ±SEM amplitudes of inward (black circles) and outward (black squares) currents in olfactory sensory neurons (C, n = 10) and outward (black triangles) currents in supporting cells (F, n = 12) versus the test potential.

These electrophysiological data show that voltage-gated currents in human olfactory sensory neurons have both transient inward currents and outward currents as in other vertebrate species. On the other side, human supporting cells displayed only outward voltage-gated currents, differently from mice, where also transient inward currents have been reported.

Firing patterns of human olfactory sensory neurons

To investigate the firing patterns of human olfactory sensory neurons in the acute slice preparation, we used whole-cell current-clamp recordings. The responses of three representative neurons to current injections from −2 to 10 pA of 2 s duration show the different types of spiking patterns we measured (Figure 3). The neuron at the top in Figure 3 generated a tonic firing consisting of sustained train of action potentials in response to current injection of 2 pA and displayed an increasing number of spikes up to 6 pA current steps.

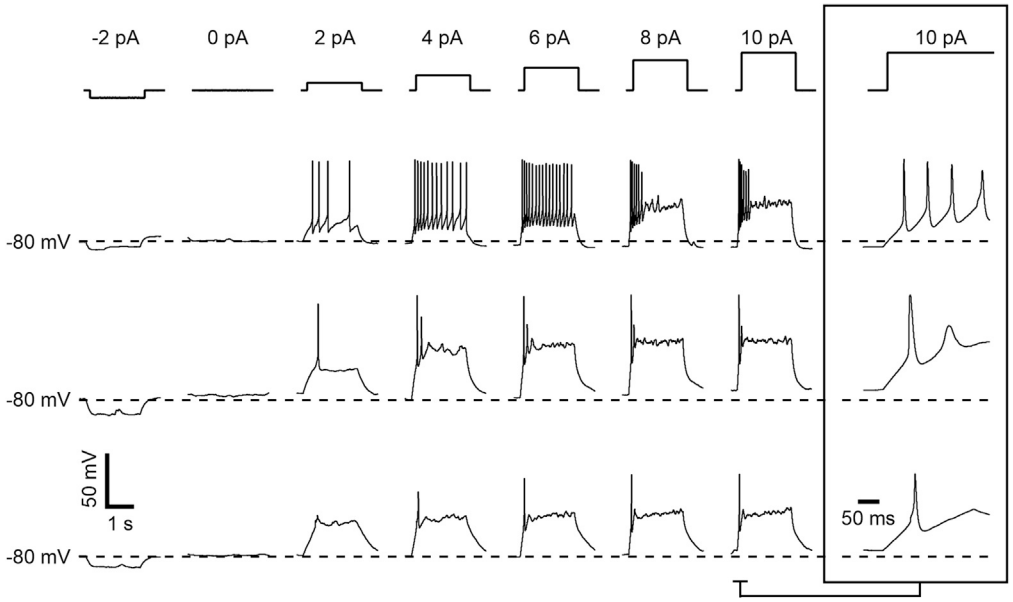


Figure 3. Firing patterns of olfactory sensory neurons recorded from acute slices of the human olfactory epithelium

Spiking activity of three different olfactory sensory neurons recorded in whole-cell current clamp in response to current steps of 2 s duration varying from −2 to 10 pA, with 2 pA increments, as indicated in the upper panel. Insets at the right show the details of firing activity generated with a 10 pA step and plotted on an expanded timescale for each cell.

At higher current injections of 8 and 10 pA, the same neuron generated a phasic firing with a brief train of action potential of decreasing amplitude followed by small oscillations around a voltage plateau. The other two neurons fired only one or two action potentials in response to current injections of 2–4 pA up to 10 pA, followed by a voltage plateau (middle and bottom recordings in Figure 3). Of eight neurons, two displayed tonic firing at current steps between 2 and 6 pA followed by phasic firing at 8 and 10 pA, while six fired only one or a few action potentials.

These experiments show that whole-cell current-clamp experiments in slices from human olfactory epithelium are able to capture the electrophysiological heterogeneity in firing behavior of different olfactory sensory neurons, a characteristic common to other vertebrate species.[36,63,64]

Responses to stimuli

To test if the olfactory transduction cascade is active in neurons of the human olfactory epithelium in acute slice preparation, we applied IBMX, a PDE inhibitor that acts on the transduction cascade by reducing the hydrolysis of cAMP. In the whole-cell voltage-clamp configuration at the holding potential of −80 mV, some neurons did not respond to stimulation with IBMX, although they generated an inward current when a solution containing high K^+ was applied to test the neuron viability (Figure 4A). Other neurons responded to 3 s stimulation of IBMX with an inward current that was slowly increasing its amplitude and then returning to baseline after IBMX removal (Figure 4B). We found that 33% (3 out of 9) of the neurons tested with IBMX displayed an inward current in response to IBMX with an average peak value of -37 ± 18 pA (n = 3), while the average value of the response to high K^+ of the same neurons was -200 ± 17 pA (n = 3). The remaining 67% (6 out of 9) did not respond to IBMX although they responded to high K^+.

We also recorded the spiking pattern in response to IBMX or high K^+ in the current-clamp configuration. The same neuron of Figure 4B displayed firing both in response to IBMX and to high K^+ (Figure 4C). We analyzed the first action potential by using phase plot analysis, in which changes of membrane potentials with time (dV/dt) are plotted as a function of membrane potential (Figure 4D). The action potential is represented by a loop, with the upper and lower parts representing the depolarization and repolarization phases, respectively. Phase plots were rather similar for the first action potential in both IBMX and high K^+ with the following values (Figure 4D): threshold −54 mV for IBMX and −55 mV for high K^+; peak amplitude

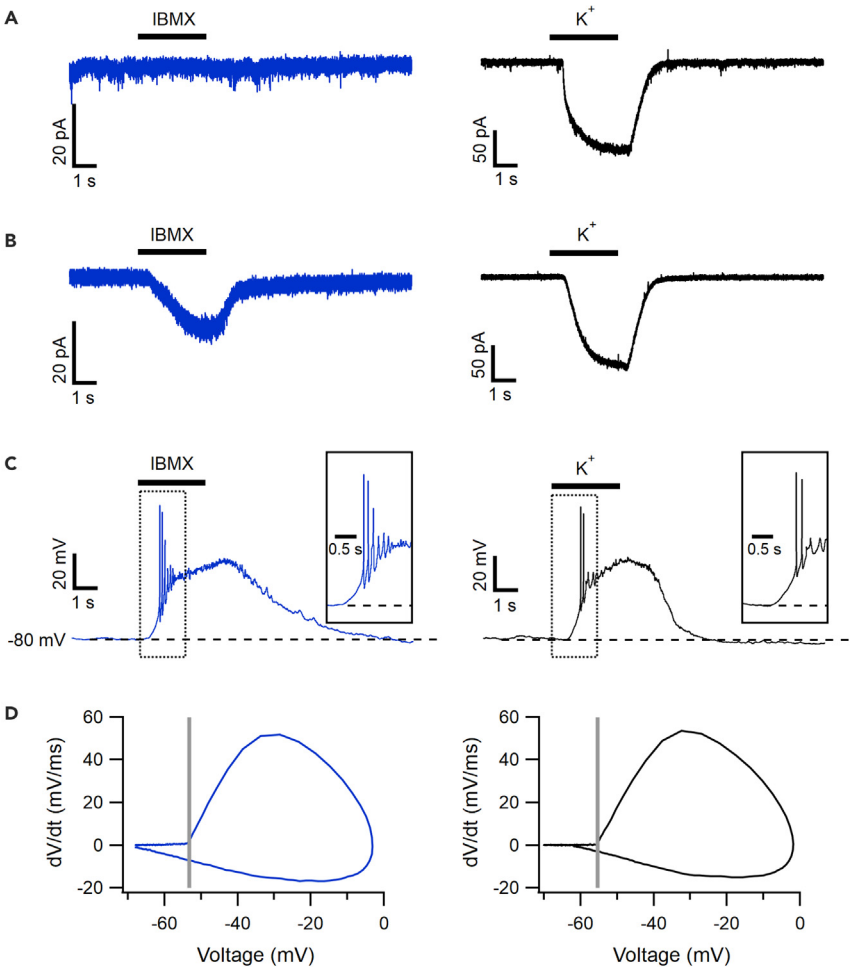


Figure 4. Responses of human olfactory sensory neurons to the phosphodiesterase inhibitor IBMX

(A) Example of an olfactory sensory neuron non-responding to 1 mM IBMX (blue trace; left) but responding to high K^+ with an inward current (black trace; right). Holding potential was −80 mV.

(B) Representative trace of an olfactory sensory neuron responding both to 1 mM IBMX and high K^+ with an inward current.

(C) Spiking activity measured in whole-cell current clamp in the same olfactory sensory neuron shown in (B) stimulated with 1 mM IBMX or high K^+. Insets show details of the spiking activity at the beginning of the stimulation on an expanded timescale.

(D) Phase plots of the first action potentials from the responses shown in (C). The crossing of vertical line with the upper loop indicates the voltage threshold for the first action potential. Stimulus duration for IBMX and high K^+ was 3 s.

−3 mV for IBMX and −2 mV for high K^+; the maximal slope of the depolarization phase was 52 mV/ms for IBMX and 54 mV/ms for high K^+; the maximal slope of the repolarization phase was −17 mV/ms for IBMX and −15 mV/ms for high K^+. Two other neurons responding to IBMX did not reach the voltage threshold for action potential generation.

To investigate if human olfactory sensory neurons in the slice preparation respond to odorants, we prepared two mixtures of odorants (mix 1 and mix 2, see STAR Methods) and recorded current responses under the voltage-clamp configuration at a holding potential of −80 mV. We found that two out of five neurons that we considered viable, as they responded to high K^+, responded to one of the two odorant mixtures with an inward transduction current. In one neuron, the peak amplitude of the current response was −18 pA with odorant mix 1 and -14 pA with IBMX, while mix 2 was not tested (Figure 5A). In another neuron, odorant mix 1 did not activate any current, while mix 2 elicited an inward current of −27 pA peak amplitude (Figure 5B).

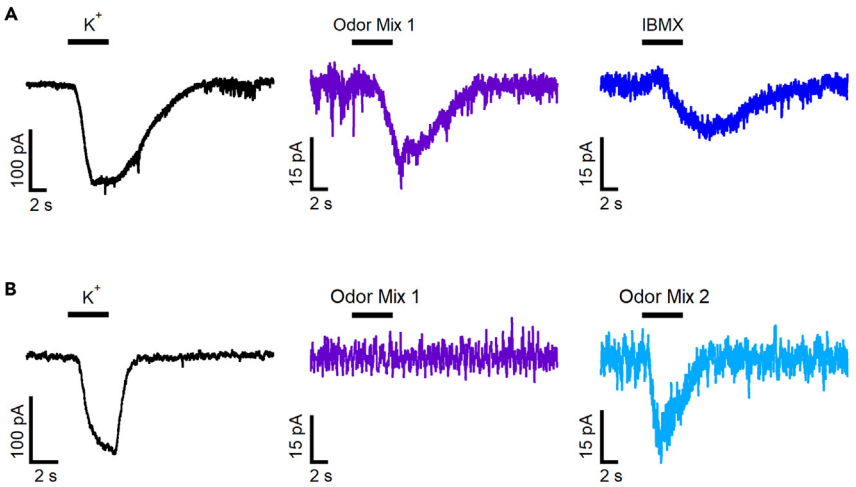


Figure 5. Responses of human olfactory sensory neurons to odorant mixtures

(A) One olfactory sensory neuron responding to high K^+, odorant mix 1, and 1 mM IBMX with inward currents.

(B) Another olfactory sensory neuron non-responding to odorant mix 1 but responding to high K^+ and to odorant mix 2 with an inward current. Holding potential was – 80 mV and stimulus duration was 5 s.

Altogether, these results show that human olfactory sensory neurons in acute slices of the olfactory epithelium have an intact transduction cascade and can respond differently to odorant mixtures. The transduction cascade involves PDE and cAMP which acts as a second messenger, since application of IBMX produces inward currents and elicits action potentials.

DISCUSSION

In this study, we have provided the first demonstration that it is possible to obtain acute slices of the human olfactory epithelium from biopsies that are viable for electrophysiological experiments, crucial to unveil the molecular logic of the very first events of human olfaction.

The resting electrical properties, input resistance, and resting membrane potential, that we measured from human olfactory sensory neurons in slices, were found to be similar to those reported by Restrepo et al.[51] from isolated human olfactory neurons and to those measured in other vertebrates.[60] However, in contrast to previous reports that recorded inward voltage-gated currents in only one out of eleven[51] or one out of fourteen[59] freshly dissociated human olfactory sensory neurons, we consistently recorded both voltage-gated transient inward currents and outward currents in olfactory neurons that were clearly visualized with a fluorescence dye. Our results suggest that avoiding enzymatic dissociation may be crucial for preserving the electrophysiological properties of these neurons. Therefore, recording from slices of the olfactory epithelium is a more suitable approach for studying the functionality of human olfactory sensory neurons.

In addition, we have also successfully recorded voltage-gated currents from human supporting cells and have found notable differences when compared with previous measurements taken in mice. Recordings from supporting cells in mouse acute slices showed the presence of very large leak currents, which could be reduced by using gap junction blockers, while we did not observe any large leak currents in our measurements from human slices. This observation may be due to species-specific differences in the density and/or composition of cellular gap junctions in the olfactory epithelium. Indeed, mouse supporting cells are electrically coupled by gap junctions composed at least by connexin 43 and 45,[65,66] while data about connexins in human supporting cells are still lacking. The composition of connexins within a gap junction can greatly influence its properties, such as sensitivity to changes in voltage and current density.[67] Diverse properties of gap junctions in olfactory supporting cells could lead to distinct electrophysiological properties and intercellular communication patterns, potentially contributing to the observed differences in leak currents between humans and mice.

Moreover, while mouse supporting cells displayed both voltage-gated transient inward currents and outward currents,[61,62] our measurements from human slices consistently showed only outward currents. Interestingly, TMEM16F is expressed in human supporting cells,[15] while in mice, it has only been found in the cilia of olfactory neurons.[68] These biophysical and molecular differences could have significant implications for our understanding of the contribution of supporting cells to the physiology in different species.

In human olfactory sensory neurons, we recorded action potential firing in the current-clamp configuration and observed that some human olfactory neurons responded to small depolarizing current steps of only 2–4 pA and 2 s duration with one or a few spikes, while others displayed a train of action potentials. Increasing current injections up to 10 pA, some neurons displayed tonic firing in the range from 2 to 6 pA, while at higher current injections (8 and 10 pA), the same neurons showed brief action potential trains followed by a voltage plateau. Our findings are consistent with previous measurements in amphibians or rodents, indicating that different firing properties can be displayed also by human olfactory sensory neurons.[36,63,64]

Although the olfactory epithelium from amphibians and rodents has provided insights into the olfactory transduction, the mechanisms underlying this process in human olfactory sensory neurons still need to be understood. While transcriptomic data from the human olfactory epithelium have confirmed the expression of several genes known to be involved in the transduction cascade in rodent olfactory sensory neurons,[8–11] the expression and localization of the proteins have only been confirmed for the alpha and gamma subunits of the G protein using immunostaining data.[11,13] Here, we used immunohistochemistry and showed that AC3, the protein responsible for cAMP production, is expressed in the dendritic knob and cilia of human olfactory neurons, indicating a potential role of cAMP as a second messenger in olfactory transduction in humans, similar to what has been observed in rodents and amphibians. Furthermore, we demonstrated the localization of Ca^{2+}-activated Cl^{-} channel TMEM16B in the dendritic knob and cilia, suggesting that it could have a significant role in human olfactory transduction, similar to previous findings in mice.[35]

By using patch-clamp recordings, we unveiled some crucial elements of the transduction in human olfactory sensory neurons. Specifically, we demonstrated that some olfactory neurons have a basal concentration of cAMP that is hydrolyzed by PDE in resting conditions. Indeed, when we applied the PDE inhibitor IBMX in whole-cell voltage clamp, we recorded an inward current in some viable neurons, but not all. Not only we found that a cAMP increase induced by PDE inhibition with IBMX produced inward currents in voltage clamp but it also elicited action potential firing as measured in the current-clamp configuration. This indicates that cAMP build-up in olfactory sensory neurons can generate transduction currents capable of driving action potential firing.

Previous studies in mice have revealed that the constitutive activity of some odorant receptors leads to spontaneous transduction events in olfactory neurons, while other odorant receptors have a lower activity and do not induce spontaneous events.[44–46] Our experiments with IBMX suggest that human olfactory neuron may also exhibit spontaneous activity, depending on the specific odorant receptor expressed. In rodents, it has been shown that the spontaneous activity of odorant receptors is important to define the glomerular map in the olfactory bulb.[69–71] Whether this also occurs in human is an important question, although difficult to answer.

Recording odorant responses in olfactory sensory neurons is a challenging task, as each neuron only expresses one type of odorant receptor, which is activated by a limited number of odorants. To increase the probability of eliciting a response, we prepared two odorant mixtures that contained compounds known to be ethologically relevant for humans, including some that have previously been shown to activate human odorant receptors *in vitro*.[72–74] In whole-cell voltage clamp, we recorded inward currents in response to each odorant mixture in different human neurons, thus showing that the transduction cascade initiated by odorant binding to specific receptor is fully functional in human olfactory sensory neurons in our slice preparation.

These recorded odorant responses, though not comprehensive, can pave the way for future experiments to understand human olfaction at the periphery by testing a large number of odorants, including food odorants.[74] In the future, calcium imaging from slices could increase the output of responding olfactory sensory neurons in a physiologically relevant context for odorant responses.

Acute slices of the human olfactory epithelium from biopsies are a valuable tool for investigating functional mechanisms behind olfactory dysfunctions, including those related to severe acute respiratory syndrome coronavirus 2 (SARS-CoV-2) infection and to long-term post-COVID-19.[7,19] Morphological changes in the olfactory epithelium of SARS-CoV-2-infected or long-term post-COVID-19 patients[10,18,19] and molecular data on cell types expressing proteins for viral entry[8,9,15] led to various hypotheses on smell loss pathogenesis. Electrophysiological recordings from human olfactory epithelium slices of hyposmic, anosmic, or parosmic patients could reveal changes in biophysical properties and odorant-evoked responses. Pharmacological manipulation would allow probing molecular pathways and characterizing various cell types' contributions. Since the SARS-CoV-2 virus primarily targets supporting cells in the olfactory epithelium, the use of ion-selective microelectrodes could help understand how the epithelial microenvironment changes with the loss of functionality of supporting cells. In addition, we have previously proposed that TMEM16F, which is expressed in human supporting cells,[15] may be involved in COVID-19 pathogenesis in the olfactory epithelium as it has been shown in the lung.[75] Thus, the use of TMEM16F blockers could identify and validate a potential target for treatment of COVID-19-related olfactory loss.

In summary, our data provide the first electrophysiological recordings of odorant responses in human olfactory sensory neurons from acute slices of the olfactory epithelium. We have demonstrated that the transduction mechanism involves PDE and that cAMP serves as a second messenger. Our findings lay the groundwork for future research using acute slices of the human olfactory epithelium, positioning humans as an ideal model for studying olfaction.

Limitations of the study

Data reported in this study are limited to recordings from acute slices of human olfactory epithelium from nasal biopsies of healthy patients. We could not use biopsies from patients with COVID-19 because the biosafety level of our electrophysiological laboratory was not considered sufficient for handling SARS-CoV-2-infected tissues. Another limitation of our study is the use of a limited number of odorants that were only tested in mixtures. Nonetheless, we proved that human olfactory sensory neurons in acute slices respond to odorants and paved the way for a more comprehensive future functional characterization.

STAR★METHODS

Detailed methods are provided in the online version of this paper and include the following:

- KEY RESOURCES TABLE
- RESOURCE AVAILABILITY
  - Lead contact
  - Materials availability
  - Data and code availability
- EXPERIMENTAL MODEL AND STUDY PARTICIPANT DETAILS
  - Human nasal tissue
- METHOD DETAILS
  - Immunohistochemistry
  - Preparation of acute slices of human nasal tissue
  - Electrophysiological recordings
  - Experiments were performed at room temperature (20–25°C)
- QUANTIFICATION AND STATISTICAL ANALYSIS

ACKNOWLEDGMENTS

We thank the patients who gave their consent for this study.

AUTHOR CONTRIBUTIONS

A.M., A.H.C., and M.D. conceptualized the project and designed experiments. A.H.C. and K.G.V. performed immunohistochemistry and confocal microscopy. A.H.C., C.A.S.T., G.G., C.R., and F.A.M. made slices, performed patch-clamp recordings and data analysis. P.B.R., M.T., P.B., and G.T. collected human biopsies. A.M., M.D., and A.H.C. wrote the manuscript with comments from all the other authors.

DECLARATION OF INTERESTS

The authors declare no competing financial interests.

INCLUSION AND DIVERSITY

We worked to ensure gender balance in the recruitment of human subjects.

Received: April 13, 2023
Revised: May 19, 2023
Accepted: June 16, 2023
Published: June 21, 2023

REFERENCES

1. Iannuzzi, L., Salzo, A.E., Angarano, G., Palmieri, V.O., Portincasa, P., Saracino, A., Gelardi, M., Dibattista, M., and Quaranta, N. (2020). Gaining Back What Is Lost: Recovering the Sense of Smell in Mild to Moderate Patients After COVID-19. Chem. Senses *45*, 875–881. https://doi.org/10.1093/chemse/bjaa066.

2. Parma, V., Ohla, K., Veldhuizen, M.G., Niv, M.Y., Kelly, C.E., Bakke, A.J., Cooper, K.W., Bouysset, C., Pirastu, N., Dibattista, M., et al. (2020). More Than Smell-COVID-19 Is Associated With Severe Impairment of Smell, Taste, and Chemesthesis. Chem. Senses *45*, 609–622. https://doi.org/10.1093/chemse/bjaa041.

3. Cecchetto, C., Di Pizio, A., Genovese, F., Calcinoni, O., Macchi, A., Dunkel, A., Ohla, K., Spinelli, S., Farruggia, M.C., Joseph, P.V., et al. (2021). Assessing the extent and timing of chemosensory impairments during COVID-19 pandemic. Sci. Rep. *11*, 17504. https://doi.org/10.1038/s41598-021-96987-0.

4. Gerkin, R.C., Ohla, K., Veldhuizen, M.G., Joseph, P.V., Kelly, C.E., Bakke, A.J., Steele, K.E., Farruggia, M.C., Pellegrino, R., Pepino, M.Y., et al. (2021). Recent Smell Loss Is the Best Predictor of COVID-19 Among Individuals With Recent Respiratory Symptoms. Chem. Senses *46*, bjaa081. https://doi.org/10.1093/chemse/bjaa081.

5. Boscolo-Rizzo, P., Hummel, T., Hopkins, C., D'Alessandro, A., Menini, A., Dibattista, M., and Tirelli, G. (2022). Comprehensive Chemosensory Psychophysical Evaluation of Self-reported Gustatory Dysfunction in Patients With Long-term COVID-19: A Cross-sectional Study. JAMA Otolaryngol. Neck Surg. *148*, 281–282. https://doi.org/10.1001/jamaoto.2021.3993.

6. Butowt, R., Bilinska, K., and von Bartheld, C.S. (2023). Olfactory dysfunction in COVID-19: new insights into the underlying mechanisms. Trends Neurosci. *46*, 75–90. https://doi.org/10.1016/j.tins.2022.11.003.

7. Boscolo-Rizzo, P., Hummel, T., Invitto, S., Spinato, G., Tomasoni, M., Emanuelli, E., Tofanelli, M., Cavicchia, A., Grill, V., Vaira, L.A., et al. (2023). Psychophysical assessment of olfactory and gustatory function in post-mild COVID-19 patients: A matched case-control study with 2-year follow-up. Int. Forum Allergy Rhinol. https://doi.org/10.1002/alr.23148.

8. Brann, D.H., Tsukahara, T., Weinreb, C., Lipovsek, M., Van den Berge, K., Gong, B., Chance, R., Macaulay, I.C., Chou, H.-J., Fletcher, R.B., et al. (2020). Non-neuronal expression of SARS-CoV-2 entry genes in the olfactory system suggests mechanisms underlying COVID-19-associated anosmia. Sci. Adv. *6*, eabc5801. https://doi.org/10.1126/sciadv.abc5801.

9. Fodoulian, L., Tuberosa, J., Rossier, D., Boillat, M., Kan, C., Pauli, V., Egervari, K., Lobrinus, J.A., Landis, B.N., Carleton, A., and Rodriguez, I. (2020). SARS-CoV-2 Receptors and Entry Genes Are Expressed in the Human Olfactory Neuroepithelium and Brain. iScience *23*, 101839. https://doi.org/10.1016/j.isci.2020.101839.

10. Khan, M., Yoo, S.-J., Clijsters, M., Backaert, W., Vanstapel, A., Speleman, K., Lietaer, C., Choi, S., Hether, T.D., Marcelis, L., et al. (2021). Visualizing in deceased COVID-19 patients how SARS-CoV-2 attacks the respiratory and olfactory mucosae but spares the olfactory bulb. Cell *184*, 5932–5949.e15. https://doi.org/10.1016/j.cell.2021.10.027.

11. Durante, M.A., Kurtenbach, S., Sargi, Z.B., Harbour, J.W., Choi, R., Kurtenbach, S., Goss, G.M., Matsunami, H., and Goldstein, B.J. (2020). Single-cell analysis of olfactory neurogenesis and differentiation in adult humans. Nat. Neurosci. *23*, 323–326. https://doi.org/10.1038/s41593-020-0587-9.

12. Morrison, E.E., and Costanzo, R.M. (1992). Morphology of olfactory epithelium in humans and other vertebrates. Microsc. Res. Tech. *23*, 49–61. https://doi.org/10.1002/jemt.1070230105.

13. Holbrook, E.H., Wu, E., Curry, W.T., Lin, D.T., and Schwob, J.E. (2011). Immunohistochemical characterization of human olfactory tissue. Laryngoscope *121*, 1687–1701. https://doi.org/10.1002/lary.21856.

14. Morrison, E.E., and Costanzo, R.M. (1990). Morphology of the human olfactory epithelium. J. Comp. Neurol. *297*, 1–13. https://doi.org/10.1002/cne.902970102.

15. Hernandez-Clavijo, A., Gonzalez-Velandia, K.Y., Rangaswamy, U., Guarneri, G., Boscolo-Rizzo, P., Tofanelli, M., Gardenal, N., Sanges, R., Dibattista, M., Tirelli, G., and Menini, A. (2022). Supporting Cells of the Human Olfactory Epithelium Co-Express the Lipid Scramblase TMEM16F and ACE2 and May Cause Smell Loss by SARS-CoV-2 Spike-Induced Syncytia. Cell. Physiol. Biochem. *56*, 254–269. https://doi.org/10.33594/000000531.

16. Moran, D.T., Rowley, J.C., Jafek, B.W., and Lovell, M.A. (1982). The fine structure of the olfactory mucosa in man. J. Neurocytol. *11*, 721–746. https://doi.org/10.1007/BF01153516.

17. Graziadei, P.P., and Graziadei, G.A. (1979). Neurogenesis and neuron regeneration in the olfactory system of mammals. I. Morphological aspects of differentiation and structural organization of the olfactory sensory neurons. J. Neurocytol. *8*, 1–18. https://doi.org/10.1007/BF01206454.

18. Zazhytska, M., Kodra, A., Hoagland, D.A., Frere, J., Fullard, J.F., Shayya, H., McArthur, N.G., Moeller, R., Uhl, S., Omer, A.D., et al. (2022). Non-cell-autonomous disruption of nuclear architecture as a potential cause of COVID-19-induced anosmia. Cell *185*, 1052–1064.e12. https://doi.org/10.1016/j.cell.2022.01.024.

19. Finlay, J.B., Brann, D.H., Abi Hachem, R., Jang, D.W., Oliva, A.D., Ko, T., Gupta, R., Wellford, S.A., Moseman, E.A., Jang, S.S., et al. (2022). Persistent post–COVID-19 smell loss is associated with immune cell infiltration and altered gene expression in olfactory epithelium. Sci. Transl. Med. *14*, eadd0484. https://doi.org/10.1126/scitranslmed.add0484.

20. Kleene, S.J. (2008). The electrochemical basis of odor transduction in vertebrate olfactory cilia. Chem. Senses *33*, 839–859. https://doi.org/10.1093/chemse/bjn048.

21. Pifferi, S., Menini, A., and Kurahashi, T. (2010). Signal Transduction in Vertebrate Olfactory Cilia. In The Neurobiology of Olfaction Frontiers in Neuroscience, A. Menini, ed. (CRC Press/Taylor & Francis).

22. Boccaccio, A., Menini, A., and Pifferi, S. (2021). The cyclic AMP signaling pathway in the rodent main olfactory system. Cell Tissue Res. *383*, 429–443. https://doi.org/10.1007/s00441-020-03391-7.

23. Genovese, F., Reisert, J., and Kefalov, V.J. (2021). Sensory Transduction in Photoreceptors and Olfactory Sensory Neurons: Common Features and Distinct

Characteristics. Front. Cell. Neurosci. *15*, 761416. https://doi.org/10.3389/fncel.2021.761416.

24. Kaupp, U.B. (2010). Olfactory signalling in vertebrates and insects: differences and commonalities. Nat. Rev. Neurosci. *11*, 188–200. https://doi.org/10.1038/nrn2789.

25. Nakamura, T., and Gold, G.H. (1987). A cyclic nucleotide-gated conductance in olfactory receptor cilia. Nature *325*, 442–444. https://doi.org/10.1038/325442a0.

26. Kurahashi, T. (1990). The response induced by intracellular cyclic AMP in isolated olfactory receptor cells of the newt. J. Physiol. *430*, 355–371. https://doi.org/10.1113/jphysiol.1990.sp018295.

27. Zufall, F., Firestein, S., and Shepherd, G.M. (1994). Cyclic nucleotide-gated ion channels and sensory transduction in olfactory receptor neurons. Annu. Rev. Biophys. Biomol. Struct. *23*, 577–607. https://doi.org/10.1146/annurev.bb.23.060194.003045.

28. Pifferi, S., Boccaccio, A., and Menini, A. (2006). Cyclic nucleotide-gated ion channels in sensory transduction. FEBS Lett. *580*, 2853–2859. https://doi.org/10.1016/j.febslet.2006.03.086.

29. Kleene, S.J., and Gesteland, R.C. (1991). Calcium-activated chloride conductance in frog olfactory cilia. J. Neurosci. *11*, 3624–3629. https://doi.org/10.1523/JNEUROSCI.11-11-03624.1991.

30. Kurahashi, T., and Yau, K.W. (1993). Co-existence of cationic and chloride components in odorant-induced current of vertebrate olfactory receptor cells. Nature *363*, 71–74. https://doi.org/10.1038/363071a0.

31. Stephan, A.B., Shum, E.Y., Hirsh, S., Cygnar, K.D., Reisert, J., and Zhao, H. (2009). ANO2 is the cilial calcium-activated chloride channel that may mediate olfactory amplification. Proc. Natl. Acad. Sci. USA *106*, 11776–11781. https://doi.org/10.1073/pnas.0903304106.

32. Pifferi, S., Dibattista, M., and Menini, A. (2009). TMEM16B induces chloride currents activated by calcium in mammalian cells. Pflügers Archiv *458*, 1023–1038. https://doi.org/10.1007/s00424-009-0684-9.

33. Pifferi, S., Cenedese, V., and Menini, A. (2012). Anoctamin 2/TMEM16B: a calcium-activated chloride channel in olfactory transduction: Anoctamin 2/TMEM16B in olfactory transduction. Exp. Physiol. *97*, 193–199. https://doi.org/10.1113/expphysiol.2011.058230.

34. Pietra, G., Dibattista, M., Menini, A., Reisert, J., and Boccaccio, A. (2016). The Ca2+-activated Cl- channel TMEM16B regulates action potential firing and axonal targeting in olfactory sensory neurons. J. Gen. Physiol. *148*, 293–311. https://doi.org/10.1085/jgp.201611622.

35. Dibattista, M., Pifferi, S., Boccaccio, A., Menini, A., and Reisert, J. (2017). The long tale of the calcium activated Cl^- channels in olfactory transduction. Channels *11*, 399–414. https://doi.org/10.1080/19336950.2017.1307489.

36. Firestein, S., and Werblin, F.S. (1987). Gated currents in isolated olfactory receptor neurons of the larval tiger salamander. Proc. Natl. Acad. Sci. USA *84*, 6292–6296. https://doi.org/10.1073/pnas.84.17.6292.

37. Kurahashi, T., and Shibuya, T. (1990). Ca2(+)-dependent adaptive properties in the solitary olfactory receptor cell of the newt. Brain Res. *515*, 261–268. https://doi.org/10.1016/0006-8993(90)90605-b.

38. Kawai, F., Kurahashi, T., and Kaneko, A. (1996). T-type Ca2+ channel lowers the threshold of spike generation in the newt olfactory receptor cell. J. Gen. Physiol. *108*, 525–535. https://doi.org/10.1085/jgp.108.6.525.

39. Borisy, F.F., Ronnett, G.V., Cunningham, A.M., Juilfs, D., Beavo, J., and Snyder, S.H. (1992). Calcium/calmodulin-activated phosphodiesterase expressed in olfactory receptor neurons. J. Neurosci. *12*, 915–923. https://doi.org/10.1523/JNEUROSCI.12-03-00915.1992.

40. Yan, C., Zhao, A.Z., Bentley, J.K., Loughney, K., Ferguson, K., and Beavo, J.A. (1995). Molecular cloning and characterization of a calmodulin-dependent phosphodiesterase enriched in olfactory sensory neurons. Proc. Natl. Acad. Sci. USA *92*, 9677–9681. https://doi.org/10.1073/pnas.92.21.9677.

41. Frings, S., and Lindemann, B. (1991). Current recording from sensory cilia of olfactory receptor cells in situ. I. The neuronal response to cyclic nucleotides. J. Gen. Physiol. *97*, 1–16. https://doi.org/10.1085/jgp.97.1.1.

42. Firestein, S., Darrow, B., and Shepherd, G.M. (1991). Activation of the sensory current in salamander olfactory receptor neurons depends on a G protein-mediated cAMP second messenger system. Neuron *6*, 825–835. https://doi.org/10.1016/0896-6273(91)90178-3.

43. Lowe, G., and Gold, G.H. (1995). Olfactory transduction is intrinsically noisy. Proc. Natl. Acad. Sci. USA *92*, 7864–7868. https://doi.org/10.1073/pnas.92.17.7864.

44. Reisert, J. (2010). Origin of basal activity in mammalian olfactory receptor neurons. J. Gen. Physiol. *136*, 529–540. https://doi.org/10.1085/jgp.201010528.

45. Connelly, T., Savigner, A., and Ma, M. (2013). Spontaneous and sensory-evoked activity in mouse olfactory sensory neurons with defined odorant receptors. J. Neurophysiol. *110*, 55–62. https://doi.org/10.1152/jn.00910.2012.

46. Dibattista, M., and Reisert, J. (2016). The Odorant Receptor-Dependent Role of Olfactory Marker Protein in Olfactory Receptor Neurons. J. Neurosci. *36*, 2995–3006. https://doi.org/10.1523/JNEUROSCI.4209-15.2016.

47. Margolis, F.L. (1972). A brain protein unique to the olfactory bulb. Proc. Natl. Acad. Sci. USA *69*, 1221–1224. https://doi.org/10.1073/pnas.69.5.1221.

48. Dibattista, M., Al Koborssy, D., Genovese, F., and Reisert, J. (2021). The functional relevance of olfactory marker protein in the vertebrate olfactory system: a never-ending story. Cell Tissue Res. *383*, 409–427. https://doi.org/10.1007/s00441-020-03349-9.

49. Malnic, B. (2007). Searching for the ligands of odorant receptors. Mol. Neurobiol. *35*, 175–181. https://doi.org/10.1007/s12035-007-0013-2.

50. Olender, T., Keydar, I., Pinto, J.M., Tatarskyy, P., Alkelai, A., Chien, M.-S., Fishilevich, S., Restrepo, D., Matsunami, H., Gilad, Y., and Lancet, D. (2016). The human olfactory transcriptome. BMC Genom. *17*, 619. https://doi.org/10.1186/s12864-016-2960-3.

51. Restrepo, D., Okada, Y., Teeter, J.H., Lowry, L.D., Cowart, B., and Brand, J.G. (1993). Human olfactory neurons respond to odor stimuli with an increase in cytoplasmic Ca2+. Biophys. J. *64*, 1961–1966. https://doi.org/10.1016/S0006-3495(93)81565-0.

52. Rawson, N.E., Gomez, G., Cowart, B., Brand, J.G., Lowry, L.D., Pribitkin, E.A., and Restrepo, D. (1997). Selectivity and Response Characteristics of Human Olfactory Neurons. J. Neurophysiol. *77*, 1606–1613. https://doi.org/10.1152/jn.1997.77.3.1606.

53. Rawson, N.E., Gomez, G., Cowart, B.J., Kriete, A., Pribitkin, E., and Restrepo, D. (2012). Age-associated loss of selectivity in human olfactory sensory neurons. Neurobiol. Aging *33*, 1913–1919. https://doi.org/10.1016/j.neurobiolaging.2011.09.036.

54. Tareilus, E., Noé, J., and Breer, H. (1995). Calcium signals in olfactory neurons. Biochim. Biophys. Acta *1269*, 129–138. https://doi.org/10.1016/0167-4889(95)00105-2.

55. Leinders-Zufall, T., Rand, M.N., Shepherd, G.M., Greer, C.A., and Zufall, F. (1997). Calcium entry through cyclic nucleotide-gated channels in individual cilia of olfactory receptor cells: spatiotemporal dynamics. J. Neurosci. *17*, 4136–4148. https://doi.org/10.1523/JNEUROSCI.17-11-04136.1997.

56. Leinders-Zufall, T., Greer, C.A., Shepherd, G.M., and Zufall, F. (1998). Imaging odor-induced calcium transients in single olfactory cilia: specificity of activation and role in transduction. J. Neurosci. *18*, 5630–5639. https://doi.org/10.1523/JNEUROSCI.18-15-05630.1998.

57. Gomez, G., Rawson, N.E., Cowart, B., Lowry, L.D., Pribitkin, E.A., and Restrepo, D. (2000). Modulation of odor-induced increases in [Ca(2+)](i) by inhibitors of protein kinases A and C in rat and human olfactory receptor neurons. Neuroscience *98*, 181–189. https://doi.org/10.1016/s0306-4522(00)00112-3.

58. Thüraüf, N., Gjuric, M., Kobal, G., and Hatt, H. (1996). Cyclic nucleotide-gated channels in identified human olfactory receptor neurons. Eur. J. Neurosci. *8*, 2080–2089. https://doi.org/10.1111/j.1460-9568.1996.tb00729.x.

59. Tamari, K., Takeuchi, H., Kobayashi, M., Takeuchi, K., Kurahashi, T., and Yamamoto, T. (2019). Electrical properties of cells from human olfactory epithelium. Auris Nasus Larynx *46*, 734–741. https://doi.org/10.1016/j.anl.2019.01.006.

60. Schild, D., and Restrepo, D. (1998). Transduction mechanisms in vertebrate olfactory receptor cells. Physiol. Rev. *78*, 429–466. https://doi.org/10.1152/physrev.1998.78.2.429.

61. Vogalis, F., Hegg, C.C., and Lucero, M.T. (2005). Ionic conductances in sustentacular cells of the mouse olfactory epithelium. J. Physiol. *562*, 785–799. https://doi.org/10.1113/jphysiol.2004.079228.

62. Henriques, T., Agostinelli, E., Hernandez-Clavijo, A., Maurya, D.K., Rock, J.R., Harfe, B.D., Menini, A., and Pifferi, S. (2019). TMEM16A calcium-activated chloride currents in supporting cells of the mouse olfactory epithelium. J. Gen. Physiol. *151*, 954–966. https://doi.org/10.1085/jgp.201812310.

63. Madrid, R., Sanhueza, M., Alvarez, O., and Bacigalupo, J. (2003). Tonic and phasic receptor neurons in the vertebrate olfactory epithelium. Biophys. J. *84*, 4167–4181. https://doi.org/10.1016/S0006-3495(03)75141-8.

64. Tomaru, A., and Kurahashi, T. (2005). Mechanisms determining the dynamic range of the bullfrog olfactory receptor cell. J. Neurophysiol. *93*, 1880–1888. https://doi.org/10.1152/jn.00303.2004.

65. Zhang, C., Finger, T.E., and Restrepo, D. (2000). Mature olfactory receptor neurons express connexin 43. J. Comp. Neurol. *426*, 1–12. https://doi.org/10.1002/1096-9861(20001009)426:1<1::AID-CNE1>3.0.CO;2-Y.

66. Rash, J.E., Davidson, K.G.V., Kamasawa, N., Yasumura, T., Kamasawa, M., Zhang, C., Michaels, R., Restrepo, D., Ottersen, O.P., Olson, C.O., and Nagy, J.I. (2005). Ultrastructural localization of connexins (Cx36, Cx43, Cx45), glutamate receptors and aquaporin-4 in rodent olfactory mucosa, olfactory nerve and olfactory bulb. J. Neurocytol. *34*, 307–341. https://doi.org/10.1007/s11068-005-8360-2.

67. Spray, D.C. (1996). Physiological Properties of Gap Junction Channels in the Nervous System. In Gap Junctions in the Nervous System Neuroscience Intelligence Unit, D.C. Spray and R. Dermietzel, eds. (Springer), pp. 39–59. https://doi.org/10.1007/978-3-662-21935-5_3.

68. Henkel, B., Drose, D.R., Ackels, T., Oberland, S., Spehr, M., and Neuhaus, E.M. (2015). Co-expression of anoctamins in cilia of olfactory sensory neurons. Chem. Senses *40*, 73–87. https://doi.org/10.1093/chemse/bju061.

69. Yu, C.R., Power, J., Barnea, G., O'Donnell, S., Brown, H.E.V., Osborne, J., Axel, R., and Gogos, J.A. (2004). Spontaneous neural activity is required for the establishment and maintenance of the olfactory sensory map. Neuron *42*, 553–566. https://doi.org/10.1016/s0896-6273(04)00224-7.

70. Imai, T., Suzuki, M., and Sakano, H. (2006). Odorant receptor-derived cAMP signals direct axonal targeting. Science *314*, 657–661. https://doi.org/10.1126/science.1131794.

71. Lorenzon, P., Redolfi, N., Podolsky, M.J., Zamparo, I., Franchi, S.A., Pietra, G., Boccaccio, A., Menini, A., Murthy, V.N., and Lodovichi, C. (2015). Circuit formation and function in the olfactory bulb of mice with reduced spontaneous afferent activity. J. Neurosci. *35*, 146–160. https://doi.org/10.1523/JNEUROSCI.0613-14.2015.

72. Chatelain, P., Veithen, A., Wilkin, F., and Philippeau, M. (2014). Deorphanization and Characterization of Human Olfactory Receptors in Heterologous Cells. Chem. Biodivers. *11*, 1764–1781. https://doi.org/10.1002/cbdv.201400083.

73. Gonzalez-Kristeller, D.C., do Nascimento, J.B.P., Galante, P.A.F., and Malnic, B. (2015). Identification of agonists for a group of human odorant receptors. Front. Pharmacol. *6*, 35. https://doi.org/10.3389/fphar.2015.00035.

74. Haag, F., Di Pizio, A., and Krautwurst, D. (2022). The key food odorant receptive range of broadly tuned receptor OR2W1. Food Chem. *375*, 131680. https://doi.org/10.1016/j.foodchem.2021.131680.

75. Braga, L., Ali, H., Secco, I., Chiavacci, E., Neves, G., Goldhill, D., Penn, R., Jimenez-Guardeño, J.M., Ortega-Prieto, A.M., Bussani, R., et al. (2021). Drugs that inhibit TMEM16 proteins block SARS-CoV-2 spike-induced syncytia. Nature *594*, 88–93. https://doi.org/10.1038/s41586-021-03491-6.

76. Aigouy, B., and Mirouse, V. (2013). ScientiFig: a tool to build publication-ready scientific figures. Nat. Methods *10*, 1048. https://doi.org/10.1038/nmeth.2692.

77. Shimazaki, R., Boccaccio, A., Mazzatenta, A., Pinato, G., Migliore, M., and Menini, A. (2006). Electrophysiological properties and modeling of murine vomeronasal sensory neurons in acute slice preparations. Chem. Senses *31*, 425–435. https://doi.org/10.1093/chemse/bjj047.

78. Dibattista, M., Mazzatenta, A., Grassi, F., Tirindelli, R., and Menini, A. (2008). Hyperpolarization-Activated Cyclic Nucleotide-Gated Channels in Mouse Vomeronasal Sensory Neurons. J. Neurophysiol. *100*, 576–586. https://doi.org/10.1152/jn.90263.2008.

79. Wong, W.M., Nagel, M., Hernandez-Clavijo, A., Pifferi, S., Menini, A., Spehr, M., and Meeks, J.P. (2018). Sensory Adaptation to Chemical Cues by Vomeronasal Sensory Neurons. eNeuro *5*. ENEURO.0223-18.2018. https://doi.org/10.1523/ENEURO.0223-18.2018.

80. Sarno, N., Hernandez-Clavijo, A., Boccaccio, A., Menini, A., and Pifferi, S. (2022). Slow Inactivation of Sodium Channels Contributes to Short-Term Adaptation in Vomeronasal Sensory Neurons. eneuro *9*. ENEURO.0471-21.2022. https://doi.org/10.1523/ENEURO.0471-21.2022.

81. Agostinelli, E., Gonzalez-Velandia, K.Y., Hernandez-Clavijo, A., Kumar Maurya, D., Xerxa, E., Lewin, G.R., Dibattista, M., Menini, A., and Pifferi, S. (2021). A Role for STOML3 in Olfactory Sensory Transduction. eNeuro *8*. ENEURO.0565-20.2021. https://doi.org/10.1523/ENEURO.0565-20.2021.

STAR★METHODS

KEY RESOURCES TABLE

REAGENT or RESOURCE	SOURCE	IDENTIFIER
Antibodies		
Polyclonal goat anti-OMP	Wako	Cat# 019–22291; RRID:AB_664696
Monoclonal mouse anti-β Tubulin III	BioLegend	Cat# 801202; RRID:AB_10063408
Polyclonal rabbit anti-ERMN	Novus	Cat# NBP1-84802; RRID:AB_11039928
Polyclonal rabbit anti-AC3	Santa Cruz	Cat# sc-588; RRID:AB_630839
Polyclonal rabbit anti-TMEM16B	Novus	Cat# NBP1-90739; RRID:AB_11033237
Donkey anti-rabbit Alexa Fluor Plus 594	Life Technologies	Cat# A32754; RRID:AB_2762827
Donkey anti-rabbit Alexa Fluor 488	Life Technologies	Cat# A21206; RRID:AB_2535792
Donkey anti-goat Alexa Fluor 647	Life Technologies	Cat# A32849; RRID:AB_2762840
Donkey anti-mouse Alexa Fluor 594	Life Technologies	Cat# A-21203; RRID:AB_141633
Donkey anti-mouse Alexa Fluor 488	Life Technologies	Cat# A32766; RRID:AB_2762823
Chemicals, peptides, and recombinant proteins		
3-isobutyl-1-methylxanthine (IBMX)	Sigma Aldrich	Cat# I5879
Acetophenone	Sigma Aldrich	Cat# A10701
Cineole	Sigma Aldrich	Cat# C8144
Eugenol	Sigma Aldrich	Cat# E51791
Heptaldehyde	Sigma Aldrich	Cat# H2120
Isoamyl acetate	Sigma Aldrich	Cat# 112674
(R)-(−)-carvone	Sigma Aldrich	Cat# 124931
(S)-(+)-carvone	Sigma Aldrich	Cat# 435759
Geraniol	Sigma Aldrich	Cat# 163333
Hexanal	Sigma Aldrich	Cat# 115606
7-hydroxycitronellal	Sigma Aldrich	Cat# 82934
(R)-(+)-limonene	Sigma Aldrich	Cat# 183164
Octanal	Sigma Aldrich	Cat# O5608
Software and algorithms		
ImageJ	National Institute of Health https://imagej.net/ij/index.html	RRID:SCR_003070
Micromanager	University of California at San Francisco https://micro-manager.org/	RRID:SCR_016865
NIS-Elements Nikon	Nikon https://www.microscope.healthcare.nikon.com/en_EU/products/software	RRID:SCR_014329
pClamp 10.6 PC software	Molecular Devices https://www.moleculardevices.com/products	RRID:SCR_011323
Clampfit 10.6	Molecular Devices https://www.moleculardevices.com/products	RRID:SCR_011323
Igor Pro 8 software	WaveMetrics https://www.wavemetrics.com/	RRID:SCR_000325

RESOURCE AVAILABILITY

Lead contact

Further information and requests for resources should be directed to and will be fulfilled by the lead contact, Anna Menini (anna.menini@sissa.it).

Materials availability

This study did not generate new unique reagents.

Data and code availability

- All data reported in this paper will be shared by the lead contact upon request.
- This paper does not report original code.
- Any additional information required to reanalyze the data reported in this paper is available from the lead contact upon request.

EXPERIMENTAL MODEL AND STUDY PARTICIPANT DETAILS

Human nasal tissue

Samples from human nasal tissue were obtained at the Section of Otolaryngology of the Department of Medical, Surgical and Health Sciences, University of Trieste, Trieste, Italy. The study was approved by the Ethics Committee on Clinical Investigation of the University of Trieste (nr 232/2016 and 110/2021), Friuli Venezia Giulia Region (CEUR-17236), each patient provided written informed consent and all experiments conform to the regulatory standards.

Biopsies were performed in the operating room from patients under general anesthesia at the end of the scheduled endoscopic sinonasal surgery. Two-three biopsy specimens were obtained from one nostril from the superior septum within the olfactory cleft and adjacent to the middle turbinate using a sickle knife and Blakesley forceps or cupped forceps. Once collected, biopsy specimens to be used for electrophysiology were immediately immersed in ice-cold artificial cerebrospinal fluid (ACSF) containing (in mM): 120 NaCl, 25 $NaHCO_3$, 5 KCl, 1 $CaCl_2$, 1 $MgSO_4$, 10 HEPES, 10 glucose, pH 7.4, while those to be used for immunohistochemistry were immersed in paraformaldehyde (PFA) at 4% in PBS. Samples containing olfactory epithelium were obtained from 9 Caucasian patients (5 males and 4 females, age between 24 and 70 years).

METHOD DETAILS

Immunohistochemistry

Human tissue samples used for immunohistochemistry were fixed in paraformaldehyde (PFA) at 4% in PBS pH 7.4 for 4 to 10 h at 4°C. After fixation, the tissue was kept in PBS pH 7.4 at 4°C, typically from 2 to 24 h. For cryoprotection of biopsies, the tissue was equilibrated overnight in 30% (w/v) sucrose in PBS at 4°C. Then, the tissue was embedded in cryostat embedding medium (BioOptica) and immediately frozen at −80°C. 16 μm sections were cut on a cryostat and mounted on Superfrost Plus Adhesion Microscope Slides (ThermoFisher Scientific). Sections were air-dried for 3 h and used the same day or stored at −20°C for later use. Cryostat embedding medium was removed from the tissue by incubating the slices in PBS for 15 min. The tissue was treated for 15 min with 0.5% (w/v) sodium dodecyl sulfate (SDS) in PBS for antigen retrieval, then washed and incubated in blocking solution (5% normal donkey serum, 0.2% Triton X-100 in PBS) for 90 min and finally incubated overnight at 4°C with the primary antibodies diluted in blocking solution. In the following day, the unbound primary antibodies were removed with PBS washes, then sections were incubated with Alexa Fluor conjugated secondary antibodies (1:500 dilution) in TPBS (0.2% Tween 20 in PBS) for 2 h at room temperature, washed and mounted with Vectashield (Vector Laboratories) or FluoromontG (ThermoFisher). DAPI (5 mg/mL) was added to the solution containing secondary antibody to stain the nuclei.

The following primary antibodies (dilution; catalog number, company) were used: polyclonal goat anti-OMP (1:1000; 019-22291, Wako), monoclonal mouse anti-β Tubulin III (TUJ1) (1:200; 801202, BioLegend), polyclonal rabbit anti-ERMN (1:200; NBP1-84802, Novus). Polyclonal rabbit anti-AC3 (1:100; sc-588, Santa Cruz) and polyclonal rabbit anti-TMEM16B (1:200, NBP1-90739, Novus). The following secondary antibodies were used: donkey anti-rabbit Alexa Fluor Plus 594 (1:500; A32754, Life Technologies), donkey anti-rabbit Alexa Fluor 488 (1:500; A21206, Life Technologies), donkey anti-goat Alexa Fluor 647 (1:500; A32849, Life Technologies), donkey anti-mouse Alexa Fluor 594 (1:500, A-21203, Life Technologies), donkey anti-mouse Alexa Fluor 488 (1:500, A32766, Life Technologies).

Control experiments, excluding primary antibodies, were performed for each immunolocalization. We performed at least 2 independent human tissue replicates for each antibody tested. All attempts at replication were successful.

Z-stack images were acquired using NIS-Elements Nikon software at 1024 × 1024 pixels resolution of each single image and analyzed with ImageJ software (National Institute of Health, USA). Max projections of Z-stacks or individual images within the stacks were used to display results. Figure assembly was performed on ImageJ (National Institutes of Health) using ScientiFig plugin.[76] No image modification was performed other than brightness and contrast adjustment.

Preparation of acute slices of human nasal tissue

Acute slices of human nasal epithelium used for electrophysiological experiments were prepared following a similar protocol to the one used for mouse olfactory and vomeronasal epithelium.[15,62,77–81] Within about 30 min from the biopsy, the human nasal epithelium was embedded in 3% Type I-A agarose (Sigma) prepared in ACSF once the agar had cooled to 38°C. Upon solidification, the agar block was fixed in a glass Petri dish and sliced with a vibratome (Vibratome 1000 Plus, Sectioning System) at 200 to 250 μm thickness in oxygenated ACSF solution. Slices were then left to recover for >30 min in chilled and oxygenated ACSF before electrophysiological experiments were initiated.

Electrophysiological recordings

Slices were transferred to a recording chamber and continuously perfused with oxygenated (95% O2, and 5% CO2) ACSF by gravity flow. Each slice was anchored to the base of the recording chamber using a homemade U-shaped silver wire, holding down the agar support without touching the slice itself. Slices were viewed with an upright microscope (Olympus BX51WI) by infrared differential contrast optics with water immersion 20X or 60X objectives. The olfactory epithelium was easily distinguished from the respiratory one because the first had no moving cilia while the second had long beating cilia.

Whole-cell recordings were performed by patching the soma of the cells. Patch pipettes pulled from borosilicate capillaries (WPI) with a PC-10 puller (Narishige) had a resistance of 3–6 MΩ. The intracellular solution filling the patch pipette contained (in mM) 80 K-Gluconate, 60 KCl, 2 Mg-ATP, 10 HEPES, and 1 EGTA, adjusted to pH 7.2 with KOH. To visualize the morphology of the cell, 0.01 mg/ml Alexa Fluor 594 carboxylic acid (Thermo Fisher, A33082) was dissolved in the patch pipette solution, diffused into the cell and the fluorescence image of the cell was observed under red fluorescence filter. Olfactory sensory neurons and supporting cells were clearly identified by their morphology (Figures 2A and 2D). Recordings in the whole-cell voltage- or current-clamp configurations were obtained with a Multiclamp 700B amplifier controlled by Clampex 10 via a Digidata 1440 (Molecular Devices). Data were low-pass filtered at 2 kHz and sampled at 10 kHz.

Experiments were performed at room temperature (20–25°C)

Responses of olfactory sensory neurons to stimuli were tested with 1 mM 3-isobutyl-1-methylxanthine (IBMX) and two odorant mixtures. Mix 1 was composed of acetophenone, cineole, eugenol, heptaldehyde, isoamyl acetate, while mix 2 was composed of (R)-(−)-carvone, (S)-(+)-carvone, geraniol, hexanal, 7-hydroxycitronellal, (R)-(+)-limonene, octanal. Each odorant was present at 100 μM. For each experiment, the response to high K^+ stimulation was used to evaluate the viability of the neuron and the time of stimulus application. Only olfactory sensory neurons that responded to high K^+ solution were included in the analysis.

1 mM IBMX was prepared weekly by directly dissolving it in ACSF solution. For odorant mixtures, each odorant was dissolved in dimethyl sulfoxide (DMSO) to prepare stock solutions at 5 M and mixtures were prepared by diluting each odorant at a final concentration of 100 μM in ACSF on the day of the experiment.

Stimuli were focally delivered to the neuron through an 8-into-1 multibarrel perfusion pencil connected to a ValveLink8.2 pinch valve perfusion system (AutoMate Scientific). The tip of the perfusion head, with a diameter of 360 μm, was placed ~500 μm away from the slice. To avoid mechanical artifacts, the slice was continuously perfused with ACSF and the flow out of the pipette was switched between ACSF and stimulus solutions.

All chemicals were purchased from Sigma-Aldrich unless otherwise stated.

QUANTIFICATION AND STATISTICAL ANALYSIS

Igor Pro 8 software (WaveMetrics, Lake Oswego, OR, USA) was used for data analysis and figure preparation. All averaged data from individual experiments in different cells are presented as mean ± standard error of the mean (SEM) and number of cells (n). These data were normally distributed (Shapiro-Wilk test).

6. Discussion

In this thesis, we address two different topics, in the first part we deeply understand the accessory olfactory system through the analysis of the VSNs and the effect of NA on excitability, and in the second part as well that we provide a new approach to obtain unknown physiological properties and currents present in OSNs of humans.

6.1.1. NA increases the excitability of VSNs

The results in the first part of this thesis provide a framework for understanding the modulatory effect of NA in VSNs, as we found that NA increases the excitability of neurons stimulated with a natural source of pheromones such as urine.

Based on the initial response to urine and the effect of NA, some of the neurons began responding only after NA treatment, while urine per se was ineffective. In this case, the stimulus in the urine might be at a too low concentration to be detected without the enhancement provided by NA or might lack the specific pheromones needed to activate the pheromone receptors expressed by those neurons. Conversely, some other VSNs responded to urine from the first stimulation, suggesting that the binding molecules in the urine were specific and sufficiently concentrated to activate these neurons. NA treatment further increased their firing frequency in response to the stimulus.

These findings indicate that NA enhances the excitability of VSNs, effectively lowering their threshold of detectability and increasing their sensitivity to stimuli. A possible mechanism might be related to changes in the transduction machinery, that affect the receptor potential and thus bring the membrane potential closer to the firing threshold. However, our results suggest that at least part of this effect is due to mechanisms involving the action potential generation. We bypassed the transduction process, injecting small current steps, and observed an increase in firing frequency under NA treatment. This suggests that NA regulates one or multiple conductances involved in action potential generation. Despite the possibility of changes in the transduction pathway, our findings highlight the significance of NA's effect on the action potential machinery, which should be investigated in detail in future work.

6.1.2. Identity of the AR expressed in VSNs

Analysis of previous scRNA-seq data set (Katreddi et al., 2022) identified the Alpha 1a receptor, a member of the Alpha 1 receptor family, as the most highly expressed subtype among the nine subtypes of ARs in mature VSNs. We supported this finding through a pharmacological approach using prazosin, a known specific inhibitor of alpha 1-AR (Michelotti et al., 2000), and methoxamine, an Alpha 1-AR agonist (DeMarinis et al., 1981). In calcium imaging experiments, prazosin abolished the calcium increase triggered by NA, and blocked its electrophysiological effect in current-clamp experiments. Conversely, methoxamine mimicked the effect of NA, confirming the functional expression of Alpha 1-AR in VSNs. However, we cannot rule out the possibility that other ARs induce a secondary effect on VSNs by releasing other regulatory molecules. Additionally, it remains unkown there are differences between the various subpopulations of VSNs in their response to NA. Further refinement of this approach, potentially through advanced genetic tools, could enhance the specificity of targeting Alpha 1a-AR expression in VSNs.

6.1.3. Calcium increase by NA stimulation and possible cellular mechanism

The Alpha 1-ARs activate the PLC-beta pathway, leading to an increase in intracellular calcium. Our experiments using BAPTA to rapidly chelate the increase of intracellular calcium, demonstrated that NA-dependent calcium increases are necessary to enhance the excitability of VSNs. These experiments were performed by injecting current into the neurons, emphasizing a regulation by calcium of voltage-gated channels. Possible candidates for this regulation are Na_V channels, such as the Na_V 1.6 channel, which is expressed in VSNs. In HEK293 cells, Na_V 1.6 has been shown to be phosphorylated by calcium-calmodulin dependent kinase II (CaMKII), leading to changes in its biophysical properties and causing a negative shift in the activation curve (Zybura et al., 2020). Another candidate is the BK channel that in combination with Ca_V, which has been shown to affect tonic firing in VSNs (Ukhanov et al., 2007). This suggests that similar mechanisms might be at play in VSNs, contributing to the NA-induced increase in excitability.

6.1.4. Sympathetic nervous system and NA on VSNs

We performed immunofluorescence assays against Tyrosine hydroxylase, the key enzyme involved in the synthesis of catecholamines such as NA and demonstrate the localization of nerve endings near the vomeronasal sensory epithelium, suggesting a possible source of NA. Another source of catecholamines is the adrenal gland. The VNO is densely supplied with blood vessels, suggesting a potential role in regulating VSNs through systemic catecholamine as adrenaline.

Recent reports have revealed the presence of catecholaminergic fibers in the non-sensory epithelium and highlighted the adrenergic control of VNO pumping. Moreover, researchers have estimated the VNO lumen volume to be approximately 85 nanoliters under resting conditions (Hamacher et al., 2024). During VNO contraction, its volume undergoes cyclic fluctuations, both decreasing and increasing. This contraction process facilitates the entry of pheromones into the VNO. These volume fluctuations can cause changes in pheromone concentration within the VNO. Since pheromones are typically present at nanomolar to picomolar concentrations, even slight volume changes can lead to substantial variations in pheromone concentration. For instance, if the VNO volume is reduced to half its size, the concentration of pheromones could double, assuming no exchange of molecules in one contraction cycle. These fluctuations can significantly influence the sensitivity and responsiveness of VSNs, as these neurons rely on precise pheromone concentrations to trigger appropriate physiological responses. To adapt to these changes, the VNO likely employs a series of regulatory molecules, such as NA, to fine-tune the firing rate and response threshold of VSNs. This dynamic regulation ensures that VSNs can accurately detect and respond to varying pheromone concentrations, maintaining effective chemosensory communication under different physiological conditions.

Further investigation to examine the exact timing and spatial patterns of NA's effects in the VNO would necessitate utilizing genetic tools to induce neurotransmitter release within the intact tissue, thus circumventing any potential artifacts linked to external perfusion system stimulation.

6.2.1. OSNs in human epithelium

We performed electrophysiological recordings of olfactory sensory neurons (OSNs) in slices of olfactory epithelium from human biopsies, allowing us to measure voltage-dependent inward and outward currents with characteristics similar to those observed in other vertebrates. Compared to previous reports on dissociated human OSNs, where the enzymatic procedure limits neuron viability (Restrepo et al., 1993), our results demonstrated that our preparation is a more appropriate method for maintaining neuron viability. We successfully recorded inward current responses to odorants in voltage clamp experiments and induced firing under stimulation by a PDE inhibitor. These results open the possibility to study the transduction cascade in greater detail, including sensory adaptation at the level of single olfactory neurons in humans, as well as the mechanisms behind olfactory dysfunctions.

These recorded odorant responses pave the way for future experiments to understand human olfaction at the periphery by testing a large number of odorants, including food odorants. Using calcium imaging from slices could increase the number of responding OSNs in a physiologically relevant context for odorant responses.

6.2.2. SCs in human epithelium

We successfully recorded outward voltage-gated currents from human supporting cells and found notable differences compared to previous measurements in mice, where there is an additional voltage-dependent inward current absent in humans. Another difference in mice supporting cells is the presence of a large leak current dependent on gap junction expression, whereas no large leak currents were observed in human slices.

This difference might be due to variations in the density and composition of cellular gap junctions. However, information about connexins in human supporting cells is still lacking. The composition of connexins can significantly influence gap junction properties, affecting voltage sensitivity and current density, which leads to different electrophysiological properties and intercellular communication patterns.

7. References

Amberg, G. C., Koh, S. D., Imaizumi, Y., Ohya, S., & Sanders, K. M. (2003). A-type potassium currents in smooth muscle. *American Journal of Physiology. Cell Physiology*, *284*(3), C583-595. https://doi.org/10.1152/ajpcell.00301.2002

Amjad, A., Hernandez-Clavijo, A., Pifferi, S., Maurya, D. K., Boccaccio, A., Franzot, J., Rock, J., & Menini, A. (2015). Conditional knockout of TMEM16A/anoctamin1 abolishes the calcium-activated chloride current in mouse vomeronasal sensory neurons. *The Journal of General Physiology*, *145*(4), 285–301. https://doi.org/10.1085/jgp.201411348

Araneda, R. C., Kini, A. D., & Firestein, S. (2000). The molecular receptive range of an odorant receptor. *Nature Neuroscience*, *3*(12), 1248–1255. https://doi.org/10.1038/81774

Berghard, A., & Buck, L. B. (1996). Sensory transduction in vomeronasal neurons: Evidence for G alpha o, G alpha i2, and adenylyl cyclase II as major components of a pheromone signaling cascade. *Journal of Neuroscience*, *16*(3), 909–918. https://doi.org/10.1523/JNEUROSCI.16-03-00909.1996

Bezanilla, F., & Armstrong, C. M. (1972). Negative Conductance Caused by Entry of Sodium and Cesium Ions into the Potassium Channels of Squid Axons. *Journal of General Physiology*, *60*(5), 588–608. https://doi.org/10.1085/jgp.60.5.588

Bigiani, A., Mucignat-Caretta, C., Montani, G., & Tirindelli, R. (2005). Pheromone reception in mammals. In *Reviews of Physiology, Biochemistry and Pharmacology* (pp. 1–35). Springer. https://doi.org/10.1007/s10254-004-0038-0

Boccaccio, A. (2018). Patch-Clamp Recordings from Mouse Olfactory Sensory Neurons. In F. M. Simoes de Souza & G. Antunes (Eds.), *Olfactory Receptors: Methods and Protocols* (pp. 113–122). Springer. https://doi.org/10.1007/978-1-4939-8609-5_9

Boccaccio, A., & Menini, A. (2007). Temporal development of cyclic nucleotide-gated and Ca2+ -activated Cl- currents in isolated mouse olfactory sensory neurons. *Journal of Neurophysiology*, *98*(1), 153–160. https://doi.org/10.1152/jn.00270.2007

Boccaccio, A., Menini, A., & Pifferi, S. (2021). The cyclic AMP signaling pathway in the rodent main olfactory system. *Cell and Tissue Research*, *383*(1), 429–443. https://doi.org/10.1007/s00441-020-03391-7

Bolz, F., Kasper, S., Bufe, B., Zufall, S., & Pyrski, M. (2017). Organization and Plasticity of Sodium Channel Expression in the Mouse Olfactory and Vomeronasal Epithelia. *Frontiers in Neuroanatomy*, *11*. https://doi.org/10.3389/fnana.2017.00028

Bushdid, C., Magnasco, M. O., Vosshall, L. B., & Keller, A. (2014). Humans can discriminate more than 1 trillion olfactory stimuli. *Science (New York, N.Y.)*, *343*(6177), 1370–1372. https://doi.org/10.1126/science.1249168

Carter, L. A., MacDonald, J. L., & Roskams, A. J. (2004). Olfactory horizontal basal cells demonstrate a conserved multipotent progenitor phenotype. *The Journal of Neuroscience: The Official Journal of the Society for Neuroscience*, *24*(25), 5670–5683. https://doi.org/10.1523/JNEUROSCI.0330-04.2004

Catterall, W. A., Perez-Reyes, E., Snutch, T. P., & Striessnig, J. (2005). International Union of Pharmacology. XLVIII. Nomenclature and structure-function relationships of voltage-gated calcium channels. *Pharmacological Reviews*, *57*(4), 411–425. https://doi.org/10.1124/pr.57.4.5

Cavaliere, R. M., Ghirardi, F., & Tirindelli, R. (2014). Lacrimal gland removal impairs sexual behavior in mice. *Frontiers in Neuroanatomy*, *8*, 101. https://doi.org/10.3389/fnana.2014.00101

Chamero, P., Katsoulidou, V., Hendrix, P., Bufe, B., Roberts, R., Matsunami, H., Abramowitz, J., Birnbaumer, L., Zufall, F., & Leinders-Zufall, T. (2011). G protein Gαo is essential for vomeronasal function and aggressive behavior in mice. *Proceedings of the National Academy of Sciences of the United States of America*, *108*(31), 12898–12903. https://doi.org/10.1073/pnas.1107770108

Chamero, P., Marton, T. F., Logan, D. W., Flanagan, K., Cruz, J. R., Saghatelian, A., Cravatt, B. F., & Stowers, L. (2007). Identification of protein pheromones that promote aggressive behaviour. *Nature*, *450*(7171), 899–902. https://doi.org/10.1038/nature05997

Cichy, A., Ackels, T., Tsitoura, C., Kahan, A., Gronloh, N., Söchtig, M., Engelhardt, C. H., Ben-Shaul, Y., Müller, F., Spehr, J., & Spehr, M. (2015). Extracellular pH Regulates Excitability of Vomeronasal Sensory Neurons. *Journal of Neuroscience*, *35*(9), 4025–4039. https://doi.org/10.1523/JNEUROSCI.2593-14.2015

Clapham, D. E., & Neer, E. J. (1997). G protein beta gamma subunits. *Annual Review of Pharmacology and Toxicology*, *37*, 167–203. https://doi.org/10.1146/annurev.pharmtox.37.1.167

Czesnik, D., Kuduz, J., Schild, D., & Manzini, I. (2006). ATP activates both receptor and sustentacular supporting cells in the olfactory epithelium of Xenopus laevis tadpoles. *European Journal of Neuroscience*, *23*(1), 119–128. https://doi.org/10.1111/j.1460-9568.2005.04533.x

De Blasi, A. (1990). Beta-adrenergic receptors: Structure, function and regulation. *Drugs Under Experimental and Clinical Research*, *16*(3), 107–112.

Del Punta, K., Leinders-Zufall, T., Rodriguez, I., Jukam, D., Wysocki, C. J., Ogawa, S., Zufall, F., & Mombaerts, P. (2002). Deficient pheromone responses in mice lacking a cluster of vomeronasal receptor genes. *Nature*, *419*(6902), 70–74. https://doi.org/10.1038/nature00955

DeMarinis, R. M., Bryan, W. M., Shah, D. H., Hieble, J. P., & Pendleton, R. G. (1981). Alpha-adrenergic agents. 1. Direct-acting alpha 1 agonists related to methoxamine. *Journal of Medicinal Chemistry*, *24*(12), 1432–1437. https://doi.org/10.1021/jm00144a012

Dewan, A., Pacifico, R., Zhan, R., Rinberg, D., & Bozza, T. (2013). Non-redundant coding of aversive odours in the main olfactory pathway. *Nature*, *497*(7450), 486–489. https://doi.org/10.1038/nature12114

Dhallan, R. S., Yau, K.-W., Schrader, K. A., & Reed, R. R. (1990). Primary structure and functional expression of a cyclic nucleotide-activated channel from olfactory neurons. *Nature*, *347*(6289), 184–187. https://doi.org/10.1038/347184a0

Dibattista, M., Amjad, A., Maurya, D. K., Sagheddu, C., Montani, G., Tirindelli, R., & Menini, A. (2012). Calcium-activated chloride channels in the apical region of mouse vomeronasal sensory neurons. *The Journal of General Physiology*, *140*(1), 3–15. https://doi.org/10.1085/jgp.201210780

Dibattista, M., Mazzatenta, A., Grassi, F., Tirindelli, R., & Menini, A. (2008). Hyperpolarization-activated cyclic nucleotide-gated channels in mouse vomeronasal sensory neurons. *Journal of Neurophysiology*, *100*(2), 576–586. https://doi.org/10.1152/jn.90263.2008

Dibattista, M., & Menini, A. (2009). [Review of *TMEM16B induces chloride currents activated by calcium in mammalian cells*, by S. Pifferi]. *Pflugers Archiv: European Journal of Physiology*, *458*(6), 1023–1038. https://doi.org/10.1007/s00424-009-0684-9

Dibattista, M., Pifferi, S., Hernandez-Clavijo, A., & Menini, A. (2024). The physiological roles of anoctamin2/TMEM16B and anoctamin1/TMEM16A in chemical senses. *Cell Calcium*, *120*, 102889. https://doi.org/10.1016/j.ceca.2024.102889

Dolphin, A. C. (2018). Voltage-gated calcium channels: Their discovery, function and importance as drug targets. *Brain and Neuroscience Advances*, *2*, 2398212818794805. https://doi.org/10.1177/2398212818794805

Døving, K. B., & Trotier, D. (1998). Structure and function of the vomeronasal organ. *Journal of Experimental Biology*, *201*(21), 2913–2925. https://doi.org/10.1242/jeb.201.21.2913

Drouin, C., Bobadilla, A.-C., & Tassin, J.-P. (2017). Norepinephrine☆. In *Reference Module in Neuroscience and Biobehavioral Psychology*. Elsevier. https://doi.org/10.1016/B978-0-12-809324-5.03130-8

Duda, T., Fik-Rymarkiewicz, E., Venkataraman, V., Krishnan, A., & Sharma, R. K. (2004). Calcium-modulated ciliary membrane guanylate cyclase transduction machinery: Constitution and operational principles. *Molecular and Cellular Biochemistry*, *267*(1–2), 107–122. https://doi.org/10.1023/b:mcbi.0000049372.33965.4f

Dulac, C., & Axel, R. (1995). A novel family of genes encoding putative pheromone receptors in mammals. *Cell*, *83*(2), 195–206. https://doi.org/10.1016/0092-8674(95)90161-2

Durante, M. A., Kurtenbach, S., Sargi, Z. B., Harbour, J. W., Choi, R., Kurtenbach, S., Goss, G. M., Matsunami, H., & Goldstein, B. J. (2020). Single-cell analysis of olfactory neurogenesis and differentiation in adult humans. *Nature Neuroscience*, *23*(3), 323–326. https://doi.org/10.1038/s41593-020-0587-9

Eckstein, E., Pyrski, M., Pinto, S., Freichel, M., Vennekens, R., & Zufall, F. (2020). Cyclic regulation of Trpm4 expression in female vomeronasal neurons driven by ovarian sex hormones. *Molecular and Cellular Neurosciences*, *105*, 103495. https://doi.org/10.1016/j.mcn.2020.103495

Elgayar, S. A. M., Saad-Eldin, H. M., & Haussein, O. A. (2017). Morphology of cat vomeronasal organ non-sensory epithelium during postnatal development. *Anatomy & Cell Biology*, *50*(1), 17–25. https://doi.org/10.5115/acb.2017.50.1.17

Fieni, F., Ghiaroni, V., Tirindelli, R., Pietra, P., & Bigiani, A. (2003). Apical and basal neurones isolated from the mouse vomeronasal organ differ for voltage-dependent currents. *The Journal of Physiology*, *552*(Pt 2), 425–436. https://doi.org/10.1113/jphysiol.2003.052035

Firestein, S. (2001). How the olfactory system makes sense of scents. *Nature*, *413*(6852), 211–218. https://doi.org/10.1038/35093026

Firestein, S., & Menini, A. (1999). The smell of adrenaline. *Nature Neuroscience*, *2*(2), 106–108. https://doi.org/10.1038/5661

Freitag, J., Ludwig, G., Andreini, I., Rössler, P., & Breer, H. (1998). Olfactory receptors in aquatic and terrestrial vertebrates. *Journal of Comparative Physiology. A, Sensory, Neural, and Behavioral Physiology*, *183*(5), 635–650. https://doi.org/10.1007/s003590050287

Gavras, I., & Gavras, H. (2001). Role of alpha2-adrenergic receptors in hypertension. *American Journal of Hypertension*, *14*(6 Pt 2), 171S-177S. https://doi.org/10.1016/s0895-7061(01)02085-4

Genovese, F., Reisert, J., & Kefalov, V. J. (2021). Sensory Transduction in Photoreceptors and Olfactory Sensory Neurons: Common Features and Distinct Characteristics. *Frontiers in Cellular Neuroscience*, *15*, 761416. https://doi.org/10.3389/fncel.2021.761416

Ghiaroni, V., Fieni, F., Tirindelli, R., Pietra, P., & Bigiani, A. (2003). Ion Conductances in Supporting Cells Isolated From the Mouse Vomeronasal Organ. *Journal of Neurophysiology*, *89*(1), 118–127. https://doi.org/10.1152/jn.00545.2002

Goldin, A. L., Barchi, R. L., Caldwell, J. H., Hofmann, F., Howe, J. R., Hunter, J. C., Kallen, R. G., Mandel, G., Meisler, M. H., Netter, Y. B., Noda, M., Tamkun, M. M., Waxman, S. G., Wood, J. N., & Catterall, W. A. (2000). Nomenclature of voltage-gated sodium channels. *Neuron*, *28*(2), 365–368. https://doi.org/10.1016/s0896-6273(00)00116-1

Gomez, G., Rawson, N. E., Cowart, B., Lowry, L. D., Pribitkin, E. A., & Restrepo, D. (2000). Modulation of odor-induced increases in [Ca(2+)](i) by inhibitors of protein kinases A and C in rat and human olfactory receptor neurons. *Neuroscience*, *98*(1), 181–189. https://doi.org/10.1016/s0306-4522(00)00112-3

Graham, R. M. (1990). Adrenergic receptors: Structure and function. *Cleveland Clinic Journal of Medicine*, *57*(5), 481–491. https://doi.org/10.3949/ccjm.57.5.481

Haberly, L. B. (2001). Parallel-distributed Processing in Olfactory Cortex: New Insights from Morphological and Physiological Analysis of Neuronal Circuitry. *Chemical Senses*, *26*(5), 551–576. https://doi.org/10.1093/chemse/26.5.551

Haga, S., Hattori, T., Sato, T., Sato, K., Matsuda, S., Kobayakawa, R., Sakano, H., Yoshihara, Y., Kikusui, T., & Touhara, K. (2010). The male mouse pheromone ESP1 enhances female sexual receptive behaviour through a specific vomeronasal receptor. *Nature*, *466*(7302), 118–122. https://doi.org/10.1038/nature09142

Hall, R. A. (2011). Autonomic modulation of olfactory signaling. *Science Signaling*, *4*(155), pe1. https://doi.org/10.1126/scisignal.2001672

Hamacher, C., Degen, R., Franke, M., Switacz, V. K., Fleck, D., Katreddi, R. R., Hernandez-Clavijo, A., Strauch, M., Horio, N., Hachgenei, E., Spehr, J., Liberles, S. D., Merhof, D., Forni, P. E., Zimmer-Bensch, G., Ben-Shaul, Y., & Spehr, M. (2024). A revised conceptual framework for mouse vomeronasal pumping and stimulus sampling. *Current Biology: CB*, S0960-9822(24)00034-4. https://doi.org/10.1016/j.cub.2024.01.036

Hassenklöver, T., Schwartz, P., Schild, D., & Manzini, I. (2009). Purinergic Signaling Regulates Cell Proliferation of Olfactory Epithelium Progenitors. *Stem Cells*, *27*(8), 2022–2031. https://doi.org/10.1002/stem.126

He, H.-Q., & Ye, R. D. (2017). The Formyl Peptide Receptors: Diversity of Ligands and Mechanism for Recognition. *Molecules : A Journal of Synthetic Chemistry and Natural Product Chemistry*, *22*(3), 455. https://doi.org/10.3390/molecules22030455

Hegg, C. C., Irwin, M., & Lucero, M. T. (2009). Calcium store-mediated signaling in sustentacular cells of the mouse olfactory epithelium. *Glia*, *57*(6), 634–644. https://doi.org/10.1002/glia.20792

Heginbotham, L., Abramson, T., & MacKinnon, R. (1992). A functional connection between the pores of distantly related ion channels as revealed by mutant K+ channels. *Science (New York, N.Y.)*, *258*(5085), 1152–1155. https://doi.org/10.1126/science.1279807

Heinemann, S. H., Terlau, H., Stühmer, W., Imoto, K., & Numa, S. (1992). Calcium channel characteristics conferred on the sodium channel by single mutations. *Nature*, *356*(6368), 441–443. https://doi.org/10.1038/356441a0

Henriques, T., Agostinelli, E., Hernandez-Clavijo, A., Maurya, D. K., Rock, J. R., Harfe, B. D., Menini, A., & Pifferi, S. (2019). TMEM16A calcium-activated chloride

currents in supporting cells of the mouse olfactory epithelium. *The Journal of General Physiology*, *151*(7), 954–966. https://doi.org/10.1085/jgp.201812310

Hernandez-Clavijo, A., Gonzalez-Velandia, K. Y., Rangaswamy, U., Guarneri, G., Boscolo-Rizzo, P., Tofanelli, M., Gardenal, N., Sanges, R., Dibattista, M., Tirelli, G., & Menini, A. (2022). Supporting Cells of the Human Olfactory Epithelium Co-Express the Lipid Scramblase TMEM16F and ACE2 and May Cause Smell Loss by SARS-CoV-2 Spike-Induced Syncytia. *Cellular Physiology and Biochemistry: International Journal of Experimental Cellular Physiology, Biochemistry, and Pharmacology*, *56*(3), 254–269. https://doi.org/10.33594/000000531

Hernandez-Clavijo, A., Sarno, N., Gonzalez-Velandia, K. Y., Degen, R., Fleck, D., Rock, J. R., Spehr, M., Menini, A., & Pifferi, S. (2021). TMEM16A and TMEM16B Modulate Pheromone-Evoked Action Potential Firing in Mouse Vomeronasal Sensory Neurons. *eNeuro*, *8*(5). https://doi.org/10.1523/ENEURO.0179-21.2021

Herness, S., Zhao, F.-L., Kaya, N., Lu, S.-G., Shen, T., & Sun, X.-D. (2002). Adrenergic signalling between rat taste receptor cells. *The Journal of Physiology*, *543*(Pt 2), 601–614. https://doi.org/10.1113/jphysiol.2002.020438

Herrada, G., & Dulac, C. (1997). A Novel Family of Putative Pheromone Receptors in Mammals with a Topographically Organized and Sexually Dimorphic Distribution. *Cell*, *90*(4), 763–773. https://doi.org/10.1016/S0092-8674(00)80536-X

Hodgkin, A. L., & Huxley, A. F. (1952). Currents carried by sodium and potassium ions through the membrane of the giant axon of Loligo. *The Journal of Physiology*, *116*(4), 449–472. https://doi.org/10.1113/jphysiol.1952.sp004717

Hoffman, B. B., & Lefkowitz, R. J. (1982). Adrenergic receptors in the heart. *Annual Review of Physiology*, *44*, 475–484. https://doi.org/10.1146/annurev.ph.44.030182.002355

Holbrook, E. H., Wu, E., Curry, W. T., Lin, D. T., & Schwob, J. E. (2011). Immunohistochemical characterization of human olfactory tissue. *The Laryngoscope*, *121*(8), 1687–1701. https://doi.org/10.1002/lary.21856

Holy, T. E., Dulac, C., & Meister, M. (2000). Responses of Vomeronasal Neurons to Natural Stimuli. *Science*, *289*(5484), 1569–1572. https://doi.org/10.1126/science.289.5484.1569

Hong, S. P., Yang, M. J., Bae, J. H., Choi, D. R., Kim, Y.-C., Yang, M.-S., Oh, B., Kang, K. W., Lee, S.-M., Kim, B., Kim, Y.-D., Ahn, J. H., & Koh, G. Y. (2023). Three-dimensional morphologic and molecular atlases of nasal vasculature. *Nature Cardiovascular Research*, *2*(5), 449–466. https://doi.org/10.1038/s44161-023-00257-3

Hoover, K. C. (2010). Smell with inspiration: The evolutionary significance of olfaction. *American Journal of Physical Anthropology*, *143 Suppl 51*, 63–74. https://doi.org/10.1002/ajpa.21441

Huang, G.-Z., Taniguchi, M., Zhou, Y.-B., Zhang, J.-J., Okutani, F., Murata, Y., Yamaguchi, M., & Kaba, H. (2018). A2-Adrenergic receptor activation promotes long-term potentiation at excitatory synapses in the mouse accessory olfactory bulb. *Learning & Memory (Cold Spring Harbor, N.Y.)*, *25*(4), 147–157. https://doi.org/10.1101/lm.046391.117

Ibarra-Soria, X., Levitin, M. O., Saraiva, L. R., & Logan, D. W. (2014). The olfactory transcriptomes of mice. *PLoS Genetics*, *10*(9), e1004593. https://doi.org/10.1371/journal.pgen.1004593

Ihara, S., Yoshikawa, K., & Touhara, K. (2013). Chemosensory signals and their receptors in the olfactory neural system. *Neuroscience*, *254*, 45–60. https://doi.org/10.1016/j.neuroscience.2013.08.063

Insel, P. A. (1989). Structure and Function of Alpha-Adrenergic Receptors. *The American Journal of Medicine*, *87*(2, Supplement 1), S12–S18. https://doi.org/10.1016/0002-9343(89)90108-3

Ishii, T., & Mombaerts, P. (2011). Coordinated coexpression of two vomeronasal receptor V2R genes per neuron in the mouse. *Molecular and Cellular Neurosciences*, *46*(2), 397–408. https://doi.org/10.1016/j.mcn.2010.11.002

Isogai, Y., Si, S., Pont-Lezica, L., Tan, T., Kapoor, V., Murthy, V. N., & Dulac, C. (2011). Molecular organization of vomeronasal chemoreception. *Nature*, *478*(7368), 241–245. https://doi.org/10.1038/nature10437

Iwanaga, T., & Nio-Kobayashi, J. (2020). Unique blood vasculature and innervation in the cavernous tissue of murine vomeronasal organs. *Biomedical Research (Tokyo, Japan)*, *41*(5), 243–251. https://doi.org/10.2220/biomedres.41.243

Jacobson, L., Trotier, D., & Døving, K. B. (1998). Anatomical description of a new organ in the nose of domesticated animals by Ludvig Jacobson (1813). *Chemical Senses*, *23*(6), 743–754. https://doi.org/10.1093/chemse/23.6.743

Jones, D. T., & Reed, R. R. (1989). Golf: An Olfactory Neuron Specific-G Protein Involved in Odorant Signal Transduction. *Science*, *244*(4906), 790–795. https://doi.org/10.1126/science.2499043

Karlson, P., & Luscher, M. (1959). Pheromones': A new term for a class of biologically active substances. *Nature*, *183*(4653), 55–56. https://doi.org/10.1038/183055a0

Katada, S., Hirokawa, T., Oka, Y., Suwa, M., & Touhara, K. (2005). Structural basis for a broad but selective ligand spectrum of a mouse olfactory receptor: Mapping the odorant-binding site. *The Journal of Neuroscience: The Official Journal of the Society for Neuroscience*, *25*(7), 1806–1815. https://doi.org/10.1523/JNEUROSCI.4723-04.2005

Katreddi, R. R., Taroc, E. Z. M., Hicks, S. M., Lin, J. M., Liu, S., Xiang, M., & Forni, P. E. (2022). Notch signaling determines cell-fate specification of the two main types of vomeronasal neurons of rodents. *Development (Cambridge, England)*, *149*(13), dev200448. https://doi.org/10.1242/dev.200448

Kaupp, U. B. (2010). Olfactory signalling in vertebrates and insects: Differences and commonalities. *Nature Reviews Neuroscience*, *11*(3), 188–200. https://doi.org/10.1038/nrn2789

Kawai, F. (1999). Simulation analysis of effects of adrenaline on spike generation in olfactory receptor cells. *Chemical Senses*, *24*(6), 701–704. https://doi.org/10.1093/chemse/24.6.701

Kawai, F. (2024). Somatic ion channels and action potentials in olfactory receptor cells and vomeronasal receptor cells. *Journal of Neurophysiology*, *131*(3), 455–471. https://doi.org/10.1152/jn.00137.2023

Kawai, F., Kurahashi, T., & Kaneko, A. (1999). Adrenaline enhances odorant contrast by modulating signal encoding in olfactory receptor cells. *Nature Neuroscience*, *2*(2), 133–138. https://doi.org/10.1038/5686

Kelliher, K. R., Spehr, M., Li, X.-H., Zufall, F., & Leinders-Zufall, T. (2006). Pheromonal recognition memory induced by TRPC2-independent vomeronasal sensing. *The European Journal of Neuroscience*, *23*(12), 3385–3390. https://doi.org/10.1111/j.1460-9568.2006.04866.x

Kim, & Nimigean, C. (2016). Voltage-Gated Potassium Channels: A Structural Examination of Selectivity and Gating. *Cold Spring Harbor Perspectives in Biology*, *8*(5), a029231. https://doi.org/10.1101/cshperspect.a029231

Kim, S., Ma, L., Jensen, K. L., Kim, M. M., Bond, C. T., Adelman, J. P., & Yu, C. R. (2012). Paradoxical contribution of SK3 and GIRK channels to the activation of mouse vomeronasal organ. *Nature Neuroscience*, *15*(9), 1236–1244. https://doi.org/10.1038/nn.3173

Kim, S., Ma, L., Unruh, J., McKinney, S., & Yu, C. R. (2015). Intracellular chloride concentration of the mouse vomeronasal neuron. *BMC Neuroscience*, *16*, 90. https://doi.org/10.1186/s12868-015-0230-y

Kim, S., Ma, L., & Yu, C. R. (2011). Requirement of calcium-activated chloride channels in the activation of mouse vomeronasal neurons. *Nature Communications*, *2*(1), Article 1. https://doi.org/10.1038/ncomms1368

Kimoto, H., Haga, S., Sato, K., & Touhara, K. (2005). Sex-specific peptides from exocrine glands stimulate mouse vomeronasal sensory neurons. *Nature*, *437*(7060), 898–901. https://doi.org/10.1038/nature04033

Kleene, S. J. (2008). The Electrochemical Basis of Odor Transduction in Vertebrate Olfactory Cilia. *Chemical Senses*, *33*(9), 839–859. https://doi.org/10.1093/chemse/bjn048

Kurahashi, T., & Menini, A. (1997). Mechanism of odorant adaptation in the olfactory receptor cell. *Nature*, *385*(6618), 725–729. https://doi.org/10.1038/385725a0

Kurahashi, T., & Yau, K.-W. (1993). Co-existence of cationic and chloride components in odorant-induced current of vertebrate olfactory receptor cells. *Nature*, *363*(6424), 71–74. https://doi.org/10.1038/363071a0

Lagostena, L., & Menini, A. (2003). Whole-cell Recordings and Photolysis of Caged Compounds in Olfactory Sensory Neurons Isolated from the Mouse. *Chemical Senses*, *28*(8), 705–716. https://doi.org/10.1093/chemse/bjg063

Le, Y., Murphy, P. M., & Wang, J. M. (2002). Formyl-peptide receptors revisited. *Trends in Immunology*, *23*(11), 541–548. https://doi.org/10.1016/S1471-4906(02)02316-5

Leinders-Zufall, T., Brennan, P., Widmayer, P., S, P. C., Maul-Pavicic, A., Jäger, M., Li, X.-H., Breer, H., Zufall, F., & Boehm, T. (2004). MHC class I peptides as chemosensory signals in the vomeronasal organ. *Science (New York, N.Y.)*, *306*(5698), 1033–1037. https://doi.org/10.1126/science.1102818

Leinders-Zufall, T., Cockerham, R. E., Michalakis, S., Biel, M., Garbers, D. L., Reed, R. R., Zufall, F., & Munger, S. D. (2007). Contribution of the receptor guanylyl cyclase GC-D to chemosensory function in the olfactory epithelium. *Proceedings of the National Academy of Sciences of the United States of America*, *104*(36), 14507–14512. https://doi.org/10.1073/pnas.0704965104

Lewcock, J. W., & Reed, R. R. (2004). A feedback mechanism regulates monoallelic odorant receptor expression. *Proceedings of the National Academy of Sciences of the United States of America*, *101*(4), 1069–1074. https://doi.org/10.1073/pnas.0307986100

Leypold, B. G., Yu, C. R., Leinders-Zufall, T., Kim, M. M., Zufall, F., & Axel, R. (2002). Altered sexual and social behaviors in trp2 mutant mice. *Proceedings of the National Academy of Sciences of the United States of America*, *99*(9), 6376–6381. https://doi.org/10.1073/pnas.082127599

Li, R.-C., Lin, C.-C., Ren, X., Wu, J. S., Molday, L. L., Molday, R. S., & Yau, K.-W. (2018). Ca2+-activated Cl current predominates in threshold response of mouse olfactory receptor neurons. *Proceedings of the National Academy of Sciences of the United States of America*, *115*(21), 5570–5575. https://doi.org/10.1073/pnas.1803443115

Li, Zhou, X., Wang, S., Michailidis, I., Gong, Y., Su, D., Li, H., Li, X., & Yang, J. (2017). Structure of a eukaryotic cyclic-nucleotide-gated channel. *Nature*, *542*(7639), 60–65. https://doi.org/10.1038/nature20819

Liberles, S. D. (2015). Trace amine-associated receptors: Ligands, neural circuits, and behaviors. *Current Opinion in Neurobiology*, *34*, 1–7. https://doi.org/10.1016/j.conb.2015.01.001

Liberles, S. D., & Buck, L. B. (2006). A second class of chemosensory receptors in the olfactory epithelium. *Nature*, *442*(7103), 645–650. https://doi.org/10.1038/nature05066

Liberles, S. D., Horowitz, L. F., Kuang, D., Contos, J. J., Wilson, K. L., Siltberg-Liberles, J., Liberles, D. A., & Buck, L. B. (2009). Formyl peptide receptors are candidate chemosensory receptors in the vomeronasal organ. *Proceedings of the National Academy of Sciences of the United States of America*, *106*(24), 9842–9847. https://doi.org/10.1073/pnas.0904464106

Liman, E. R., & Buck, L. B. (1994). A second subunit of the olfactory cyclic nucleotide-gated channel confers high sensitivity to cAMP. *Neuron*, *13*(3), 611–621. https://doi.org/10.1016/0896-6273(94)90029-9

Liman, E. R., & Corey, D. P. (1996). Electrophysiological Characterization of Chemosensory Neurons from the Mouse Vomeronasal Organ. *Journal of Neuroscience*, *16*(15), 4625–4637. https://doi.org/10.1523/JNEUROSCI.16-15-04625.1996

Liman, E. R., Corey, D. P., & Dulac, C. (1999). TRP2: A candidate transduction channel for mammalian pheromone sensory signaling. *Proceedings of the National Academy of Sciences of the United States of America*, *96*(10), 5791–5796. https://doi.org/10.1073/pnas.96.10.5791

Lucas, P., Ukhanov, K., Leinders-Zufall, T., & Zufall, F. (2003). A Diacylglycerol-Gated Cation Channel in Vomeronasal Neuron Dendrites Is Impaired in *TRPC2* Mutant Mice. *Neuron*, *40*(3), 551–561. https://doi.org/10.1016/S0896-6273(03)00675-5

Ma, M., Chen, W. R., & Shepherd, G. M. (1999). Electrophysiological characterization of rat and mouse olfactory receptor neurons from an intact epithelial preparation. *Journal of Neuroscience Methods*, *92*(1–2), 31–40. https://doi.org/10.1016/s0165-0270(99)00089-8

Marban, E., Yamagishi, T., & Tomaselli, G. F. (1998). Structure and function of voltage-gated sodium channels. *The Journal of Physiology*, *508*(Pt 3), 647–657. https://doi.org/10.1111/j.1469-7793.1998.647bp.x

Maresh, A., Rodriguez Gil, D., Whitman, M. C., & Greer, C. A. (2008). Principles of glomerular organization in the human olfactory bulb—Implications for odor processing. *PloS One*, *3*(7), e2640. https://doi.org/10.1371/journal.pone.0002640

Matsunami, H., & Buck, L. B. (1997). A Multigene Family Encoding a Diverse Array of Putative Pheromone Receptors in Mammals. *Cell*, *90*(4), 775–784. https://doi.org/10.1016/S0092-8674(00)80537-1

Matthews, H. R., & Reisert, J. (2003). Calcium, the two-faced messenger of olfactory transduction and adaptation. *Current Opinion in Neurobiology*, *13*(4), 469–475. https://doi.org/10.1016/s0959-4388(03)00097-7

Maue, R. A., & Dionne, V. E. (1987). Patch-clamp studies of isolated mouse olfactory receptor neurons. *The Journal of General Physiology*, *90*(1), 95–125. https://doi.org/10.1085/jgp.90.1.95

McCorry, L. K. (2007). Physiology of the Autonomic Nervous System. *American Journal of Pharmaceutical Education*, *71*(4), 78.

McDougal, D. H., & Gamlin, P. D. (2015). Autonomic control of the eye. *Comprehensive Physiology*, *5*(1), 439–473. https://doi.org/10.1002/cphy.c140014

Mechin, V., Pageat, P., Teruel, E., & Asproni, P. (2021). Histological and Immunohistochemical Characterization of Vomeronasal Organ Aging in Mice.

Animals : An Open Access Journal from MDPI, *11*(5), 1211. https://doi.org/10.3390/ani11051211

Menco, B., Carr, V., Ezeh, P., Liman, E., & Yankova, M. (2001). Ultrastructural localization of G-proteins and the channel protein TRP2 to microvilli of rat vomeronasal receptor cells. *The Journal of Comparative Neurology*, *438*(4), 468–489. https://doi.org/10.1002/cne.1329

Menco, B., & Morrison, E. E. (2003). Morphology of the Mammalian Olfactory Epithelium: Form, Fine Structure, Function and Pathology. In *Handbook of Olfaction and Gustation* (pp. 17–49).

Menini, A., Lagostena, L., & Boccaccio, A. (2004). Olfaction: From Odorant Molecules to the Olfactory Cortex. *Physiology*, *19*(3), 101–104. https://doi.org/10.1152/nips.1507.2003

Meredith, M., Marques, D. M., O'Connell, R. O., & Stern, F. L. (1980). Vomeronasal pump: Significance for male hamster sexual behavior. *Science (New York, N.Y.)*, *207*(4436), 1224–1226. https://doi.org/10.1126/science.7355286

Meredith, M., & O'Connell, R. J. (1979). Efferent control of stimulus access to the hamster vomeronasal organ. *The Journal of Physiology*, *286*, 301–316. https://doi.org/10.1113/jphysiol.1979.sp012620

Michelotti, G. A., Price, D. T., & Schwinn, D. A. (2000). Alpha 1-adrenergic receptor regulation: Basic science and clinical implications. *Pharmacology & Therapeutics*, *88*(3), 281–309. https://doi.org/10.1016/s0163-7258(00)00092-9

Migeotte, I., Communi, D., & Parmentier, M. (2006). Formyl peptide receptors: A promiscuous subfamily of G protein-coupled receptors controlling immune responses. *Cytokine & Growth Factor Reviews*, *17*(6), 501–519. https://doi.org/10.1016/j.cytogfr.2006.09.009

Miller, C. H., Campbell, P., & Sheehan, M. J. (2020). Distinct evolutionary trajectories of V1R clades across mouse species. *BMC Evolutionary Biology*, *20*, 99. https://doi.org/10.1186/s12862-020-01662-z

Molday, R. S. (1996). Calmodulin regulation of cyclic-nucleotide-gated channels. *Current Opinion in Neurobiology*, *6*(4), 445–452. https://doi.org/10.1016/s0959-4388(96)80048-1

Mombaerts, P. (2004). Genes and ligands for odorant, vomeronasal and taste receptors. *Nature Reviews Neuroscience*, *5*(4), 263–278. https://doi.org/10.1038/nrn1365

Morrison, E. E., & Costanzo, R. M. (1990). Morphology of the human olfactory epithelium. *The Journal of Comparative Neurology*, *297*(1), 1–13. https://doi.org/10.1002/cne.902970102

Namadurai, S., Yereddi, N. R., Cusdin, F. S., Huang, C. L.-H., Chirgadze, D. Y., & Jackson, A. P. (2015). A new look at sodium channel β subunits. *Open Biology*, *5*(1), 140192. https://doi.org/10.1098/rsob.140192

Neely, A., & Hidalgo, P. (2014). Structure-function of proteins interacting with the α1 pore-forming subunit of high-voltage-activated calcium channels. *Frontiers in Physiology*, *5*, 209. https://doi.org/10.3389/fphys.2014.00209

Newcomb, R., Szoke, B., Palma, A., Wang, G., Chen, X., Hopkins, W., Cong, R., Miller, J., Urge, L., Tarczy-Hornoch, K., Loo, J. A., Dooley, D. J., Nadasdi, L., Tsien, R. W., Lemos, J., & Miljanich, G. (1998). Selective Peptide Antagonist of the Class E Calcium Channel from the Venom of the Tarantula Hysterocrates gigas. *Biochemistry*, *37*(44), 15353–15362. https://doi.org/10.1021/bi981255g

Norlin, E. M., Gussing, F., & Berghard, A. (2003). Vomeronasal Phenotype and Behavioral Alterations in Gαi2 Mutant Mice. *Current Biology*, *13*(14), 1214–1219. https://doi.org/10.1016/S0960-9822(03)00452-4

Novotny, M. V., Ma, W., Wiesler, D., & Zídek, L. (1999). Positive identification of the puberty-accelerating pheromone of the house mouse: The volatile ligands associating with the major urinary protein. *Proceedings. Biological Sciences*, *266*(1432), 2017–2022. https://doi.org/10.1098/rspb.1999.0880

O'Donnell, J., Zeppenfeld, D., McConnell, E., Pena, S., & Nedergaard, M. (2012). Norepinephrine: A neuromodulator that boosts the function of multiple cell types to optimize CNS performance. *Neurochemical Research*, *37*(11), 2496–2512. https://doi.org/10.1007/s11064-012-0818-x

Okano, M., & Takagi, S. F. (1974). Secretion and electrogenesis of the supporting cell in the olfactory epithelium. *The Journal of Physiology*, *242*(2), 353–370. https://doi.org/10.1113/jphysiol.1974.sp010711

Ostrin, L. A., & Glasser, A. (2010). Autonomic drugs and the accommodative system in rhesus monkeys. *Experimental Eye Research*, *90*(1), 104–112. https://doi.org/10.1016/j.exer.2009.09.015

Pankevich, D. E., Cherry, J. A., & Baum, M. J. (2006). Effect of vomeronasal organ removal from male mice on their preference for and neural Fos responses to female urinary odors. *Behavioral Neuroscience*, *120*(4), 925–936. https://doi.org/10.1037/0735-7044.120.4.925

Park, S. H., Podlaha, O., Grus, W. E., & Zhang, J. (2011). The microevolution of V1r vomeronasal receptor genes in mice. *Genome Biology and Evolution*, *3*, 401–412. https://doi.org/10.1093/gbe/evr039

Philipp, M., Brede, M., & Hein, L. (2002). Physiological significance of α2-adrenergic receptor subtype diversity: One receptor is not enough. *American Journal of Physiology-Regulatory, Integrative and Comparative Physiology*, *283*(2), R287–R295. https://doi.org/10.1152/ajpregu.00123.2002

Pietra, G., Dibattista, M., Menini, A., Reisert, J., & Boccaccio, A. (2016). The Ca2+-activated Cl- channel TMEM16B regulates action potential firing and axonal targeting in olfactory sensory neurons. *The Journal of General Physiology*, *148*(4), 293–311. https://doi.org/10.1085/jgp.201611622

Pifferi, S., Cenedese, V., & Menini, A. (2012). Anoctamin 2/TMEM16B: A calcium-activated chloride channel in olfactory transduction. *Experimental Physiology*, *97*(2), 193–199. https://doi.org/10.1113/expphysiol.2011.058230

Pifferi, S., Dibattista, M., & Menini, A. (2009). TMEM16B induces chloride currents activated by calcium in mammalian cells. *Pflügers Archiv - European Journal of Physiology*, *458*(6), 1023–1038. https://doi.org/10.1007/s00424-009-0684-9

Pifferi, S., Menini, A., & Kurahashi, T. (2010). Signal Transduction in Vertebrate Olfactory Cilia. In A. Menini (Ed.), *The Neurobiology of Olfaction*. CRC Press/Taylor & Francis. http://www.ncbi.nlm.nih.gov/books/NBK55986/

Pifferi, S., Pascarella, G., Boccaccio, A., Mazzatenta, A., Gustincich, S., Menini, A., & Zucchelli, S. (2006). Bestrophin-2 is a candidate calcium-activated chloride channel involved in olfactory transduction. *Proceedings of the National Academy of Sciences of the United States of America*, *103*(34), 12929–12934. https://doi.org/10.1073/pnas.0604505103

Potter, S. M., Zheng, C., Koos, D. S., Feinstein, P., Fraser, S. E., & Mombaerts, P. (2001). Structure and Emergence of Specific Olfactory Glomeruli in the Mouse. *Journal of Neuroscience*, *21*(24), 9713–9723. https://doi.org/10.1523/JNEUROSCI.21-24-09713.2001

Purves, D., Augustine, G. J., Fitzpatrick, D., Katz, L. C., LaMantia, A.-S., McNamara, J. O., & Williams, S. M. (2001). The Olfactory Epithelium and Olfactory Receptor Neurons. In *Neuroscience. 2nd edition*. Sinauer Associates. https://www.ncbi.nlm.nih.gov/books/NBK10896/

Ranjan, R., Logette, E., Marani, M., Herzog, M., Tâche, V., Scantamburlo, E., Buchillier, V., & Markram, H. (2019). A Kinetic Map of the Homomeric Voltage-Gated Potassium Channel (Kv) Family. *Frontiers in Cellular Neuroscience*, *13*, 358. https://doi.org/10.3389/fncel.2019.00358

Rasche, S., Toetter, B., Adler, J., Tschapek, A., Doerner, J. F., Kurtenbach, S., Hatt, H., Meyer, H., Warscheid, B., & Neuhaus, E. M. (2010). Tmem16b is Specifically Expressed in the Cilia of Olfactory Sensory Neurons. *Chemical Senses*, *35*(3), 239–245. https://doi.org/10.1093/chemse/bjq007

Reisert, J., & Matthews, H. R. (1998). Na+-dependent Ca2+ extrusion governs response recovery in frog olfactory receptor cells. *The Journal of General Physiology*, *112*(5), 529–535. https://doi.org/10.1085/jgp.112.5.529

Reiten, I., Uslu, F. E., Fore, S., Pelgrims, R., Ringers, C., Diaz Verdugo, C., Hoffman, M., Lal, P., Kawakami, K., Pekkan, K., Yaksi, E., & Jurisch-Yaksi, N. (2017). Motile-Cilia-Mediated Flow Improves Sensitivity and Temporal Resolution of Olfactory Computations. *Current Biology*, *27*(2), 166–174. https://doi.org/10.1016/j.cub.2016.11.036

Restrepo, D., Okada, Y., Teeter, J. H., Lowry, L. D., Cowart, B., & Brand, J. G. (1993). Human olfactory neurons respond to odor stimuli with an increase in cytoplasmic Ca2+. *Biophysical Journal*, *64*(6), 1961–1966.

Rivière, S., Challet, L., Fluegge, D., Spehr, M., & Rodriguez, I. (2009). Formyl peptide receptor-like proteins are a novel family of vomeronasal chemosensors. *Nature*, *459*(7246), 574–577. https://doi.org/10.1038/nature08029

Roberts, S. A., Simpson, D. M., Armstrong, S. D., Davidson, A. J., Robertson, D. H., McLean, L., Beynon, R. J., & Hurst, J. L. (2010). Darcin: A male pheromone that stimulates female memory and sexual attraction to an individual male's odour. *BMC Biology*, *8*, 75. https://doi.org/10.1186/1741-7007-8-75

Rodriguez, I., Del Punta, K., Rothman, A., Ishii, T., & Mombaerts, P. (2002). Multiple new and isolated families within the mouse superfamily of V1r vomeronasal receptors. *Nature Neuroscience*, *5*(2), 134–140. https://doi.org/10.1038/nn795

Roppolo, D., Vollery, S., Kan, C.-D., Lüscher, C., Broillet, M.-C., & Rodriguez, I. (2007). Gene cluster lock after pheromone receptor gene choice. *The EMBO Journal*, *26*(14), 3423–3430. https://doi.org/10.1038/sj.emboj.7601782

Rump, L. C., Bohmann, C., Schaible, U., Schöllhorn, J., & Limberger, N. (1995). Alpha 2C-adrenoceptor-modulated release of noradrenaline in human right atrium. *British Journal of Pharmacology*, *116*(6), 2617–2624. https://doi.org/10.1111/j.1476-5381.1995.tb17216.x

Rünnenburger, K., Breer, H., & Boekhoff, I. (2002). Selective G protein beta gamma-subunit compositions mediate phospholipase C activation in the vomeronasal organ. *European Journal of Cell Biology*, *81*(10), 539–547. https://doi.org/10.1078/0171-9335-00277

Ryba, N. J., & Tirindelli, R. (1997). A new multigene family of putative pheromone receptors. *Neuron*, *19*(2), 371–379. https://doi.org/10.1016/s0896-6273(00)80946-0

Sarno, N., Hernandez-Clavijo, A., Boccaccio, A., Menini, A., & Pifferi, S. (2022). Slow Inactivation of Sodium Channels Contributes to Short-Term Adaptation in Vomeronasal Sensory Neurons. *eNeuro*, *9*(3). https://doi.org/10.1523/ENEURO.0471-21.2022

Sharma, A., Kumar, R., Aier, I., Semwal, R., Tyagi, P., & Varadwaj, P. (2019). Sense of Smell: Structural, Functional, Mechanistic Advancements and Challenges in Human Olfactory Research. *Current Neuropharmacology*, *17*(9), 891–911. https://doi.org/10.2174/1570159X17666181206095626

Sherborne, A. L., Thom, M. D., Paterson, S., Jury, F., Ollier, W. E. R., Stockley, P., Beynon, R. J., & Hurst, J. L. (2007). The genetic basis of inbreeding avoidance in house mice. *Current Biology: CB*, *17*(23), 2061–2066. https://doi.org/10.1016/j.cub.2007.10.041

Shimazaki, R., Boccaccio, A., Mazzatenta, A., Pinato, G., Migliore, M., & Menini, A. (2006). Electrophysiological properties and modeling of murine vomeronasal sensory neurons in acute slice preparations. *Chemical Senses*, *31*(5), 425–435. https://doi.org/10.1093/chemse/bjj047

Silva, L., & Antunes, A. (2017). Vomeronasal Receptors in Vertebrates and the Evolution of Pheromone Detection. *Annual Review of Animal Biosciences*, *5*, 353–370. https://doi.org/10.1146/annurev-animal-022516-022801

Silvotti, L., Moiani, A., Gatti, R., & Tirindelli, R. (2007). Combinatorial co-expression of pheromone receptors, V2Rs. *Journal of Neurochemistry*, *103*(5), 1753–1763. https://doi.org/10.1111/j.1471-4159.2007.04877.x

Spehr, M. (2010). Sniffing out social signals. *E-Neuroforum*, *1*(1), 9–16. https://doi.org/10.1007/s13295-010-0002-1

Spehr, M., & Munger, S. D. (2009). Olfactory receptors: GPCRs and beyond. *Journal of Neurochemistry*, *109*(6), 1570–1583. https://doi.org/10.1111/j.1471-4159.2009.06085.x

Stowers, L., Holy, T. E., Meister, M., Dulac, C., & Koentges, G. (2002). Loss of sex discrimination and male-male aggression in mice deficient for TRP2. *Science (New York, N.Y.)*, *295*(5559), 1493–1500. https://doi.org/10.1126/science.1069259

Stowers, L., & Kuo, T.-H. (2015). Mammalian pheromones; emerging properties and mechanisms of detection. *Current Opinion in Neurobiology*, *34*, 103–109. https://doi.org/10.1016/j.conb.2015.02.005

Strosberg, A. D. (1995). Structure, function, and regulation of the three beta-adrenergic receptors. *Obesity Research*, *3 Suppl 4*, 501S-505S. https://doi.org/10.1002/j.1550-8528.1995.tb00219.x

Suzuki, Y., Takeda, M., & Farbman, A. I. (1996). Supporting cells as phagocytes in the olfactory epithelium after bulbectomy. *Journal of Comparative Neurology*, *376*(4), 509–517. https://doi.org/10.1002/(SICI)1096-9861(19961223)376:4<509::AID-CNE1>3.0.CO;2-5

Takeuchi, H., & Kurahashi, T. (2003). Identification of Second Messenger Mediating Signal Transduction in the Olfactory Receptor Cell. *The Journal of General Physiology*, *122*(5), 557–567. https://doi.org/10.1085/jgp.200308911

Tamari, K., Takeuchi, H., Kobayashi, M., Takeuchi, K., Kurahashi, T., & Yamamoto, T. (2019). Electrical properties of cells from human olfactory epithelium. *Auris, Nasus, Larynx*, *46*(5), 734–741. https://doi.org/10.1016/j.anl.2019.01.006

Tian, C., Yang, Y., Wang, R., Li, Y., Sun, F., Chen, J., & Zha, D. (2024). Norepinephrine protects against cochlear outer hair cell damage and noise-induced hearing loss via α2A-adrenergic receptor. *BMC Neuroscience*, *25*(1), 5. https://doi.org/10.1186/s12868-024-00845-4

Tirindelli, R. (2021). Coding of pheromones by vomeronasal receptors. *Cell and Tissue Research*, *383*(1), 367–386. https://doi.org/10.1007/s00441-020-03376-6

Tirindelli, R., Dibattista, M., Pifferi, S., & Menini, A. (2009). From pheromones to behavior. *Physiological Reviews*, *89*(3), 921–956. https://doi.org/10.1152/physrev.00037.2008

Tsujimoto, G., Tsujimoto, A., Suzuki, E., & Hashimoto, K. (1989). Glycogen phosphorylase activation by two different alpha 1-adrenergic receptor subtypes: Methoxamine selectively stimulates a putative alpha 1-adrenergic receptor subtype (alpha 1a) that couples with Ca2+ influx. *Molecular Pharmacology*, *36*(1), 166–176.

Ukhanov, K., Leinders-Zufall, T., & Zufall, F. (2007). Patch-Clamp Analysis of Gene-Targeted Vomeronasal Neurons Expressing a Defined V1r or V2r Receptor: Ionic Mechanisms Underlying Persistent Firing. *Journal of Neurophysiology*, *98*(4), 2357–2369. https://doi.org/10.1152/jn.00642.2007

Untiet, V., Moeller, L. M., Ibarra-Soria, X., Sánchez-Andrade, G., Stricker, M., Neuhaus, E. M., Logan, D. W., Gensch, T., & Spehr, M. (2016). Elevated Cytosolic Cl- Concentrations in Dendritic Knobs of Mouse Vomeronasal Sensory Neurons. *Chemical Senses*, *41*(8), 669–676. https://doi.org/10.1093/chemse/bjw077

Velásquez-Martinez, M. C., Vázquez-Torres, R., & Jiménez-Rivera, C. A. (2012). Activation of alpha1-adrenoceptors enhances glutamate release onto ventral tegmental area dopamine cells. *Neuroscience*, *216*, 18–30. https://doi.org/10.1016/j.neuroscience.2012.03.056

Vogalis, F., Hegg, C. C., & Lucero, M. T. (2005a). Electrical coupling in sustentacular cells of the mouse olfactory epithelium. *Journal of Neurophysiology*, *94*(2), 1001–1012. https://doi.org/10.1152/jn.01299.2004

Vogalis, F., Hegg, C. C., & Lucero, M. T. (2005b). Ionic conductances in sustentacular cells of the mouse olfactory epithelium. *The Journal of Physiology*, *562*(Pt 3), 785–799. https://doi.org/10.1113/jphysiol.2004.079228

Voznessenskaya, V. V., Klyuchnikova, M. A., & Laktionova, T. K. (2022). Evolution of Pheromones in Mammals. *Biology Bulletin Reviews*, *12*(1), 49–64. https://doi.org/10.1134/S2079086422010091

Waxenbaum, J. A., Reddy, V., & Varacallo, M. (2024). Anatomy, Autonomic Nervous System. In *StatPearls*. StatPearls Publishing. http://www.ncbi.nlm.nih.gov/books/NBK539845/

Webb, R. C. (2003). Smooth muscle contraction and relaxation. *Advances in Physiology Education*, *27*(4), 201–206. https://doi.org/10.1152/advan.00025.2003

Wehrwein, E. A., Orer, H. S., & Barman, S. M. (2016). Overview of the Anatomy, Physiology, and Pharmacology of the Autonomic Nervous System. *Comprehensive Physiology*, *6*(3), 1239–1278. https://doi.org/10.1002/cphy.c150037

Weiss, L., Manzini, I., & Hassenklöver, T. (2021). Olfaction across the water–air interface in anuran amphibians. *Cell and Tissue Research*, *383*(1), 301–325. https://doi.org/10.1007/s00441-020-03377-5

Wong, S. T., Trinh, K., Hacker, B., Chan, G. C. K., Lowe, G., Gaggar, A., Xia, Z., Gold, G. H., & Storm, D. R. (2000). Disruption of the Type III Adenylyl Cyclase Gene

Leads to Peripheral and Behavioral Anosmia in Transgenic Mice. *Neuron*, *27*(3), 487–497. https://doi.org/10.1016/S0896-6273(00)00060-X

Wu, J., Yan, Z., Li, Z., Qian, X., Lu, S., Dong, M., Zhou, Q., & Yan, N. (2016). Structure of the voltage-gated calcium channel Cav1.1 at 3.6 Å resolution. *Nature*, *537*(7619), 191–196. https://doi.org/10.1038/nature19321

Yan, C., Zhao, A. Z., Bentley, J. K., Loughney, K., Ferguson, K., & Beavo, J. A. (1995). Molecular cloning and characterization of a calmodulin-dependent phosphodiesterase enriched in olfactory sensory neurons. *Proceedings of the National Academy of Sciences of the United States of America*, *92*(21), 9677–9681.

Yang, C., & Delay, R. J. (2010). [Review of *Odors activate dual pathways, a TRPC2 and a AA-dependent pathway, in mouse vomeronasal neurons*, by P. Zhang]. *American Journal of Physiology - Cell Physiology*, *298*(5), C1253–C1264. https://doi.org/10.1152/ajpcell.00271.2009

Yoshinaga, S., Sato, T., Hirakane, M., Esaki, K., Hamaguchi, T., Haga-Yamanaka, S., Tsunoda, M., Kimoto, H., Shimada, I., Touhara, K., & Terasawa, H. (2013). Structure of the Mouse Sex Peptide Pheromone ESP1 Reveals a Molecular Basis for Specific Binding to the Class C G-protein-coupled Vomeronasal Receptor *. *Journal of Biological Chemistry*, *288*(22), 16064–16072. https://doi.org/10.1074/jbc.M112.436782

Yu, F. H., & Catterall, W. A. (2003). Overview of the voltage-gated sodium channel family. *Genome Biology*, *4*(3), 207.

Zhang, & Firestein, S. (2002). The olfactory receptor gene superfamily of the mouse. *Nature Neuroscience*, *5*(2), 124–133. https://doi.org/10.1038/nn800

Zhang, Kolli, T., Hivley, R., Jaber, L., Zhao, F. I., Yan, J., & Herness, S. (2010). Characterization of the expression pattern of adrenergic receptors in rat taste buds. *Neuroscience*, *169*(3), 1421–1437. https://doi.org/10.1016/j.neuroscience.2010.05.021

Zhang, P., Yang, C., & Delay, R. J. (2008). Urine Stimulation Activates BK Channels in Mouse Vomeronasal Neurons. *Journal of Neurophysiology*, *100*(4), 1824–1834. https://doi.org/10.1152/jn.90555.2008

Zhou, G., Lane, G., Cooper, S. L., Kahnt, T., & Zelano, C. (2019). Characterizing functional pathways of the human olfactory system. *eLife*, *8*, e47177. https://doi.org/10.7554/eLife.47177

Zhuang, Y., Liu, H., Edward Zhou, X., Kumar Verma, R., de Waal, P. W., Jang, W., Xu, T.-H., Wang, L., Meng, X., Zhao, G., Kang, Y., Melcher, K., Fan, H., Lambert, N. A., Eric Xu, H., & Zhang, C. (2020). Structure of formylpeptide receptor 2-Gi complex reveals insights into ligand recognition and signaling. *Nature Communications*, *11*(1), 885. https://doi.org/10.1038/s41467-020-14728-9

Zimnik, N. C., Treadway, T., Smith, R. S., & Araneda, R. C. (2013). α(1A)-Adrenergic regulation of inhibition in the olfactory bulb. *The Journal of Physiology*, *591*(7), 1631–1643. https://doi.org/10.1113/jphysiol.2012.248591

Zybura, A. S., Baucum, A. J., Rush, A. M., Cummins, T. R., & Hudmon, A. (2020). CaMKII enhances voltage-gated sodium channel Nav1.6 activity and neuronal excitability. *The Journal of Biological Chemistry*, *295*(33), 11845–11865. https://doi.org/10.1074/jbc.RA120.014062